10
8/24/92 (2)

RFP-4450
June 26, 1992

RFP-4450
June 26, 1992

CALCULATION OF BINARY PHASE DIAGRAMS BETWEEN THE ACTINIDE ELEMENTS, RARE EARTH ELEMENTS, AND TRANSITION METAL ELEMENTS

J. E. Selle

EG&G ROCKY FLATS

Rocky Flats Plant
P. O. Box 464
Golden, Colorado 80402-0464

U.S. DEPARTMENT OF ENERGY
CONTRACT DE-AC04-90DE62349

DISCLAIMER

Printed
June 26, 1992

RFP-4450
UC-704 MATERIALS
DOE/OSTI-4500-R75

RFP--4450

DE92 019119

CALCULATION OF BINARY PHASE DIAGRAMS BETWEEN THE ACTINIDE ELEMENTS, RARE EARTH ELEMENTS, AND TRANSITION METAL ELEMENTS

J. E. Selle

SUBJECT DESCRIPTORS

Actinide Elements
Binary Phase Diagrams
Phase Diagram Calculations
Rare Earth Elements
Transition Metal Elements

EG&G ROCKY FLATS, INC.
ROCKY FLATS PLANT
P. O. BOX 464
GOLDEN, COLORADO 80402-0464

PREPARED UNDER CONTRACT DE-AC04-90DE62349
FOR THE
ALBUQUERQUE OPERATIONS OFFICE
U.S. DEPARTMENT OF ENERGY

CONTENTS

CALCULATION OF BINARY PHASE DIAGRAMS BETWEEN THE ACTINIDE ELEMENTS, RARE EARTH ELEMENTS, AND TRANSITION METAL ELEMENTS

J. E. Selle

ABSTRACT

Attempts were made to apply the Kaufman method of calculating binary phase diagrams to the calculation of binary phase diagrams between the rare earths, actinides, and the refractory transition metals. Difficulties were encountered in applying the method to the rare earths and actinides, and modifications were necessary to provide accurate representation of known diagrams. To calculate the interaction parameters for rare earth-rare earth diagrams, it was necessary to use the atomic volumes for each of the phases: liquid, body-centered cubic, hexagonal close-packed, and face-centered cubic. Determination of the atomic volumes of each of these phases for each element is discussed in detail. In some cases, empirical means were necessary. Results are presented on the calculation of rare earth-rare earth, rare earth-actinide, and actinide-actinide diagrams.

For rare earth-refractory transition metal diagrams and actinide-refractory transition metal diagrams, empirical means were required to develop values for the enthalpy of vaporization for rare earth elements and values for the constant (C) required when intermediate phases are present. Results of using the values determined for each element are presented.

INTRODUCTION

A method has been proposed by Kaufman[1] for calculating binary phase diagrams, which relies only upon the thermodynamic properties of the pure elements. When initially developed, this method was successful for calculating binary phase diagrams between the refractory transition metals of the second and third long periods. Further effort by Kaufman[2] extended this work to titanium. Subsequent attempts were made by Aaronson et al. [3-5] to extend this method even further to the rare earth elements and the actinide elements. In these works, only liquidus and solidus lines were calculated. Considerable success was achieved on some systems while only limited success was achieved on others. More complete calculations were not possible because of the lack of necessary thermodynamic data.

As part of a casting development program, it became desirable to know the characteristics of the Lu-Pu and Ir-Pu binary phase diagrams. No information is available in the literature on the Lu-Pu diagram, and only limited information is available on the presence of intermetallic compounds in the Ir-Pu system.[6,7] Since the Kaufman method requires only thermodynamic data for the pure elements, it was decided to use this method to calculate the Lu-Pu and Ir-Pu phase diagrams.

The Kaufman approach assumes that solid phases of metal systems are either body-centered cubic, hexagonal close-packed, or face-centered cubic, designated ß, ε, or α, respectively. The thermodynamic data required are the enthalpy of vaporization (ΔH_{vap}) of each element, the enthalpy (ΔH), and the entropy (ΔS) of each transformation between different crystal structures of the pure elements. The latter two values are used to calculate the free energy (ΔF) of the transformation, also called the lattice stability parameter defined by the relationship:

$$\Delta F = \Delta H - T\Delta S \qquad \text{(Eq. 1)}$$

where T is the absolute temperature.

A complete set of transformations includes hypothetical transformations as well as known transformations. For instance, tantalum,

which has the body-centered cubic structure at all temperatures to the melting point, would also require lattice stability parameters for the Liquid (L)→ε, L→α, ß→ε, ß→α, and ε→α transformations as well as the L→ß transformation, even though such transformations do not actually exist. Procedures for determining these values for the refractory transition metal elements are described by Kaufman.[1]

The atomic volume of each element is also required. The enthalpy of vaporization and the atomic volumes are used to calculate the interaction parameters for the system of interest according to procedures established by Kaufman[1] and modified by Shiflet et al.[3] and this work; the lattice stability parameters, along with the interaction parameters are used to determine phase boundaries.

Two relationships are used to calculate the boundaries of a two-phase field. For the ß+L field, the equations are:

$$\Delta F^{\beta\rightarrow L}{}_i + RT\ln(1-x_L)/(1-x_\beta) = (x_\beta)^2B - (x_L)^2L \qquad \text{(Eq. 2)}$$

and

$$\Delta F^{\beta\rightarrow L}{}_j + RT\ln x_L/x_B = (1-x_\beta)^2B - (1-x_L)^2L \qquad \text{(Eq. 3)}$$

where T = absolute temperature

R = the gas constant
= 1.9872 cal/mole-deg

$\Delta F^{\beta\rightarrow L}{}_i$, $\Delta F^{\beta\rightarrow L}{}_j$ = the lattice stability parameters for the ß→L transformation for Elements i and j, respectively,

x_B = the composition of the ß/ß + L boundary,

x_L = the composition of the ß + L/L boundary, and

B, L = the interaction parameters for the body-centered cubic and liquid phases, respectively.

Since

$$\Delta F^{\beta\rightarrow L}{}_i = \Delta H^{\beta\rightarrow L}{}_i - T\Delta S^{\beta\rightarrow L}{}_i \qquad \text{(Eq. 4)}$$

and

$$\Delta F^{\beta\rightarrow L}{}_j = \Delta H^{\beta\rightarrow L}{}_j - T\Delta S^{\beta\rightarrow L}{}_j \qquad \text{(Eq. 5)}$$

then $\Delta S^{\beta\rightarrow L}{}_i = \Delta H^{\beta\rightarrow L}{}_i/T^{\beta\rightarrow L}{}_i$, and

$$\Delta S^{\beta\rightarrow L}{}_j = \Delta H^{\beta\rightarrow L}{}_j/T^{\beta\rightarrow L}{}_j \qquad \text{(Eq. 6)}$$

For any temperature other than the transformation (melting) point

$$\Delta F^{\beta\rightarrow L}{}_i = \Delta H^{\beta\rightarrow L}{}_i - T(\Delta H^{\beta\rightarrow L}{}_i)/T^{\beta\rightarrow L}{}_i$$
$$= \Delta H^{\beta\rightarrow L}{}_i(1-T/T^{\beta\rightarrow L}{}_i) \qquad \text{(Eq. 7)}$$

A similar equation is obtained for Element j.

Similar pairs of equations are used for all other two-phase fields, using the proper values for ΔF_i, ΔF_j, and the interaction parameters. Calculation of a diagram consists of determining the boundaries of all appropriate two-phase fields. The liquidus curves for each possible structure are calculated, and the curve with the highest temperature for each composition is the one used. It is possible that different structures may solidify at different compositions. The appropriate sets of curves are selected and solid-state phase boundaries are calculated, based on the higher temperature phases present.

This report summarizes an attempt to extend the Kaufman method to allow calculation of binary phase diagrams involving the rare earths and the actinides. All of the rare earths are included with the exception of promethium. Most of the modification work centered around identification of the various parameters required. Much of the information is available in the open literature or can be calculated from this information. Wherever information is not available, other means must be devised to estimate the necessary values. Typical examples are presented, where appropriate, to demonstrate the effectiveness of the parameters used.

PROCEDURE

To begin the calculation of binary phase diagrams by the Kaufman method, the following data are needed for each element:

1. Enthalpy of vaporization, ΔH_{vap}
2. Molar volume
3. Lattice stability parameters for each real and hypothetical transformation

Lattice stability parameters for some of the transformations of most rare earth and actinide metals were obtained from Hultgren et al.[8] From these, others were calculated directly from the relationships:

$$\Delta H^{1\to3} = \Delta H^{1\to2} + \Delta H^{2\to3} \qquad \text{(Eq. 8)}$$

and

$$\Delta S^{1\to3} = \Delta S^{1\to2} + \Delta S^{2\to3} \qquad \text{(Eq. 9)}$$

where the superscripts 1, 2, and 3 represent any of the phases of the element in question. In many cases, these calculations do not result in a complete set of stability parameters for a given element, and other means are required. A complete description of the procedures used and the results obtained are given in Appendix A.

To calculate a binary diagram using the Kaufman method, it is also necessary to determine interaction parameters for the various phases. Four interaction parameters are required for each binary system (L, B, E, and A), representing the parameters for the liquid, body-centered cubic, hexagonal close-packed, and face-centered cubic phases, respectively. For the liquid phase, the interaction parameter (L) is defined as:

$$L = e_o + e_p \qquad \text{(Eq. 10)}$$

where e_o is the electronic component and e_p is the "internal pressure" component. These are defined as:

$$e_o = 2[{}^0H^V_{(i+j)/2} - 1/2\,{}^0H^V_{(i)} - 1/2\,{}^0H^V_{(j)}] \qquad \text{(Eq. 11)}$$

$$e_p = 0.3(V_i^L + V_j^L)\,[(-{}^0H^V_{(i)}/V_i^L) - (-{}^0H^V_{(j)}/V_j^L)^{1/2}]^2 \qquad \text{(Eq. 12)}$$

where

V_i^L, V_j^L = molar volume of Elements i and j as liquid

${}^0H^V_{(i)}$, ${}^0H^V_{(j)}$ = enthalpy of vaporization of Elements i and j in the structure stable at the melting point

${}^0H^V_{(i+j)/2}$ = enthalpy of vaporization of an element from the group whose number is the average of those of Elements i and j.

TABLE 1. Values for the Enthalpy of Vaporization for Second and Third Row Elements (Ref. 1)

Elements	Group Number	${}^0H^V_{(i)}$ cal/g-atom
Zr/Hf	4.0	−148,000
	4.5	−157,000
Nb/Ta	5.0	−166,000
	5.5	−173,000
Mo/W	6.0	−180,000
	6.5	−180,000
Re	7.0	−168,000
	7.5	−159,000
Ru/Os	8.0	−150,000
	8.5	−141,500
Rh/Ir	9.0	−132,000
	9.5	−123,000
Pd/Pt	10.0	−114,000

The values ${}^0H^V_{(i)}$, ${}^0H^V_{(j)}$, and ${}^0H^V_{(i+j)/2}$ require further explanation. For each element of the second and third long periods (Groups IVA - VIIIA), Kaufman assigned a group number from 4 to 10. For each group number, a value for the enthalpy of vaporization was determined from the average of the two elements in the group. This is shown in Table 1. For Zr/Hf (Group 4), the average for enthalpy of vaporization is −148,000 cal/g-atom. These average values were determined for each group as shown in the table. For any binary diagram, the value of the enthalpy of vaporization is determined from the table, based on the group number of the binary diagram component. This would give ${}^0H^V_{(i)}$ and ${}^0H^V_{(j)}$. The value for ${}^0H^V_{(i+j)/2}$ is also determined from the table by averaging the group numbers of the components. Thus, for a diagram between elements with Group Numbers 4 and 8, the values used would be −148,000, −150,000, and −180,000 cal/g-atom for ${}^0H^V_{(i)}$, ${}^0H^V_{(j)}$, and ${}^0H^V_{(i+j)/2}$, respectively. Since the group number of the rare earths and the actinides is three, $e_o = 0$ for systems between these two groups of elements as well as for intra-rare earth and intra-actinide systems.

For the solid phases, calculation of the interaction parameters begins with that for the body-centered-cubic phase. The interaction parameter (B) for the body-centered-cubic phase (ß) is determined by:

$$B = L + e_1 + e_2 \qquad \text{(Eq. 13)}$$

where

$$e_1 = -0.5[{}^0H^V_{(i)}(\beta) + {}^0H^V_{(j)}(\beta)] \\ (V_i^\beta - V_j^\beta)^2(V_i^\beta + V_j^\beta)^{-2} \qquad \text{(Eq. 14)}$$

and

$$e_2 = 2[\Delta^0H^{L\rightarrow\beta}_{(i+j)/2} - 1/2\Delta^0H_{(i)}{}^{L\rightarrow\beta} \\ - 1/2\Delta^0H_{(j)}{}^{L\rightarrow\beta}] \qquad \text{(Eq. 15)}$$

where

${}^0H^V_{(i)}(\beta)$, ${}^0H^V_{(j)}$ = enthalpies of vaporization of pure body-centered-cubic i and j

$\Delta^0H^{L\rightarrow\beta}_{(i)}$, $\Delta^0H^{L\rightarrow\beta}_{(j)}$ = enthalpy change associated with the liquid → body-centered-cubic transformation in pure i and pure j, and

$\Delta^0H^{L\rightarrow\beta}_{(i+j)/2}$ = enthalpy change associated with the L→β transformation in the pure element (i+j)/2

For systems between the rare earths and actinides, $e_2 = 0$, as in the case of e_o.

According to Kaufman, the other interaction parameters are calculated by:

$$E = B + e_3 = e_p + e_1 + e_3 \qquad \text{(Eq. 16)}$$

and

$$A = E + e_4 = e_p + e_1 + e_3 + e_4 \qquad \text{(Eq. 17)}$$

where e_3 and e_4 are determined from relationships similar to Equations 4 and 8. Therefore, $e_3 = e_4 = 0$ for systems between elements of the same group. This means that A = E = B, or the interaction parameters for the solid phases are equal, which is not to be expected for any group of elements.

To obtain expected differences between interaction parameters for solid phases, a modification was made to the method of calculating these parameters. The strain energy term for different phases would be expected to be different because their atomic volumes are different. The strain energy term is given by e_1, Equation 18. According to Kaufman:

$$e_1 \propto VG(\Delta V/V)^2 \qquad \text{(Eq. 18)}$$

where

G = shear modulus

V = atomic volume of Elements i and j

ΔV = atomic volume difference between i and j

If the shear modulus, G, is proportional to H/V, then:

$$e_1 = -0.5[{}^0H^V_{(i)}(\beta) + {}^0H^V_{(j)}(\beta)] \\ (V_i - V_j)^2(V_i + V_j)^{-2}, \qquad \text{(Eq. 19)}$$

which is identical to Equation 18.

Since the strain energy term is different for each phase, this expression can be generalized by:

$$e_{1x} = -0.5[{}^0H_{(i)}(x) + {}^0H_{(j)}(x)] \\ (V^x_i - V^x_j)^2(V^x_i + V^x_j)^{-2} \qquad \text{(Eq. 20)}$$

where x = ß, ε, or α phase.

From this relationship, the interaction parameters can be determined by:

$$X = e_p + e_{1x} \qquad \text{(Eq. 21)}$$

This relationship indicates that the atomic volume of each phase is important for determinating interaction parameters. The procedures used in determining these values for the various phases are summarized in Appendix B, and the results are given in Tables B1 and B2 for the rare earths and actinides, respectively.

RESULTS

Calculated phase diagrams are presented in five different categories listed below:

1. Intra - rare earth systems
2. Intra - actinide systems
3. Rare earth - actinide systems
4. Rare earth - refractory transition metal systems
5. Actinide - refractory transition metal systems

Calculated phase diagrams in each category will be compared with experimentally determined diagrams. This is to aid in determining viability of the procedures used. Finally, the results of

TABLE 2. Interaction Parameters for Selected Intra-Rare Earth Phase Diagrams

System	L	B	E	A
Ce-Eu	16312	18010	17853	17944
Ce-La	5	41	6	7
Ce-Nd	615	696	816	785
Dy-Y	1124	1290	1319	1178
Er-Tb	799	804	853	799
Er-Yb	8010	11099	10421	10355
Eu-La	15952	17196	17421	17448
Eu-Yb	8	238	481	512
Gd-Pr	288	356	339	339
Gd-Sc	207	1063	1437	1437
Gd-Sm	4822	4824	4842	4825
Gd-Yb	14378	16239	15755	15706
Lu-Nd	1940	2308	2495	2497
Nd-Sc	1686	3082	3320	3321
Nd-Y	931	933	932	962
Sc-Y	145	1430	1803	1369

calculations of the Ir-Pu and Lu-Pu systems will be discussed.

Intra - Rare Earth Systems

Using the data for the enthalpy of vaporization and atomic volumes presented in Table B1, the interaction parameters for several intra-rare earth systems were calculated and the results are presented in Table 2. Phase diagrams calculated from these interaction parameters and the stability parameters given in Table A1 are shown in Figures 1-16.

In all the diagrams presented in this report, calculated diagrams are represented by thick lines while literature diagrams are represented by thin lines. Literature diagrams were taken from Hansen,[9] Elliott,[10] Shunk,[6] and Moffatt.[11] These systems were chosen to demonstrate different types of diagrams present in intra-rare earth systems and the ability of the proposed modification to the Kaufman method to differentiate between the various types.

Not all of the diagrams for which interaction parameters were calculated are shown in the figures. The calculated diagrams show excellent agreement with experimentally determined diagrams in most cases. Even the elements with one or more empirically determined values for the atomic volume show consistent agreement with experiment. This suggests that empirical determination of atomic volume has potential as a useful technique for establishing correct parameters and that the empirically determined values described in Appendix B are transferrable to other systems containing that element.

Some deviations from experimentally determined systems were encountered, but these deviations are only in temperature and compositional differences from experimental data. In all cases, the general features of the diagrams were correctly predicted. This suggests that the proposed variation to the Kaufman method and the data used in the calculations are essentially correct.

The least accurate calculations occur in the systems containing the monotectic reaction. The presence of the monotectic reaction in the liquid is correctly predicted in all cases. However, the temperature of the calculated maximum in the miscibility gap is not. Reasons for this inaccuracy are unknown.

Intra - Actinide Systems

Systems between four actinide elements (thorium, uranium, neptunium, and plutonium) were investigated. Interaction parameters calculated for the six diagrams between these elements are given in Table 3. The diagrams calculated from these parameters are shown in Figures 17-22.

The Np-U and Np-Pu diagrams given in Figures 17 and 18, respectively, show excellent agreement

TABLE 3. Summary of Interaction Parameters for Intra-Actinide Phase Diagrams

System	L	B	E	A
Np-Pu	1649	1938	2643	3319
Np-Th	1588	7399	7106	6893
Np-U	110	171	170	175
Pu-Th	97	6387	5475	4943
Pu-U	2849	2977	3095	3160
Th-U	2737	7478	7189	6985

for the liquid-solid and solid-solid transformations. The transformations in the Np-Pu system would be expected to show good agreement with the experimentally determined diagram, since this diagram was used to establish the effective atomic volumes empirically for the plutonium phases, as described in Appendix B. The solid-solid transformation in the Np-U system also shows good agreement with the literature. More complete agreement in the solid-solid transformation is not possible since the Kaufman method treats only line compounds and does not consider intermediate phases exhibiting extensive solid solubility.

The calculated Pu-Th diagram (Figure 19) shows the general form of the liquidus curve but does not show the extensive solid solubility of plutonium in the high-temperature body-centered-cubic phase of thorium. For the Pu-U diagram (Figure 20), the minimum in the liquidus is not predicted by the modified Kaufman method, although good agreement with the literature is shown for the solid-solid transformations.

Poor agreement is shown with the experimentally determined diagram of the Th-U system (Figure 21). The calculated diagram shows a simple eutectic with some terminal solid solubility at both ends of the diagram. This is identical to the results of Chan et al.[5] A monotectic is not predicted. Reasons for this are unclear at this time.

No diagram is available in the literature for the Np-Th system, but a calculated diagram is shown in Figure 22. The diagram is similar to the Pu-Th diagram although no data are available to predict a compound in the diagram. The calculated Np-Th diagram is also similar to the calculated Th-U diagram shown in Figure 21.

With the exception of plutonium diagrams, calculated liquidus and solidus curves shown in Figures 17-22 are similar to those determined by Chan et al.[5] This is to be expected, since the method used is the same. With the exception of differences already noted, the agreement between diagrams calculated with the modified Kaufman method and the experimental diagrams is good. The present work extends the earlier work to include solid-solid phase boundaries with reasonable success.

Rare Earth - Actinide Systems

Calculated diagrams for selected rare earth-actinide systems are given in Figures 23-31. Superimposed on each calculated diagram is the experimentally determined diagram. Values for the atomic volumes and the enthalpy of vaporization for each element were taken from Table B1, and values for the stability parameters were taken from Table A1. Interaction parameters for the diagrams calculated with these data are summarized in Table 4.

Diagrams for thorium and uranium systems are shown in Figures 23-27. These calculated diagrams show good agreement with the diagrams determined experimentally, especially the liquidus and solidus curves. In each case, the type of diagram is correctly predicted although some deviation in the solid state is found in the Gd-Th and Sc-Th diagrams.

Initial work on the calculation of selected rare earth-plutonium diagrams is shown in Figures 28-31. The four diagrams given in these figures show poor agreement with experimentally determined diagrams.

The calculated lanthanum-plutonium diagram (Figure 28) shows a simple eutectic with no

TABLE 4. Interaction Parameters for Rare Earth-Actinide Phase Diagrams Using Unaltered Values for the Enthalpy of Vaporization and Atomic Volumes

System	L	B	E	A
Ce-Th	1156	2079	2256	1896
Gd-Th	1536	1579	1566	1546
Nd-Th	4585	4588	4585	4591
Sc-Th	529	1803	2244	1980
Ce-U	8440	14670	14902	14807
La-Pu	960	5898	4902	4690
Y-Pu	522	3481	2347	2228
Ce-Pu	823	4987	4654	4351
Nd-P	2588	5711	4903	4772

TABLE 5. Values for the Enthalpy of Vaporization and Atomic Volumes Used for Rare Earth-Plutonium Phase Diagrams

System	Element	${}^{0}H^{V}$ (cal/mole)	V_L (cm^3/mole)	V_β (cm^3/mole)	V_ε (cm^3/mole)	V_α (cm^3/mole)
Sc-Pu	Sc	−90320	17.33	16.81	15.90	15.92
	Pu	−84100	14.72	14.95	15.24	15.30
Y-Pu	Y	−101500	21.53	21.01	20.49	19.79
	Pu	−101000	14.00	14.95	15.24	15.30
La-Pu	La	−103000	23.35	23.27	22.60	22.44
	Pu	−112000	14.00	17.41	17.07	17.00
Ce-Pu	Ce	−101000	20.98	20.91	20.95	20.70
	Pu	−106000	14.00	18.00	17.65	17.90
Pr-Pu	Pr	−85000	21.32	21.22	20.48	20.70
	Pu	−92000	14.00	17.41	17.07	17.00
Nd-Pu	Nd	−78300	21.62	21.21	20.58	20.48
	Pu	−85000	14.00	17.41	17.07	17.00
Sm-Pu	Sm	−49400	21.17	20.32	20.46	20.00
	Pu	−65000	14.00	17.41	17.07	17.00

evidence of a miscibility gap in the liquid phase. The calculated yttrium-plutonium diagram (Figure 29) suggests complete solid solubility in the hexagonal close-packed phase. Although the liquidus curve approximates that of the experimentally determined diagram, the limited solid solubility of plutonium in hexagonal close-packed yttrium is not predicted. Instead, the calculated diagram shows complete solid solubility.

For the cerium-plutonium diagram (Figure 30) and the neodymium-plutonium (Figure 31), the calculated eutectics are at 345 and 500 °C, respectively, rather than 626 and 628 °C, respectively, for the experimentally determined diagrams. In addition, the calculated diagrams indicate limited terminal solid solubility in both systems.

This lack of agreement for plutonium systems suggests that incorrect data are being used to calculate the interaction parameters. Alteration of the thermodynamic values (stability parameters) for the various transformations produced very little change in the calculated diagrams. The only other data used for calculations are the enthalpy of vaporization and the atomic volumes of the various phases.

Determination of the atomic volume for the different phases of plutonium was done by trial and error, using the neodymium-plutonium diagram as a reference. The atomic volumes of plutonium that gave the most reasonable agreement with the experimentally determined diagram are 14.00, 17.41, 17.07, and 17.00 cm/mole for V_L, V_β, V_ε, and V_α, respectively.

In addition to changing the effective atomic volumes, it was also necessary to change the enthalpy of vaporization of plutonium for each rare earth-plutonium system. Data for the enthalpy of vaporization and atomic volumes used in calculating satisfactory diagrams between the rare earths and plutonium are given in Table 5. Included in this table are data for scandium and yttrium (technically, not rare earths but Group III elements) along with the rare earths and actinides. Only systems with experimentally determined diagrams are included in this table. The values for the enthalpy of vaporization of plutonium included in Table 5 were determined by trial and error to yield the most satisfactory diagram compared to the experimental diagram. No experimental diagrams of plutonium with the rare earths from gadolinium to lutetium are available.

TABLE 6. Interaction Parameters for Rare Earth-Plutonium Systems Using Effective Enthalpy of Vaporization and Atomic Volumes

System	L	B	E	A
Ce-Pu	3262	3845	4023	3810
La-Pu	5941	8103	7966	7923
Nd-Pu	3450	4459	4356	4348
Pr-Pu	3404	4417	4415	4407
Sc-Pu	265	297	397	377
Sm-Pu	4150	4770	5000	4835
Y-Pu	2824	5197	5113	4706

Interaction parameters calculated for selected systems are given in Table 6, and the resulting diagrams are shown in Figures 32-38. In all cases, the form of the diagram is calculated correctly, with some deviation in actual temperatures and compositions of invariant points. For the Nd-Pu system, the calculated diagram would be expected to approximate the experimental one since this system was used to determine the effective atomic volumes for the plutonium phases. The fact that other rare earth-plutonium diagrams agree as well as they do suggests that the revised atomic volumes are useful in calculating rare earth-plutonium diagrams.

The values for the effective enthalpy of vaporization (ΔH^{vap}) of plutonium are plotted as a function of atomic number in Figure 39. Also included in this figure are data for the enthalpy of vaporization, H_v, of each element used in the calculations. The values for the rare earths show a linear decrease with atomic number, from Element 57 (lanthanum) to Element 63 (europium), with the effective values for plutonium paralleling the actual values for the rare earths.

No experimentally determined diagrams are available for systems between plutonium and Elements 64 (gadolinium) and 71 (lutetium). Only estimated diagrams are available, based on the interpretation of very limited data. However, taking advantage of the apparent repetitive nature of the enthalpy of vaporization of the rare earths,[12,13] the effective enthalpies for plutonium with systems involving the Elements Gd through Lu were estimated by a line parallel to the line for plutonium with Elements La through Eu. When these values are used, the calculated diagrams shown in Figures 40-42 are produced. Interaction parameters calculated for these systems are given in Table 7. The Gd-Pu and Dy-Pu diagrams show good agreement with the estimated diagrams while the Er-Pu diagram shows complete miscibility with plutonium in the hexagonal close-packed phase, rather than terminal solid solubility as shown in the estimated diagram. Calculation of the Lu-Pu diagram is discussed in a later section of this report.

TABLE 7. Interaction Parameters for (Gd, Dy, Er)-Plutonium Systems

System	L	B	E	A
Gd-Pu	4804	5363	5415	5408
Dy-Pu	4977	5281	5193	5271
Er-Pu	1768	1887	1925	1922

Rare Earth - Refractory Transition Metal Systems

The results obtained on rare earth refractory transition metal diagrams were different for each group of elements, but similar for elements within each group. For Groups IVA, VA, and VIA, no compounds are formed and only adjustments to the parameter ${}^0H^V_i$ were necessary. For Groups VIIA and VIIIA, adjustments to ${}^0H^V_i$ and the constant (C) were necessary. In addition, it was necessary to determine values empirically for the constants used for calculation of liquidus lines involving intermetallic compounds. The results for each group number are discussed separately.

Initial attempts at the calculation of rare earth-refractory transition metal systems yielded mixed results. In these attempts the unmodified procedure described by Kaufman[1] was used. The value used for ${}^0H^V$[RE] was -100,000 cal/mole while values for V_i, H_v, $H_2(i)$, $H_3(i)$, and $H_4(i)$ were obtained from Appendices A and B. Typical results are shown in Figures 43 and 44. From these figures, it can be seen that modifications to the procedure are required. It also became apparent that each group of the transition elements

would have to be treated separately. Procedures for each group are therefore discussed separately. It is not intended that empirical parameters be established for each rare earth-transition metal system; the intent is to determine a general procedure for establishing the necessary parameters. This procedure is intended to keep "curve fitting" to a minimum. However, it should be recognized that any "curve fitting" should produce parameters that will enhance the future capability to calculate ternary phase diagrams as well as binary diagrams.

Zirconium and Hafnium

Alteration of the value of ${}^0H_i^V$, where the element i is a rare earth element, was found to be necessary for calculating diagrams of rare earth elements with zirconium and hafnium. Empirically determined values for ${}^0H_i^V$ are given in Figure 45. Calculated interaction parameters for these diagrams are given in Table 8. Calculated diagrams for the Hf-Pr and the Dy-Zr systems using ${}^0H_i^V$= -100,000 cal/mole are given in Figures 46 and 47, respectively. The diagram for the Hf-Pr system is shown to be satisfactory while that for the Dy-Zr system is not. The calculated diagram for the Dy-Zr system, using the value for ${}^0H^V$(Dy) from Figure 45, is given in Figure 48. The diagram calculated in this manner is quite satisfactory. Reasons for this required variation in ${}^0H_i^V$ are not known at this time.

TABLE 8. Interaction Parameters for the Rare Earth Diagrams with Zirconium and Hafnium

System	L	B	E	A
Y-ZR	5564	8859	9870	9132
EU-ZR	31425	33676	34827	34726
GD-ZR	4798	7322	8464	8361
DY-ZR	6265	8135	8715	8906
ER-ZR	5328	6642	7548	7470
YB-ZR	17711	19321	19648	19511
SC-HF	-37	238	769	834
Y-HF	5797	8851	10978	10287
CE-HF	10130	14578	17841	17642
PR-HF	12548	15832	18165	18174
ER-HF	6667	7836	9542	9547

TABLE 9. Interaction Parameters for Rare Earth Diagrams with Niobium and Tantalum

System	L	B	E	A
Sc-Nb	6834	12052	8650	8650
Eu-Nb	29313	39689	36347	36314
La-Nb	16710	32182	28655	29518
Sm-Nb	26331	37013	33397	33778
Ce-Ta	20860	35516	32001	32821
Eu-Ta	36437	46584	43242	43209
Tb-Ta	14356	24399	21239	20649
Dy-Ta	21528	30453	27088	26642
Er-Ta	13332	22035	19432	17870

Niobium and Tantalum

For systems between the rare earths and niobium or tantalum, the value of ${}^0H_i^V$ for the rare earths must be modified to the values given in Figure 49. The linear curve presented is identical for the rare earths La through Eu (plus Sc and Y), and for the rare earths Gd through Lu. Values for the interaction parameters are given in Table 9. Calculated diagrams for the La-Nb, Ce-Ta, and Er-Ta systems are given in Figures 50-52, respectively. For these systems, the unmodified Kaufman method was used. Atomic volumes for the room temperature phase of the rare earth metal were used. Unfortunately, experimental work on these systems is incomplete. In fact, experimental data are available for very few rare earth systems with niobium or tantalum. The calculated diagrams agree with those diagrams estimated by other means.

Table 10 compares the various calculated diagrams with diagrams available in the literature. In all cases, agreement is found in the type of diagram. For the Dy-Ta, Tb-Ta, Ce-Ta, and Er-Ta systems, the diagrams are presumed to be monotectics, based on the similarity to the La-Ta and Y-Ta diagrams. However, it is possible that the diagrams are simple eutectics.

The calculated Sc-Nb diagram shown in Figure 53 is a simple eutectic. This diagram was calculated using a value of -110,000 cal/mole for ${}^0H_i^V$. Using the value of -116,000 cal/mole for ${}^0H_i^V$ produces a diagram showing extensive terminal solid solubility

TABLE 10. Comparison of Calculated Diagrams Between Selected Rare Earths and Niobium or Tantalum and Literature Diagrams

System	Type Diagram (Calculated)	Type Diagram (Literature)	Method	Agree/Disagree
Sc-Nb	Eutectic	Eutectic	Experimental	Agree
La-Nb	Monotectic	Monotectic	Experimental	Agree
Ce-Ta	Monotectic	Mono./Eutectic	Estimated	Agree-Mono.
Sm-Nb	Monotectic	Monotectic	Experimental	Agree
Eu-Nb	Monotectic	Monotectic	Calculated	Agree
Eu-Ta	Monotectic	Monotectic	Calculated	Agree
Tb-Ta	Monotectic	Mono./Eutectic	Estimated	Agree-Mono.
Dy-Ta	Monotectic	Mono./Eutectic	Estimated	Agree-Mono.
Er-Ta	Monotectic	Mono./Eutectic	Estimated	Agree-Mono.

as shown in Figure 54. Thus, it appears that ${}^{0}H_{i}^{V}$ has considerable effect on the shape of this diagram. The diagram given in Figure 53 is estimated between 1500 and 1725 °C because the computer program would not produce liquidus and solidus values in this temperature range.

Molybdenum and Tungsten

Establishing parameters for calculating binary phase diagrams of molybdenum or tungsten with the rare earths is difficult because very few diagrams between these classes of elements have been established experimentally. The presence of intermetallic phases in these systems is highly improbable because of the high positive heats of formation for any intermediate phases. There is a general trend toward liquid immiscibility in the form of immiscible or monotectic diagrams. Therefore, determination of the parameters for these systems was accomplished by recalculating diagrams suggested by Brewer and Lamoreaux.[14] This is not desirable, because there are no experimental data to justify the calculations.

Values for the parameter ${}^{0}H_{i}^{V}$ determined under these conditions are summarized in Figure 55. The two curves shown in the figure are analogous to those obtained for the niobium and tantalum systems, but displaced slightly. The interaction parameters obtained for the systems calculated are given in Table 11, and typical results are summarized in Figures 56 and 57. In view of the non-ideal circumstances described above, extensive comment is unwarranted.

TABLE 11. Interaction Parameters for Rare Earth Diagrams with Molybdenum and Tungsten

System	L	B	E	A
Sc-Mo	4024	13062	12090	12090
La-Mo	14578	36802	35705	36568
Nd-Mo	13045	30539	29333	29714
Eu-Mo	27690	43615	42703	42670
Gd-Mo	15796	33234	32239	32090
Tb-Mo	12878	28992	28262	27672
Ho-Mo	17264	32237	31428	30500
Er-Mo	12452	26716	26543	24981
Lu-Mo	9270	22896	21956	20699
Sc-W	19284	27659	26687	26687
Eu-W	52748	67790	66878	66845
Yb-W	49087	59822	60637	59260

Rhenium

The Group VIIA elements of the second and third long periods are technetium and rhenium. Since technetium is not found in nature, no binary phase diagrams for this element with the rare earths are available, and no effort was expended on the calculation of technetium-rare earth diagrams. All work was concentrated on the calculation of rhenium systems.

TABLE 12. Interaction Parameters for Rare Earth Diagrams with Rhenium

System	L	B	E	A
Sc-Re	-12099	-3250	1108	1208
Y-Re	-11119	6959	11552	11702
La-Re	-8487	12459	16692	17655
Pr-Re	-10672	6285	10442	11319
Gd-Re	-15430	644	4979	4930
Tb-Re	-18790	-3976	624	134
Er-Re	-19519	-6551	-1394	-2856

Calculation of these systems required changes in ${}^{0}H_i^{V}$ as shown in Figure 58. The same values for ${}^{0}H_i^{V}$ were used for the rare earths from La through Eu and for Gd through Yb. The value for lutetium is assumed to be the same as for lanthanum and gadolinium, namely -97,000 cal/mole. Interaction parameters calculated using these values for ${}^{0}H_i^{V}$ are summarized in Table 12. For all systems showing an intermetallic compound, the compound is always $LnRe_2$, where Ln is a lanthanide (rare earth) element with the hexagonal structure. In calculating the two-phase field with this compound, a constant with a value of -6,000 cal/mole was used and gave reasonably consistent results.

Selected diagrams calculated using these parameters are shown in Figures 59-61. In most cases, the compound calculates to be a congruent melting compound rather than a peritectic as observed experimentally. In the case of the Pr-Re diagram (Figure 61), the liquidus is very broad and flat and not in agreement with the estimated diagram given in the literature. For the Sc-Re system, a second compound, Sc_5Re_{24}, is also reported. In the calculation of this diagram, a value of +12,000 cal/mole was used for the constant to produce the diagram given in Figure 60.

Ruthenium, Osmium, Rhodium, and Iridium

These elements can be discussed together, since the same procedures were used for all of them in calculating phase diagrams with the rare earths. Useful values for ${}^{0}H_i^{V}$ are identical to those used for rhenium (Figure 58). These values lead to the interaction parameters summarized in Table 13, which in turn result in representative phase diagrams shown in Figures 62-65.

TABLE 13. Interaction Parameters for Rare Earth Diagrams with Ruthenium, Osmium, Rhodium, and Iridium

System	L	B	E	A
Sc-Ru	-52039	-42846	-37269	-37189
Ce-Ru	-52250	-32954	-27489	-26589
Pr-Ru	-53832	-36809	-31432	-30575
Dy-Ru	-53604	-40048	-34432	-34799
Er-Ru	-61857	-48783	-42406	-43888
Y-Os	-51594	-34585	-28772	-28692
La-Rh	-96720	-80253	-73920	-72857
Nd-Rh	-98575	-86275	-80051	-79100
Er-Rh	-105728	-96418	-89161	-90523
La-Ir	-84226	-68996	-62663	-61600
Ce-Ir	-85369	-70519	-64174	-63154

Empirically determined values for the constant used to calculate the liquidus boundaries for the intermediate phases are summarized in Figure 66. These values were determined to be those that produce melting points for compounds indicated in the experimentally determined diagram. For the hexagonal close-packed phase, the constant appears to be a linear function of compound composition. For face-centered cubic and body-centered cubic structures, the relationship is less clear. The body-centered cubic structure seems to occur only at the equiatomic position for these elements. For the face-centered cubic structure, most of the compounds occur at the AB_2 phase where B is the refractory transition metal. Most of the compounds required a constant of -11,000 cal/mole although $LaIr_2$ and $CeIr_2$ required constants of -2,000 and -5,000 cal/mole, respectively. The only other face-centered cubic compound identified for these elements was $Sc_{11}Ru_4$, which required a constant of -2,000 cal/mole. Considering the scarcity of compounds with the face-centered cubic and body-centered cubic structures, prediction of trends is not possible at this time.

Since the constant is empirically determined from the melting points of the compounds, the diagrams

would be expected to agree reasonably well with the experimentally determined diagrams. However, two general observations can be made concerning agreement between the calculated and experimental diagrams. First, the solid solubilities at both ends of the diagrams are calculated to be much greater than observed experimentally. Second, most compounds determined experimentally to be peritectic compounds are calculated to be congruent melting compounds. This seems to be the result of the trend for the liquidus to decrease more rapidly with composition than is observed experimentally.

Palladium and Platinum

Diagrams of palladium and platinum with the rare earths have presented the most difficulty in establishing a consistent set of parameters. Values for ${}^{0}H_{i}^{V}$ used for calculating these diagrams are the same as for rhenium (Figure 58). Interaction parameters derived from these values are summarized in Table 14. Typical diagrams calculated for these systems are shown in Figures 67-69. The calculated diagrams are reasonable representations of the experimentally determined diagrams. However, as was noticed in the previous section, two sources of difference are noted: terminal solid solubilities are considerably higher than experimental values; and the width of the two-phase liquid-solid fields associated with the compounds is too narrow so that most of the calculated compounds appear as congruent compounds rather than incongruent or peritectic compounds.

TABLE 14. Interaction Parameters for Systems Between Rare Earths and Palladium, and Platinum

System	L	B	E	A
Sc-Pd	−124988	−122322	−118664	−118614
Y-Pd	−133558	−123720	−119827	−119777
Ce-Pd	−137770	−126341	−122796	−121926
Sm-Pd	−133906	−126723	−123279	−122848
Eu-Pd	−132665	−125820	−122102	−122084
Gd-Pd	−138025	−129929	−126294	−126393
Ho-Pd	−140128	−133937	−130116	−130994
Nd-Pt	−120820	−113628	−110204	−109398
Er-Pt	−127481	−122675	−118218	−119730
Yb-Pt	−111037	−108400	−102975	−104302

A more serious problem is encountered with the value of the constant used in the calculation involving compounds. Values were determined empirically for each system in an attempt to establish a consistent method for determining values for other systems. The values determined by this method are summarized in Table 15. In general, the values for a given system are approximately linear with compound composition for a given structure as shown in Figures 70 and 71. For the epsilon (hexagonal close-packed) structure (Figure 70), two groups of curves are indicated, although reasons for the grouping are unclear. This, in effect, makes the estimation of correct parameters for other systems very tenuous. For the alpha (face-centered cubic) structure (Figure 71), the curves are even more dispersed, with no apparent consistency.

Actinide - Refractory Transition Metal Systems

The results of calculation of actinide-refractory transition metal diagrams are analogous to the rare earth-refractory transition metal diagrams. Values of ${}^{0}H$(actinides) were determined empirically, as were values for the constant (C) used in the calculation of the liquidus values involving intermetallic compounds. Each group will be discussed separately.

Calculation of binary phase diagrams between the actinides and the refractory transition metal elements yielded mixed results, similar to those encountered in calculating rare earth-refractory transition metal diagrams. In general, diagrams calculated from the parameters given in Tables A1 and B1 did not accurately represent experimentally determined diagrams. As a result, empirical methods were used to determine the value of ${}^{0}H^{V}$ (actinide) in the most accurately calculated system. Although this method is basically curve fitting, it is justified on the basis of potential utility in calculating ternary systems. In addition, it is hoped that these values might lead eventually to identification of an additional term or terms to be added to the Kaufman method.

TABLE 15. Values for Constant Used for Intermetallic Compound Calculations for Rare Earth Diagrams with Palladium and Platinum

System	Percent Transition Element	Experimental Melt. Temp. (°C)	Calculated Melt. Temp. (°C)	Constant (cal/mole)	Phase
Gd-Pd	0.286	~850	888	-9000	Epsilon
	0.4	~925	1032	-6500	Epsilon
	0.5	1380	1386	6000	Beta
	0.555	1355	1334	-2000	Epsilon
	O.667	~1400	1355	-2000	Alpha
	O.75	1630	1662	3000	Alpha
Pd-Sc	0.2	~1060	1069	-3500	Epsilon
	0.4	~1250	1256	1000	Epsilon
	0.5	1600	1479	12000	Beta
	0.667	~1450	1384	3000	Alpha
	0.75	1480	1499	5000	Alpha
Nd-Pt	0.3	~1000	1085	-3000	Epsilon
	0.4	~1400	1479	2000	Epsilon
	0.5	1535	1590	4000	Epsilon
	0.571	~1450	1845	4000	Alpha
	0.667	2020	2020	6500	Alpha
	0.75	>1730	2065	8000	Alpha
	0.833	~1800	1741	12000	Epsilon
Pt-Yb	0.25	~850	877	-10000	Epsilon
	0.333	~1150	1295	-1000	Epsilon
	0.375	~1400	1368	0	Epsilon
	0.444	~(1500)	1566	2500	Epsilon
	0.5	~(1550)	1594	3000	Epsilon
	0.571	(1620)	1731	5000	Epsilon
	0.667	~1550	1445	4000	Alpha
	0.75	1600	1674	6500	Alpha
Ce-Pd	0.5	(1127)	1128	-6000	Epsilon
	0.75	1437	1427	-5000	Alpha

TABLE 15. (Continued)

System	Percent Transition Element	Experimental Melt Temp. (°C)	Calculated Melt. Temp. (°C)	Constant (cal/mole)	Phase
Ho-Pd	0.286	~1100	901	-9000	Epsilon
	0.4	~1100	972	-7000	Epsilon
	0.5	1480	1498	9000	Beta
	0.556	1430	1476	1000	Epsilon
	0.667	~1350	1304	-1000	Epsilon
	0.75	1730	1702	7000	Epsilon
Er-Pt	0.25	~1250	1326	-2000	Epsilon
	0.333	~1500	1440	0	Epsilon
	0.375	~1550	1565	2000	Epsilon
	0.5	1660	1654	12000	Beta
	0.571	~1650	1590	4500	Alpha
	0.667	~1775	1749	5500	Alpha
	0.75	1840	1888	9000	Alpha
	0.833	~1750	- - -	12000	Epsilon
Eu-Pd	0.286	~700	661	-11000	Epsilon
	0.4	810	822	-8000	Epsilon
	0.5	~860	956	-6000	Epsilon
	0.667	~1350	1284	-2000	Alpha
	0.75	1425	1420	0	Alpha
	0.833	~1250	1335	2000	Epsilon
Sm-Pd	0.3	~750	761	-8000	Epsilon
	0.5	1270	1114	-3000	Epsilon
	0.571	(1260)	- - -	-2500	Alpha
	0.667	~1300	1335	1000	Epsilon
	0.75	(1620)	1631	3000	Alpha
	0.833	~1200	1375	5000	Epsilon
Y-Pd	0.714	915	995	-11000	Epsilon

Empirically determined values for ${}^{0}H^{V}$(actinide) producing the most accurate calculated diagrams are summarized in Table 16. In these calculations, the unmodified Kaufman relationships were used, along with the values for the atomic volumes given in Table 17. These values were taken from Kaufman for the refractory transition metals and from Appendix A for the room temperature phase of the actinides. As with the previous section, the results for elements from each group will be discussed separately.

TABLE 16. Heat of Vaporization ${}^{0}H^{V}$(Actinides) Used in Calculating Actinide-Transition Metal Diagrams

Transition Metal	Actinide Metal		
	Th	U	Pu
Zr	−99000	−104500	−95000
Hf	−100000	−105500	−95000
Nb	−118000	−129000	−112000
Ta	−100000	−129000	−112000
Mo	−122000	−130000	−112000
W	−120000	−130000	−112000
Re	−110000	−125000	−112000
Ru	−120000	−130000	−112000
Os	−120000	−125000	−112000
Rh	−120000	−125000	−112000
Ir	−120000	−125000	−112000
Pd	−120000	−125000	−112000
Pt	−120000	−125000	−112000

All values in cal/mole

TABLE 17. Values for Atomic Volumes Used for Actinides With Zirconium and Hafnium

System	Element	V_L	V_β	V_ε	V_α
		(cm^3/g-atom)			
Th-Zr	Th	22.10	20.99	20.58	20.18
	Zr	15.73	15.09	14.02	14.02
U-Zr	U	13.91	13.61	13.51	13.40
	Zr	15.73	15.09	14.02	14.02
Pu-Zr	Pu	14.72	14.95	15.24	15.30
	Zr	15.73	15.09	14.02	14.02
Th-Hf	Th	22.10	20.99	20.58	20.18
	Hf	16.08	15.28	13.50	13.43
U-Hf	U	13.91	13.61	13.51	13.40
	Hf	16.08	15.28	13.50	13.43
Pu-Hf	Pu	14.72	14.95	15.24	15.30
	Hf	16.08	15.28	13.50	13.43

Zirconium and Hafnium

Interaction parameters calculated using values of ${}^{0}H^{V}$(actinides) in Table 16 are given in Table 18. Diagrams calculated from these parameters are shown in Figures 72-75. With the exception of the Pu-Hf diagram, the calculated diagrams are reasonable representations of the experimental diagrams. For the Pu-Hf system, the calculated diagram indicates complete solid solubility in the body-centered cubic phase and hexagonal close-packed phases, whereas the estimated diagram from the literature suggests a peritectic-type diagram with limited terminal solid solubility. Calculated diagrams for the remaining two systems (U-Zr and Th-Hf) show good agreement with experimental diagrams.

Niobium and Tantalum

Interaction parameters calculated from values of ${}^{0}H^{V}$(actinides) given in Table 16 are summarized in Table 19, and diagrams calculated from these

TABLE 18. Interaction Parameters for Actinides with Zirconium and Hafnium

System	L	B	E	A
Th-Zr	2461	5763	6900	6468
U-Zr	4521	4857	4565	4586
Pu-Zr	−1065	−1062	−854	−833
Th-Hf	4591	7676	9964	9612
U-Hf	5529	5952	5529	5529
Pu-Hf	−4818	−4804	−4373	−4303

TABLE 19. Interaction Parameters for Actinides with Niobium and Tantalum

System	L	B	E	A
Th-Nb	5841	19368	14255	16612
U-Nb	5435	5916	3360	3643
Pu-Nb	7327	11100	7179	8151
Th-Ta	−8173	4304	−809	1548
U-Ta	7599	7982	5426	5709
Pu-Ta	7020	10613	6692	7664

parameters are shown in Figures 76-81. With the exception of the Ta-Th diagram, good agreement with experimental diagrams is shown, although the calculated terminal solid solubilities are too high. For the Ta-Th diagram, a congruent compound is indicated rather than an incongruent compound. In addition, the eutectic between thorium and the Ta-Th compound is calculated to be about 12 at. %, rather than about 1 at. % for the literature diagram. For the Nb-Pu diagram, a peritectic is calculated for the epsilon plutonium solid solution phase rather than a eutectic as indicated in the literature diagram. For the Nb-Th diagram, no liquidus data could be calculated below 1650 °C, so the eutectic in this diagram is estimated.

Molybdenum and Tungsten

Interaction parameters calculated from values of ${}^{0}H^{V}$(actinides) given in Table 16 are summarized in Table 20, and diagrams calculated from these parameters are shown in Figures 82-87. With the exception of the Mo-Th diagram (Figure 82), good agreement was obtained between the calculated and the experimental diagrams. In this diagram, the calculated liquidus values are at much higher thorium concentrations than are observed experimentally. In addition, no results could be calculated below 1800 °C.

For the Th-W and the Pu-W systems, monotectic diagrams were calculated rather than low solubility eutectics, as suggested by the experimental diagrams. However, the experimental diagrams are estimated diagrams above 2400 and 1000 °C for the Th-W and the Pu-W systems, respectively. Thus, the elevated temperature portions of both

TABLE 20. Interaction Parameters for Actinides with Molybdenum and Tungsten

System	L	B	E	A
Th-Mo	7346	27154	24471	26828
U-Mo	3506	6431	6305	6588
Pu-Mo	1073	6415	4924	5896
Th-W	21058	39841	37158	39515
U-W	12645	15071	14945	15228
Pu-W	16517	21232	19741	20713

TABLE 21. Interaction Parameters for Actinides with Rhenium

System	L	B	E	A
Th-Re	-20137	-1163	1484	3941
U-Re	-23416	-21287	-16083	-15700
Pu-Re	-14921	-9839	-6000	-4928

of these diagrams are inconclusive and could conceivably exhibit the monotectic reaction.

Rhenium

Interaction parameters calculated using values of ${}^{0}H^{V}$(actinides) given in Table 16 are summarized in Table 21. Diagrams calculated from these parameters are shown in Figures 88-90. Reasonably good agreement was obtained between the calculated and experimental diagrams. The compound melting point was calculated by varying the constant until the calculated compound melting temperature matched the experimentally determined value. The empirically determined constants for $ThRe_2$, URe_2, and $PuRe_2$ are -6000, +7000, and 0, respectively. No reason can be given for the differences among the three values.

The calculated uranium-rhenium diagram shows a peritectic reaction in the gamma phase terminal solid solution instead of the eutectic reaction determined experimentally. The calculated diagram also shows terminal solid solubility in rhenium that is not indicated experimentally. Terminal solid solubility in rhenium is also indicated in the calculated plutonium-rhenium diagram that is not shown in the experimental diagram.

Ruthenium, Osmium, Rhodium, and Iridium

Interaction parameters calculated from values of ${}^{0}H^{V}$(actinides) given in Table 16 are summarized in Table 22, and diagrams calculated from these parameters are shown in Figures 91-96. Reasonably good agreement was obtained between the calculated and experimental diagrams. In view of the empirical method used to determine the

TABLE 22. Interaction Parameters for Actinides with Ruthenium, Osmium, Rhodium, and Iridium

System	L	B	E	A
Th-Ru	-50231	-30065	-26198	-23761
U-Ru	-55119	-52731	-49915	-49552
Pu-Ru	-54972	-49618	-44559	-43507
Th-Os	-49006	-30183	-26316	-23879
U-Os	-59147	-57539	-51115	-50752
Pu-Os	-53701	-49386	-44327	-43275
Th-Rh	-91479	-75454	-70707	-68150
U-Rh	-96982	-97348	-90044	-89561
Pu-Rh	-96049	-93944	-88005	-86833
Th-Ir	-82698	-67947	-63200	-60643
U-Ir	-77698	-64356	-57052	-56569
Pu-Ir	-87300	-86169	-80230	-70058

compound melting temperature, this is to be expected.

Values for the compound constant determined empirically are given in Table 23. Values for the hexagonal close-packed (epsilon) phase are plotted in Figure 97, and those for the face-centered cubic (alpha) and body-centered cubic (beta) phases are plotted in Figure 98. For the hexagonal close-packed structure (Figure 97) the values vary approximately linearly with composition, regardless of the element considered. However, this is not the case with the cubic structures (Figure 98). The values increase with increasing transition element for a given system. However, the relative location is different for each

TABLE 23. Values for the Compound Constant for Actinides with Ruthenium, Osmium, Rhodium, and Iridium

System	Percent Transition Element	Structure	Constant	System	Percent Transition Element	Structure	Constant
Th-Rh	0.3	HCP	-6000	U-Ir	0.25	FCC	-14000
	0.5	FCC	-14000		0.4	FCC	-13000
	0.667	HCP	6000		0.5	BCC	3000
	0.75	FCC	-7000		0.667	FCC	-7000
	0.833	HCP	-10000		0.75	FCC	-6000
U-Rh	0.429	HCP	1000	Pu-Ir	0.667	FCC	3000
	0.571	HCP	4500	Th-Ru	0.3	HCP	-14000
	0.625	HCP	6000		0.4	HCP	-15000
	0.75	FCC	5000		0.5	HCP	-16000
Pu-Rh	0.333	HCP	-2000		0.667	FCC	-15000
	0.375	HCP	-500	U-Ru	0.75	FCC	15000
	0.392	HCP	0	Pu-Ru	0.25	HCP	-8000
	0.444	HCP	1000		0.375	HCP	-5000
	0.5	HCP	2000		0.5	BCC	6000
	0.571	FCC	-3000		0.667	FCC	4000
	0.667	FCC	-2000	Th-Os	0.3	HCP	-10000
	0.75	FCC	-1000		0.4	HCP	-7000
Th-Ir	0.3	HCP	-6000		0.667	FCC	-3000
	0.5	BCC	6000	U-Os	0.667	FCC	13000
	0.667	FCC	-6000	Pu-Os	0.25	HCP	-8000
	0.75	FCC	-7000		0.375	HCP	-2000
	0.833	HCP	0		0.667	HCP	7000

system, with no apparent order or predictable trend. Thus, the melting points in these systems with the hexagonal close-packed structure can be calculated fairly accurately, but not compounds with cubic structures.

Palladium and Platinum

Interaction parameters calculated from values of ${}^{0}H^{V}$(actinides) given in Table 16 are summarized in Table 24, and diagrams calculated from these parameters are shown in Figures 99-101. Considerable deviation from experimental diagrams on the high actinide end is evident. Agreement on the high transition metal end is fair.

Empirically determined values for the compound constant are given in Table 25 and plotted in Figure 102. No consistent correlation can be seen between the compound constant and composition for either the hexagonal close-packed or the face-centered cubic phases. In view of this, calculation of diagrams between the actinides and either palladium or platinum should be approached with caution. Work needs to be done to explain these inconsistencies.

TABLE 24. Interaction Parameters for Actinides with Palladium and Platinum

System	L	B	E	A
Th-Pd	−120822	−111290	−109343	−106936
U-Pd	−120822	−123622	−119118	−118785
Pu-Pd	−128399	−129323	−126184	−125162
Th-Pt	−112464	−101857	−99910	−97503
U-Pt	−116551	−119969	−115465	−115132
Pu-Pt	−116897	−118569	−115430	−115908

TABLE 25. Values for the Compound Constant for Actinides with Palladium and Platinum

System	Percent Transition Element	Structure	Constant
Th-Pd	0.333	HCP	−5000
	0.5	HCP	−2000
	0.625	HCP	0
	0.75	HCP	2000
U-Pd	0.80	FCC	11000
Pu-Pd	0.444	HCP	6000
	0.5	HCP	7000
	0.571	HCP	8000
	0.75	HCP	9000
Th-Pt	0.3	HCP	−1000
U-Pt	0.667	HCP	16000
	0.75	HCP	17000
	0.833	FCC	11000
Pu-Pt	0.375	HCP	8000
	0.5	HCP	9000
	0.667	FCC	9000
	0.75	FCC	10000

Iridium-Plutonium Diagram

The calculated Ir-Pu diagram is shown in Figure 103. Interaction parameters determined for this system are -87300, -86169, -80230, and -70058 for L, B, E, and A, respectively. The only compound for which crystal structure data are available is $PuIr_2$, which is face-centered cubic. Other compounds reported are Pu_3Ir, Pu_5Ir_3, and Pu_5Ir_4, but no crystal structure data have been reported. No melting point data are available for any of the compounds. Constants for calculating the liquidus values for the intermetallic compounds were estimated from Figures 97 and 98. For these calculations, Pu_5Ir_3 and Pu_5Ir_4 were assumed to be hexagonal while Pu_3Ir was assumed to be face-centered cubic. These assumptions had very little effect on the melting point calculation. A large region of solid solubility of iridium in body-centered cubic plutonium is indicated.

Lutetium-Plutonium Diagram

The calculated Lu-Pu diagram indicates a peritectic-type diagram with stabilization of the face-centered cubic phase of plutonium to room temperature at compositions above about

1 at. % lutetium. This is shown in Figure 104. The liquidus shows a nearly continuous increase from the melting point of plutonium to that of lutetium.

DISCUSSION

The first part of this section discusses the rare earth and actinide systems using the modified Kaufman method. The successes and limitations of the various combinations of elements are reviewed. Subsequent discussion concerns the problems encountered with the various transition metals in combination with the various refractory transition metals in combination with rare earths and actinides. Finally, the results of the calculation of the iridium-plutonium and lutetium-plutonium diagrams are described.

Rare Earth, Actinide, and Transition Metal Diagrams

Diagrams of the rare earth-rare earth, actinide-actinide, and rare earth-actinide systems can be calculated with the modified Kaufman method with moderate changes of atomic volumes required in a few cases. In the rare earth-rare earth systems, modifications were necessary for scandium, yttrium, cerium, and dysprosium.

Shiflet et al.[4] reported that the calculation of three systems involving scandium (Sc-Y, Gd-Sc, and Nd-Sc) produced unsatisfactory results. In these systems, the calculated body-centered cubic plus hexagonal close-packed regions cross the liquid body-centered cubic regions. Two possibilities were presented to explain these results: the effects of impurities; or uncertainties in the atomic volumes of the phases of scandium at high temperature. The present work has avoided the problem by changing the atomic volumes of the various phases.

Atomic volumes used by Shiflet et al. were 15.5, 15.2, and 15.04 cm^3/g-atom for the liquid, body-centered cubic and hexagonal close-packed phases, respectively. Values for these phases were determined by empirical methods using the Nd-Sc diagram as described in Appendix B, and were found to be 17.33, 16,81, and 15.90 cm^3/g-atom, respectively. Figures 11, 13, and 15 show that not only has the problem encountered by Shiflet et al. been avoided, but the agreement between the calculated and experimental diagrams of the Gd-Sc, Nd-Sc, and Sc-Y systems is excellent.

This result suggests that the atomic volume is an extremely important parameter in the Kaufman method, perhaps more so than thought previously. This should not be too surprising since it appears that the volume of an atom is dependent on the electron configuration, which also determines the crystal structure.[15,16]

Empirical determination of atomic volumes of yttrium, cerium, and dysprosium was necessary because calculated diagrams of systems containing these elements were also unsatisfactory. Only one system for each of these elements was used to calculate the atomic volumes. The resulting atomic volumes produced satisfactory systems for all other diagrams using these elements.

For actinide-actinide systems, changes were required to the atomic volumes of plutonium phases. These were determined empirically by using the neptunium-plutonium system. These parameters were also found to be satisfactory for all other intra-actinide diagrams containing plutonium. For plutonium, there is a limitation to the Kaufman method. The Kaufman method assumes that three phases are possible in the solid state: body-centered cubic, face-centered cubic, and hexagonal close-packed. For plutonium, there are six allotropes, which means that three allotropes cannot be considered. In this work, the δ' phase (body-centered tetragonal) is ignored. The epsilon phase of plutonium is body-centered cubic and the delta phase is face-centered cubic, so there can be no ambiguity over these phases. The final possible phase (hexagonal close-packed) is assigned to the gamma phase for these calculations. However, this means that alpha and beta plutonium cannot enter into these calculations, and any systems that would include these phases are not calculable. This includes Pu-U and Np-Pu. Thus, inaccuracies are

inevitable in these systems. However, considering this limitation, the results obtained with actinide-actinide systems are favorable.

For rare earth-actinide diagrams, only changes to parameters for plutonium were necessary. Alteration of the atomic volumes for the various phases and the enthalpy of vaporization were necessary to obtain satisfactory calculated diagrams.

Other than the parameters described, no changes were necessary for any of the rare earths or actinides. This was not true, however, for the rare earth-transition metal or the actinide-transition metal systems. In all cases involving transition metals, it was necessary to use the average enthalpy of vaporization, ${}^{0}H_i^{V}$, where i is the element of concern (rare earth or actinide element). In diagrams involving intermetallic compounds, empirical determination of the constant (C) was necessary in the equation:

$$F^{\Psi} = (1 - x_*)\, F_i^{\theta} + x_*\, F_j^{\theta}\, (1 - x_*)\, (L - C) \qquad \text{(Eq. 22)}$$

where

- x_* = Composition of the compound
- L = Interaction parameter for the liquid phase
- F^{Ψ} = Free energy of formation of the compound phase of composition x_*
- i, j = Elements of the system
- θ = Type of phase (α, β, or ε structures)

This constant represents the interaction parameter of the solid compound. There is, at present, no method of calculating this value, and it is standard practice with the Kaufman method to determine the value of C empirically by using the melting point and the above equation. This establishes the value for binary systems for future use in ternary systems. Thus, the Kaufman method is limited to known phases and cannot be used to calculate diagrams with no prior information. Given this, the necessity for empirically determining values of C is not unexpected.

A qualitative explanation of the results may be found in the works of Brewer,[16,17] who uses an analysis of electronic configurations to explain the various relationships and rationalizes these relationships in terms of the Engel theory of alloying.[18]

The enthalpy of vaporization and the atomic volume affect the "internal pressure," $\Delta H_i/V_i$, where ΔH_i is the heat of vaporization of the element i and V_i is its atomic volume. Changes in the atomic volume of a phase can be caused by changes in the electronic structure of the atoms. Distribution of electrons among the various states can change with alloy composition, temperature, and pressure. As metals with differing electronic concentrations are mixed, the atoms can change their electronic configurations and, therefore, their sizes. Thus, the metals do not have one characteristic size but, in some instances, a series of sizes depending on the electronic environment.

An "effective" enthalpy of vaporization may be necessary, which may be different from the measured values for the element because of the promotional energy required to bring the electronic configuration from the ground state to the excited state in the alloy. Brewer[15] suggested that the energy of vaporization of a metal to a gaseous atom of the same electronic configuration as in the solid is a more correct measure of the cohesion.

Present theories of electronic structure of atoms in solids are inadequate so that determination of an *a priori* model for the electronic structure of the rare earths or actinides under various conditions does not appear feasible at this time. Therefore, it becomes necessary to determine values for the atomic volumes and the effective enthalpies of vaporization by empirical means.

Iridium-Plutonium Diagram

In view of the assumptions made concerning crystal structure and values for the constant (C), the liquidus compositions should only be considered as approximations. The presence of

intermetallic compounds in the system is indicated by the very high, negative values for the interaction parameters, so the main area of concern is the composition of compounds, their structure, and their melting points. The high solubility of iridium in body-centered cubic plutonium is somewhat surprising. Determination of solid state boundaries was not possible, so this area of the diagram should be considered highly speculative. The extent of the calculated solid solubility would decrease if the melting point of the $IrPu_3$ compound is higher than about 800 °C or if there is a different compound, higher in plutonium than $IrPu_3$.

Lutetium-Plutonium Diagram

Considering the relative success in the calculation of diagrams of rare earth-actinide systems, the calculated Lu-Pu diagram shown in Figure 104 should be a reasonable representation of the diagram. Certainly, extensive solid solubility exists at both ends of the diagram. A highly speculative diagram (published in the literature but based on very limited data) suggests a eutectic at about 97 at. % plutonium, with solid solubility of about 20 at. % plutonium in lutetium.[19]

The internal pressures calculated for lutetium and plutonium are 5748 and 5760 cal/cm^3, respectively. These nearly identical values would suggest extensive solid solubility, unless there is a radical change in the electronic structure of the constituents. In view of the similarities between trivalent rare earths and trivalent actinides, the probability of an electronic structure change is low.

CONCLUSIONS

1. The Kaufman method has been modified to accommodate the calculation of intra-rare earth, intra-actinide, and rare earth-actinide diagrams.

2. Empirical methods were necessary to determine useful values for the atomic volumes of scandium, yttrium, cerium, dysprosium, and plutonium.

3. The modified Kaufman method was successful in predicting the type of diagrams to be expected.

4. More empirical methods were required for rare earth-transition metal and actinide-transition metal diagrams for both the enthalpy of vaporization ($^0H_i^V$) and for the compound constant (C).

5. These empirical methods produced trends that allowed interpolation for unknown systems.

6. Progression from zirconium to palladium in the second long period and from hafnium to platinum in the third long period resulted in increasing difficulty in applying empirical methods.

REFERENCES

1. L. Kaufman and H. Bernstein, *Computer Calculation of Phase Diagrams*, Academic Press, New York, NY, 1970.

2. L. Kaufman and H. Bernstein, "Calculation of Regular Solution Phase Diagrams for Titanium Base Binary Systems," *The Science, Technology, and Application of Titanium*, pp 361-372, R. I. Jaffee and N. Promisel, Eds., Pergamon Press, 1970.

3. K. F. Michaels et al., "Considerations on the Kaufman Approach to Binary Phase Diagram Calculation," *Metallurgical Transactions A, 6A*, pp 1843-1848, 1975.

4. G. J. Shiflet, J. K. Lee, and H. I. Aaronson, "Application of the Kaufman Approach to the Calculation of Intra-Rare Earth Phase Diagrams," *CALPHAD, 3*, pp 129-137, 1979.

5. K. S. Chan, J. K. Lee, and H. I. Aaronson, "Kaufman Approach to Calculation of Partial Phase Diagrams Amongst Th, U, Np, and Pu," *J. Nucl. Mater., 92*, pp 237-242, 1980.

6. F. A. Shunk, *Constitution of Binary Alloys, Second Supplement*, p 461, McGraw-Hill Book Co., New York, NY, 1969.

7. B. Erdman and C. Keller, "Actinide (Lanthanide) - Noble Metal Phases, Preparation and Properties," *J. Solid State Chem., 7*, pp 40-48, May 1973.

8. R. Hultgren et al., *Selected Values of the Thermodynamic Properties of the Elements*, ASM, Metals Park, OH.

9. M. Hansen and K. Anderko, *Constitution of Binary Alloys*, 2nd Edition, McGraw-Hill Book Co., New York, NY, 1958.

10. R. P. Elliott, *Constitution of Binary Alloys, First Supplement*, McGraw-Hill Book Co., New York, NY, 1965.

11. W. G. Moffatt, *The Handbook of Binary Phase Diagrams*, General Electric Company, Schenectady, NY, 1981.

12. K. A. Gschneider Jr., "On the Nature of 4f Bonding in the Lanthanide Elements and their Compounds," *J. Less-Common Metals, 25*, pp 405-422, 1971.

13. L. Brewer, "Energies of the Electronic Configurations of the Lanthanide and the Actinide Neutral Atoms," *J. Opt. Soc. of America, 61(8)*, pp 1101-1111, 1971.

14. L. Brewer and R. H. Lamoreaux, "Molybdenum, Physicochemical Properties of its Compounds and Alloys," *At. Energy Rev., Special Issue 7, Part II*, IAEA, Vienna, 1980.

15. L. Brewer, "Mathematical Representation of Size and Electronic Factors," *Mat. Res. Soc. Symp. 19*, pp 129-134, 1983.

16. L. Brewer, "Thermodynamics and Alloy Behavior of the BCC and FCC Phases of Plutonium and Thorium," *Plutonium 1970 and Other Actinides*, pp 650-658, W. N. Miner (Ed.), AIME, New York, NY, 1970.

17. L. Brewer, "Chemical Bonding Theory Applied to Metals," *Alloying*, pp 1-28, J. L. Walter, M. R. Jackson, and C. T. Sims (Ed.), ASM International, Metals Park, OH, 1988.

18. N. Engel, "Metallic Lattices Considered as Electron Concentration Phases," *Trans. Quarterly, 57*, pp 610-619, 1964.

19. V. Storhok, *Reactor Materials, 6(3)*, pp 14-15, 1963.

ILLUSTRATIONS
(Figures 1 Through 104)

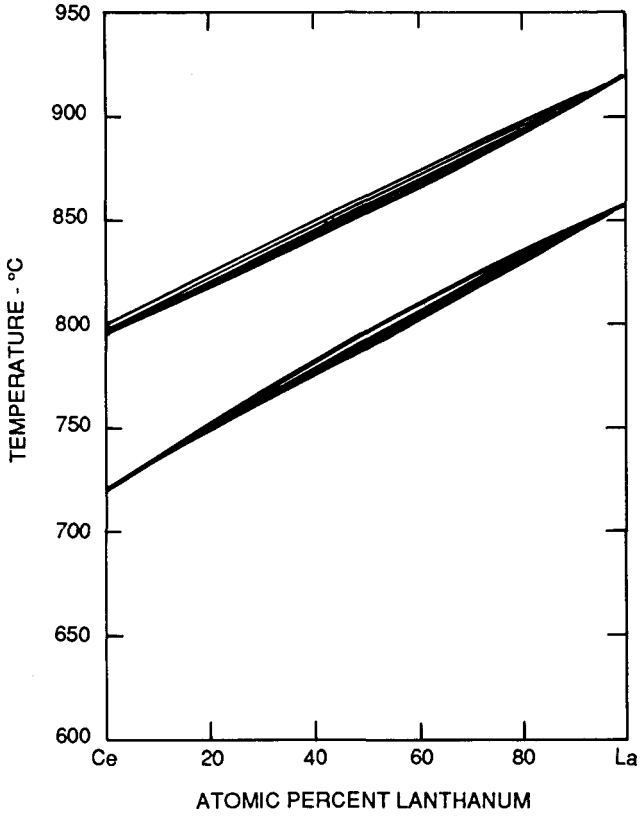

FIGURE 1. Calculated vs Experimental Ce-La Diagram. Thick lines indicate calculated diagram. Thin lines indicate literature diagram.

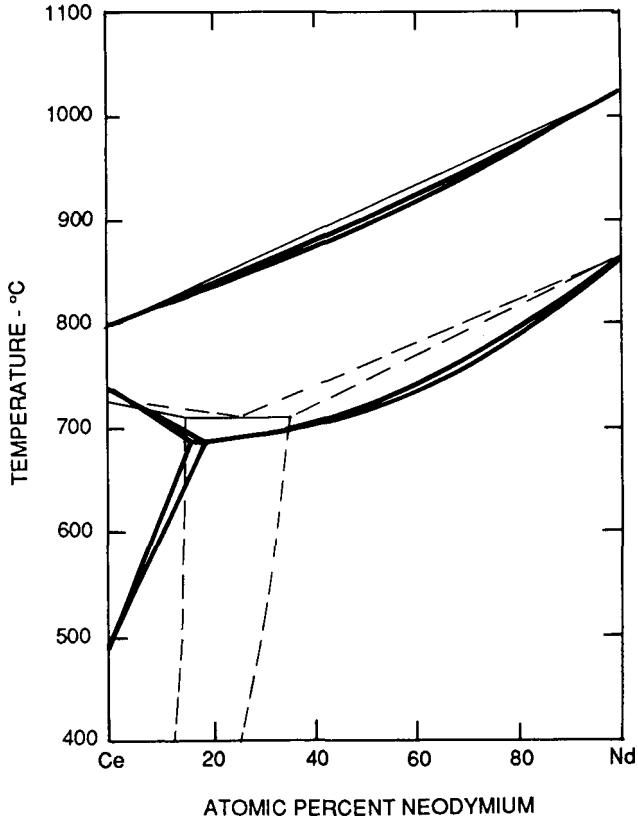

FIGURE 2. Calculated vs Experimental Ce-Nd Diagram

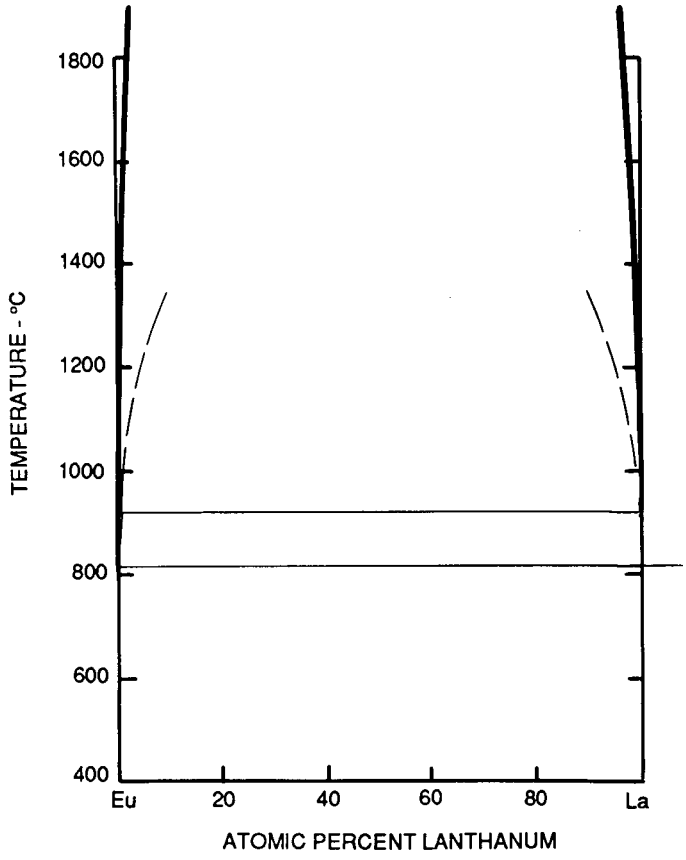

FIGURE 3. Calculated vs Estimated Eu-La Diagram

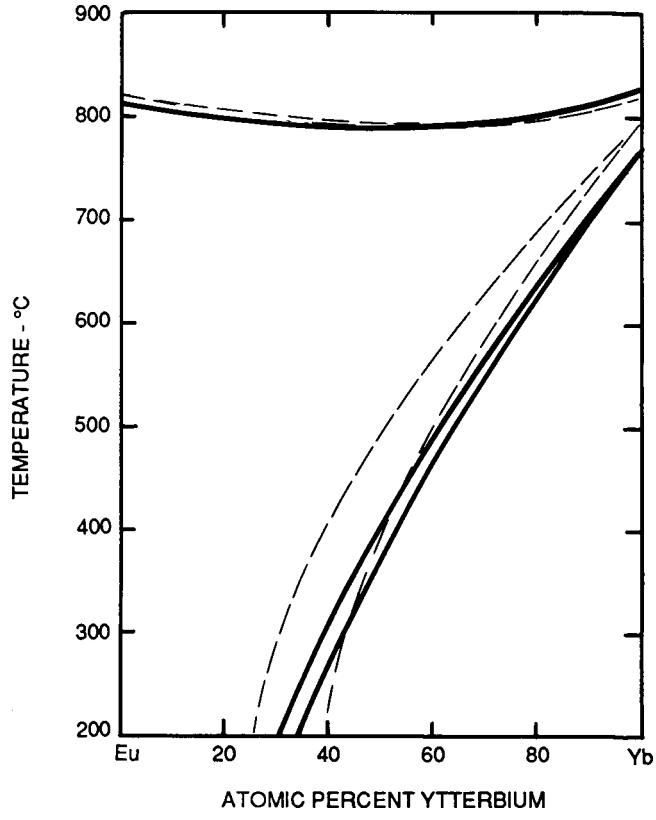

FIGURE 4. Calculated vs Estimated Eu-Yb Diagram

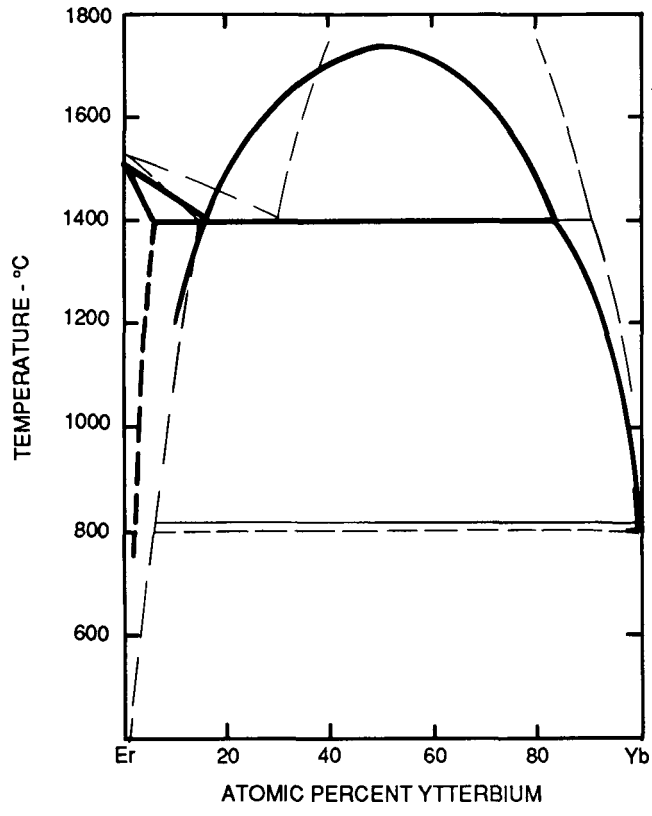

FIGURE 6. Calculated vs Estimated Er-Yb Diagram

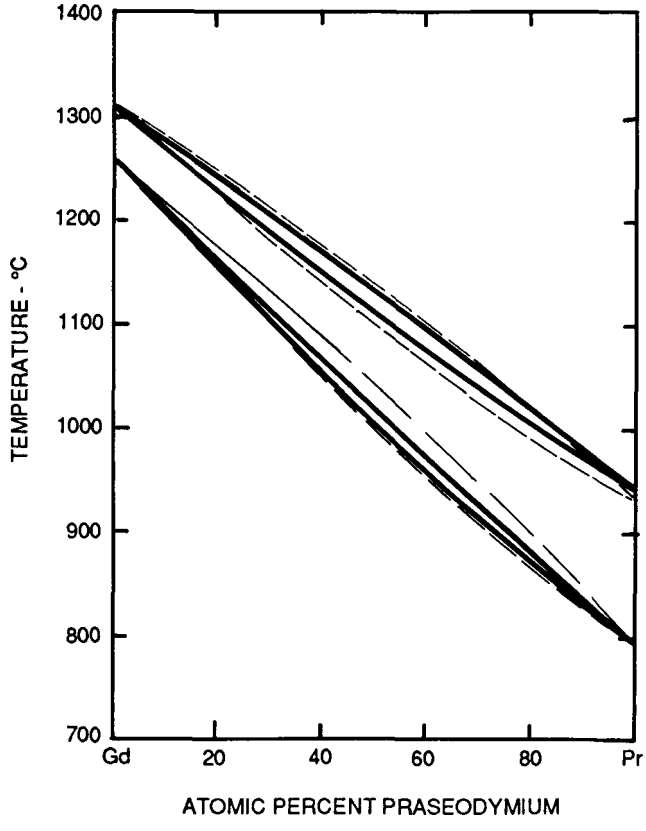

FIGURE 5. Calculated vs Estimated Gd-Pr Diagram

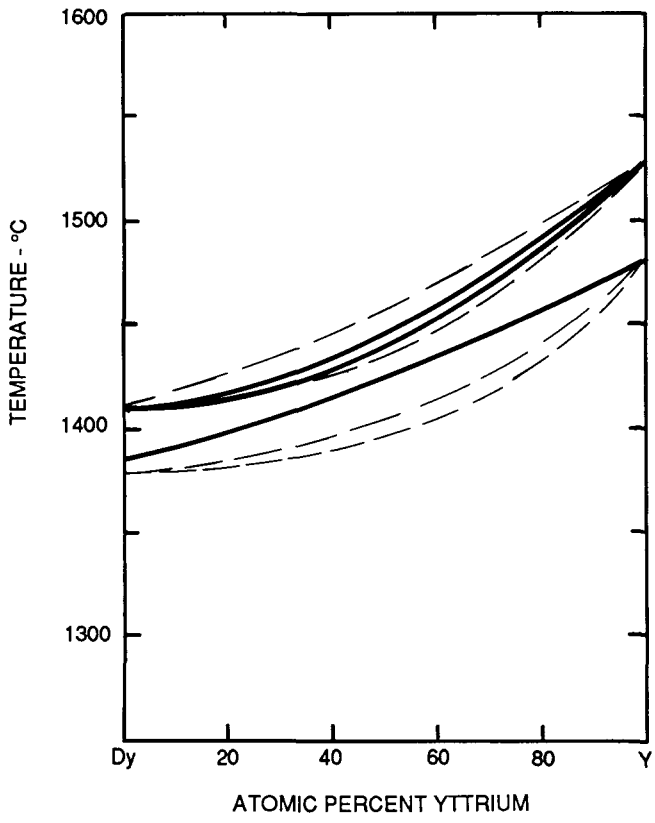

FIGURE 7. Calculated vs Estimated Dy-Y Diagram

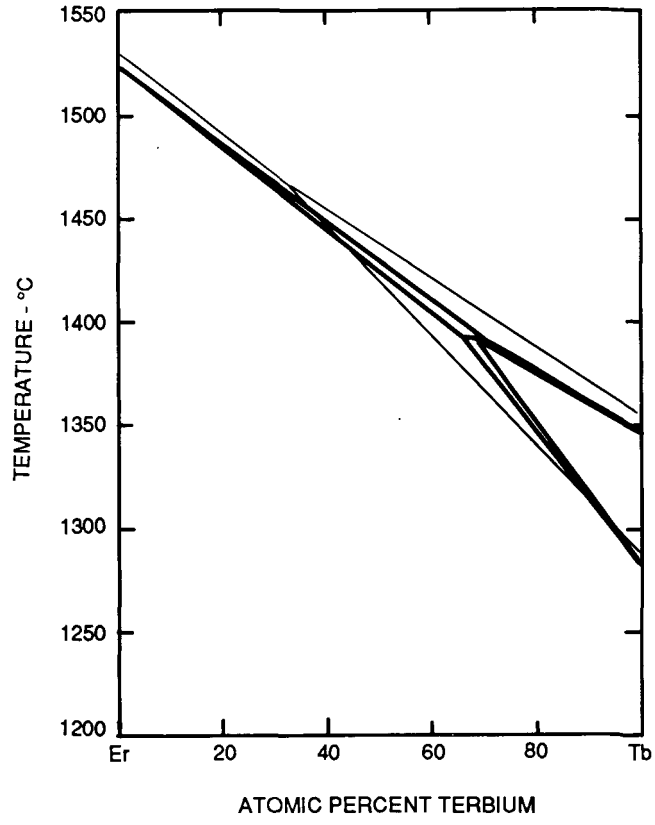

FIGURE 8. Calculated vs Experimental Er-Tb Diagram

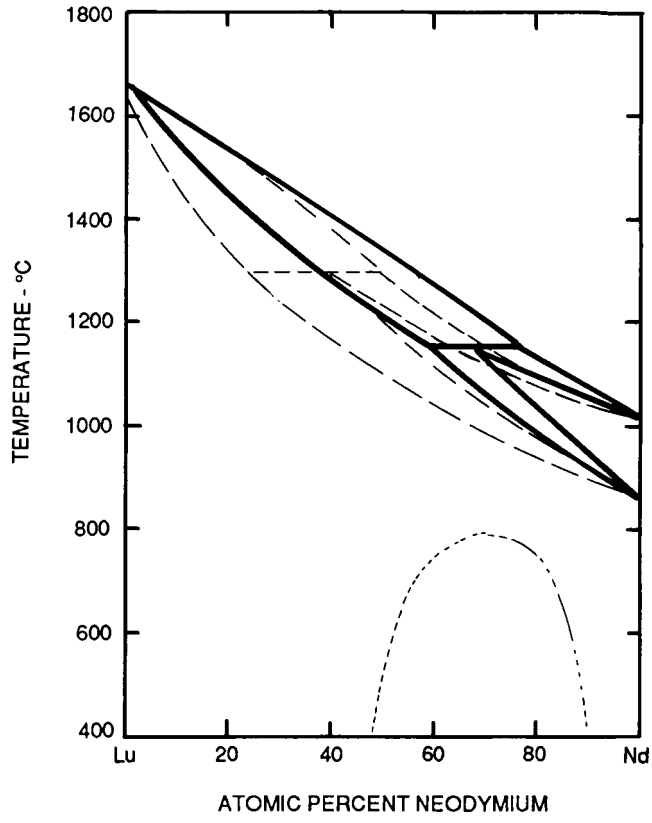

FIGURE 10. Calculated vs Estimated Lu-Nd Diagram

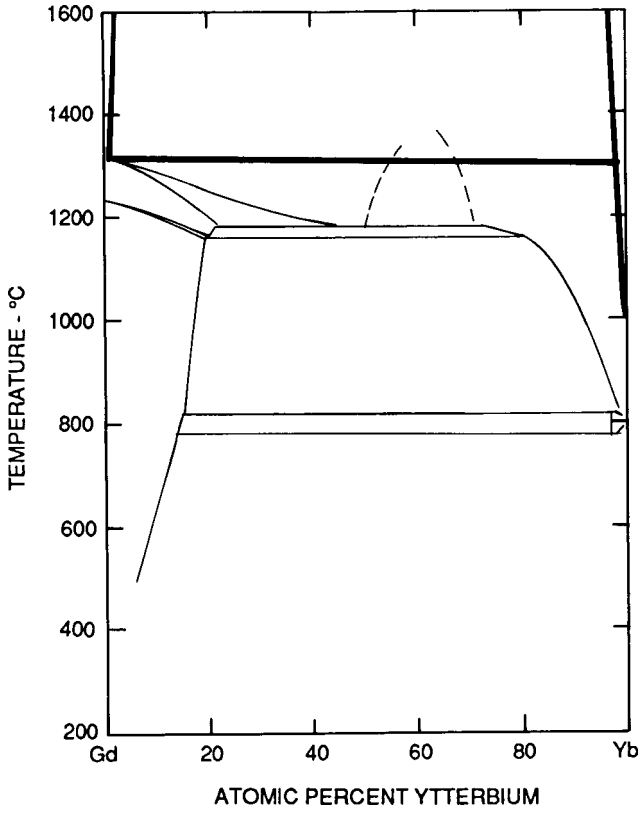

FIGURE 9. Calculated vs Experimental Gd-Yb Diagram

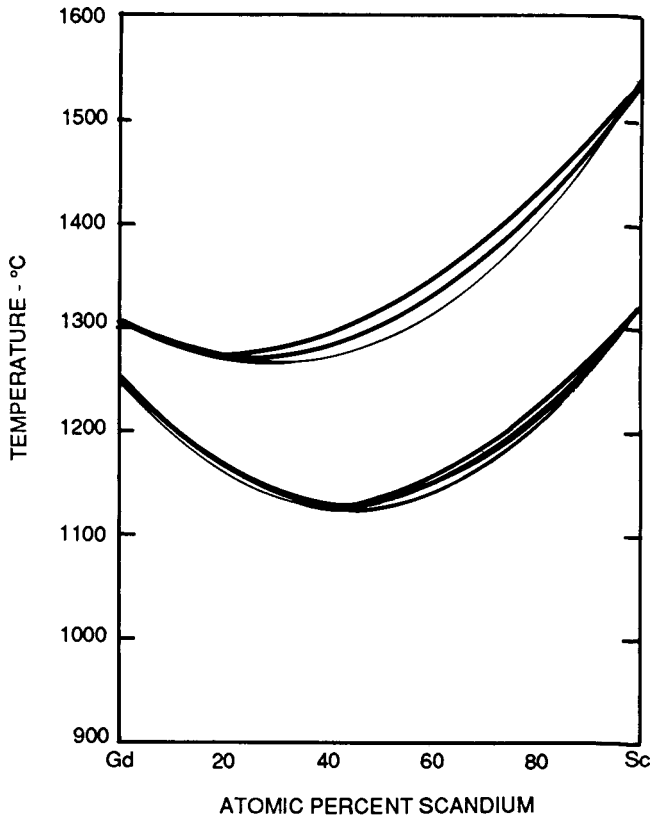

FIGURE 11. Calculated vs Experimental Gd-Sc Diagram

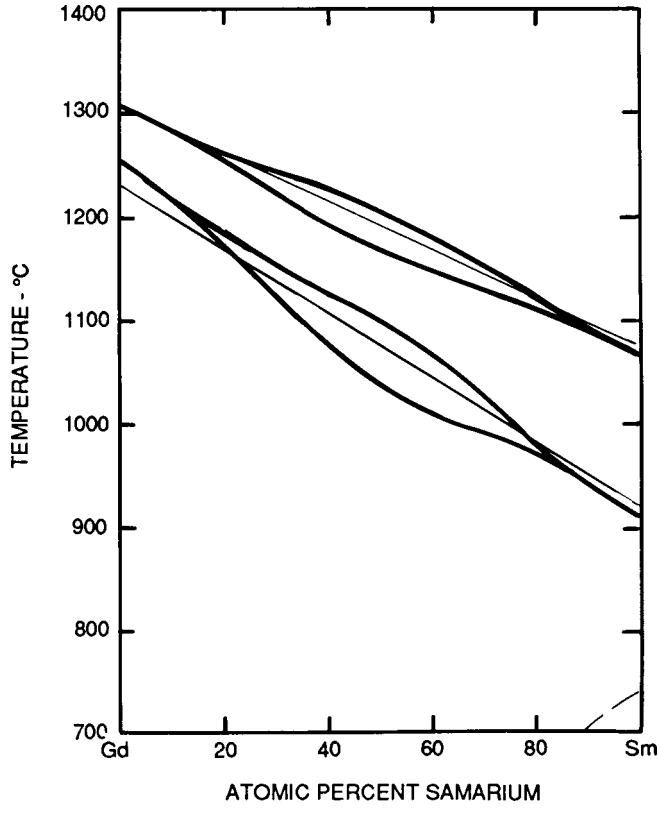

FIGURE 12. Calculated vs Experimental Gd-Sm Diagram

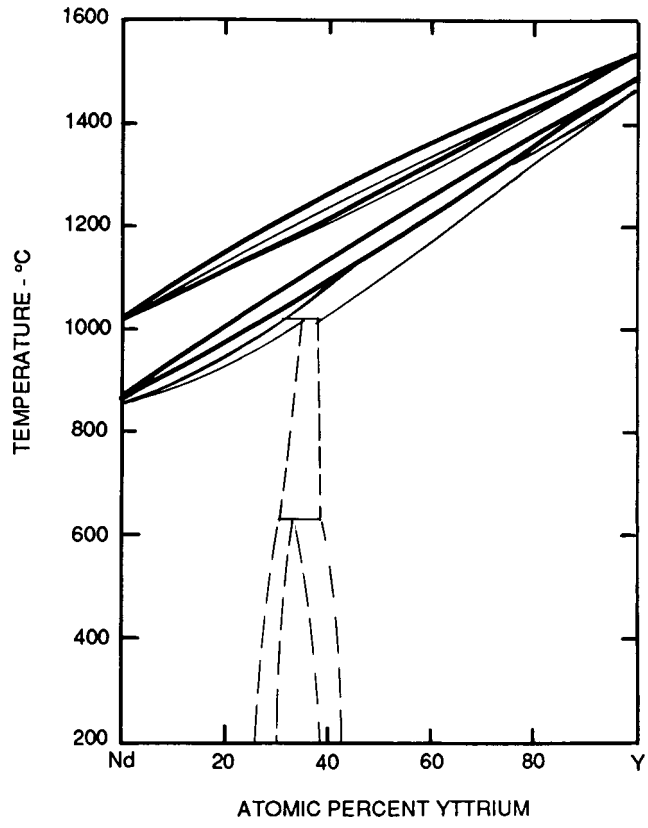

FIGURE 14. Calculated vs Experimental Nd-Y Diagram

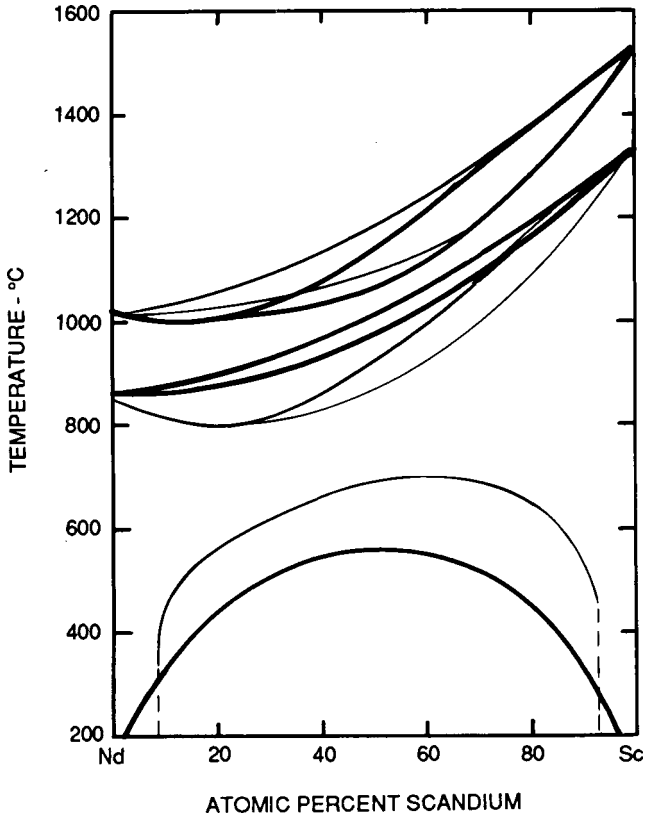

FIGURE 13. Calculated vs Experimental Nd-Sc Diagram

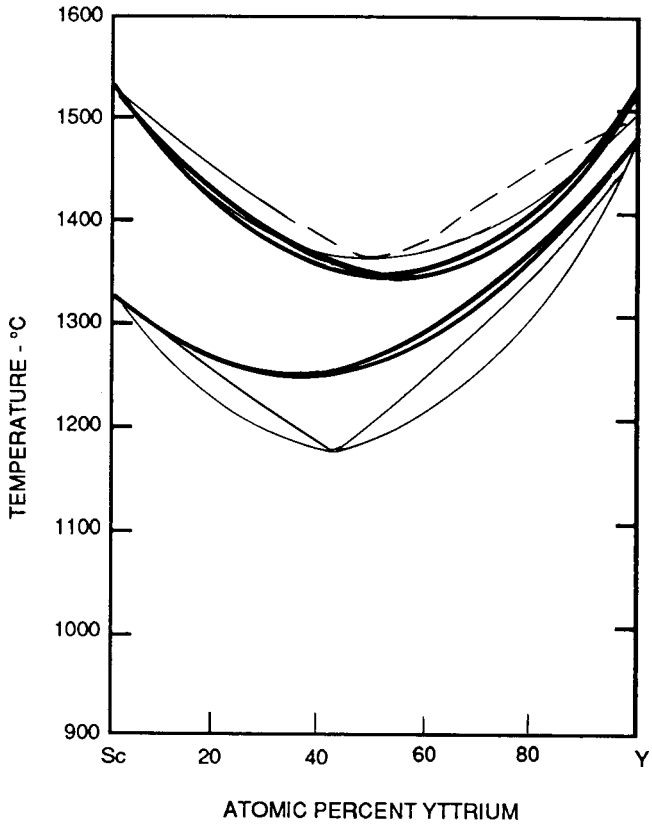

FIGURE 15. Calculated vs Experimental Sc-Y Diagram

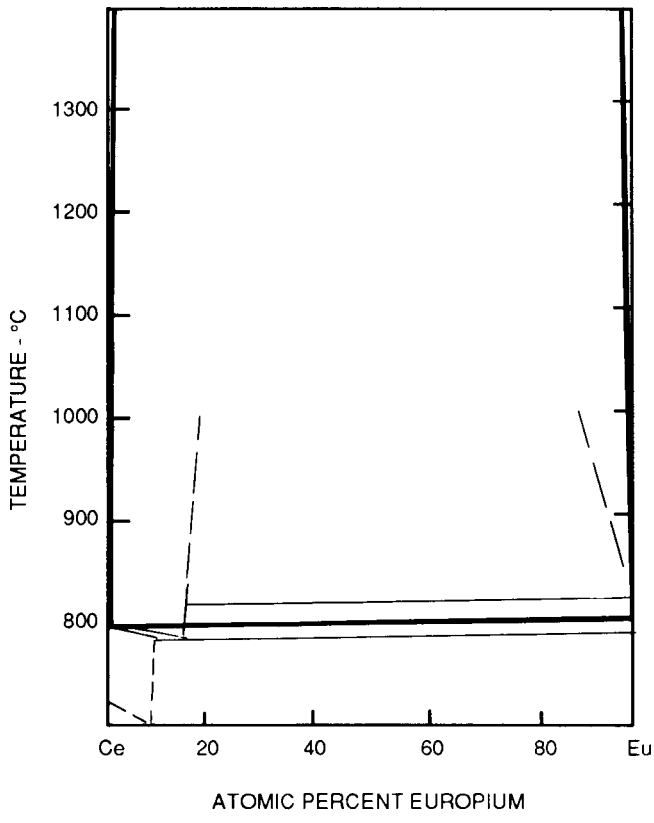

FIGURE 16. Calculated vs Estimated Ce-Eu Diagram

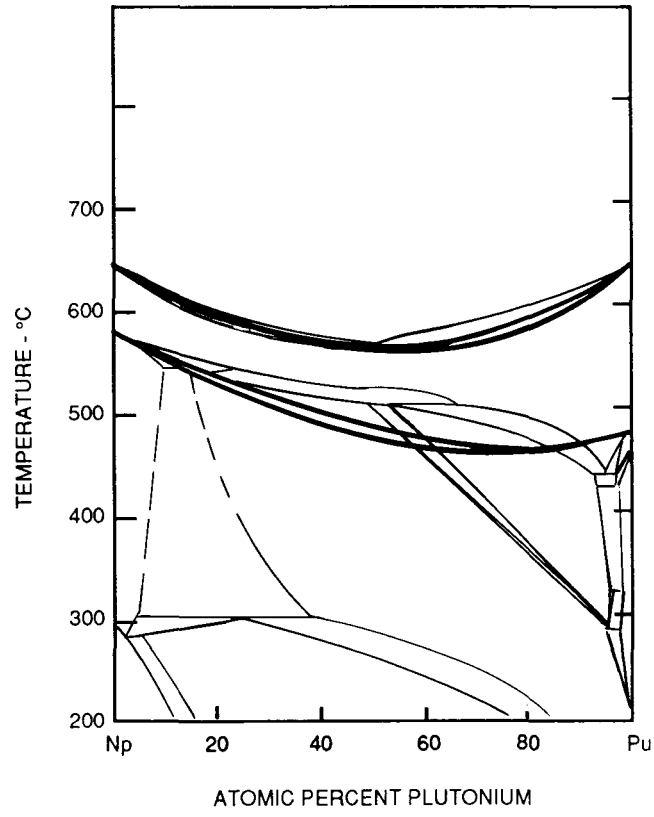

FIGURE 18. Calculated vs Experimental Np-Pu Diagram

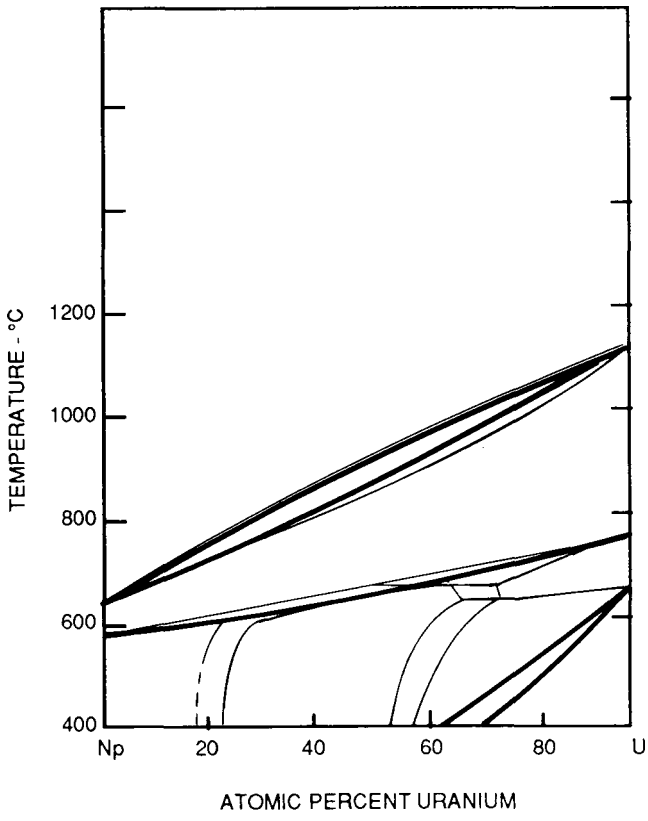

FIGURE 17. Calculated vs Experimental Np-U Diagram

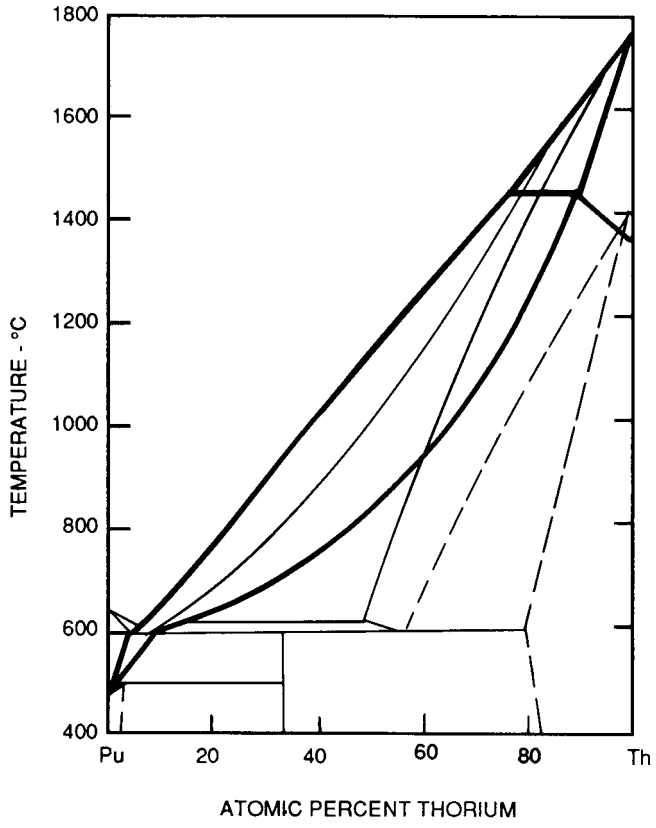

FIGURE 19. Calculated vs Experimental Pu-Th Diagram

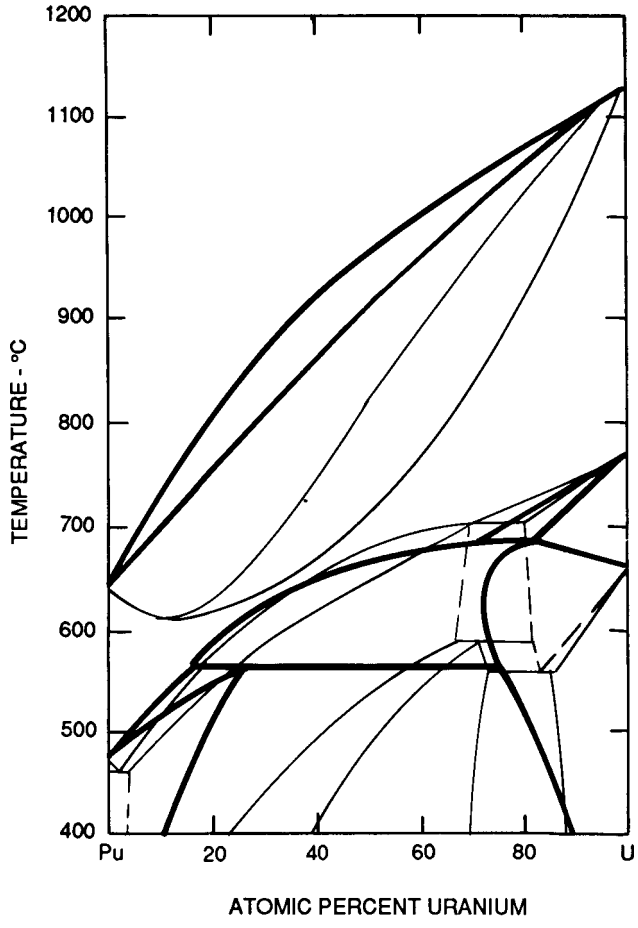

FIGURE 20. Calculated vs Experimental Pu-U Diagram

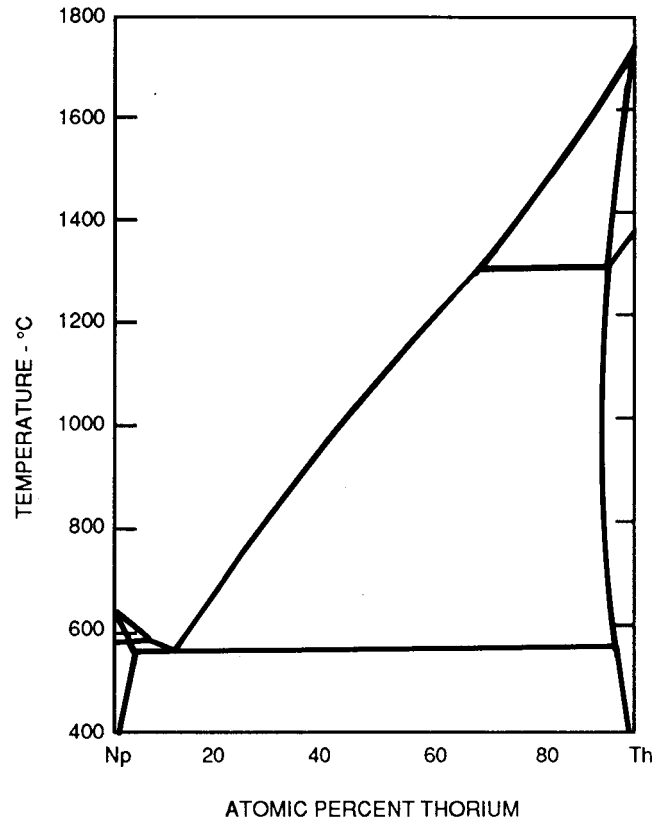

FIGURE 22. Calculated Np-Th Diagram. No literature diagram is available.

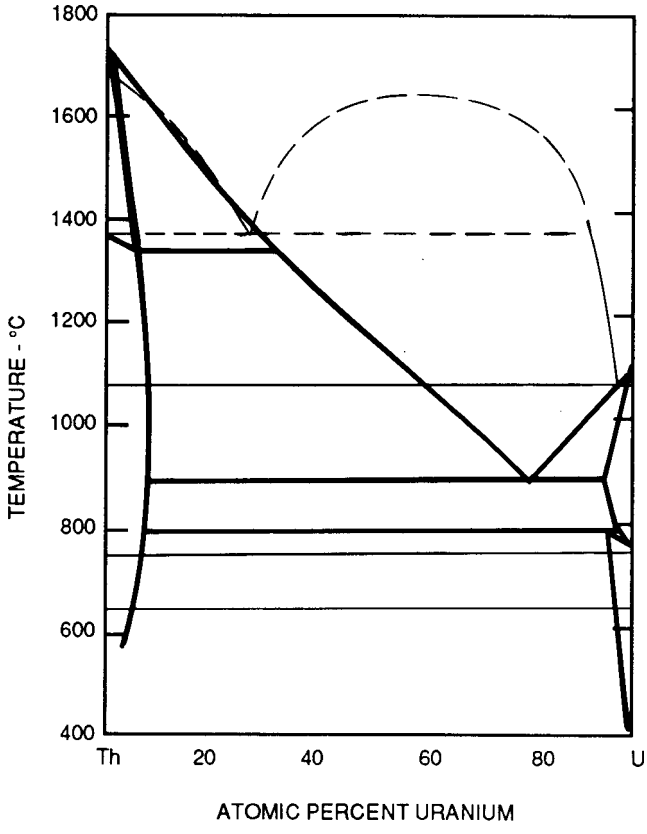

FIGURE 21. Calculated vs Experimental Th-U Diagram

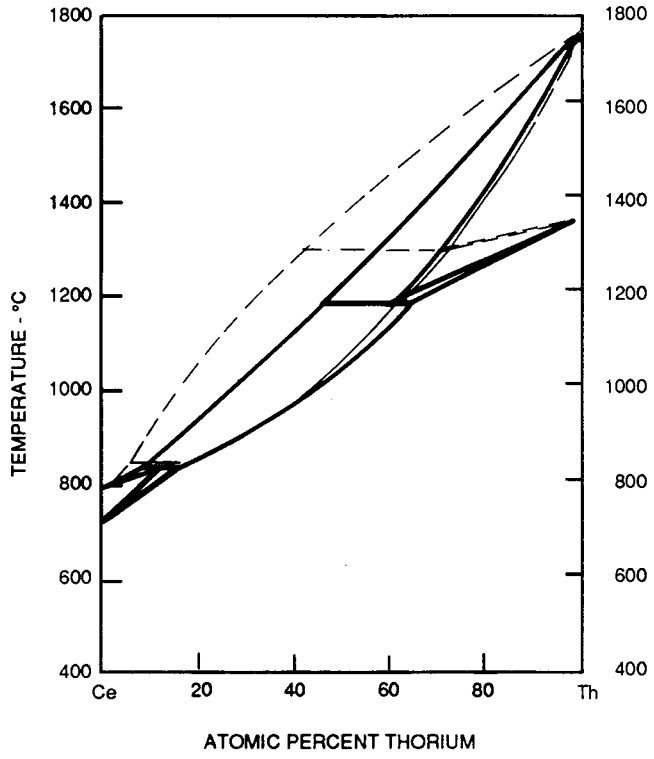

FIGURE 23. Calculated vs Estimated Ce-Th Diagram

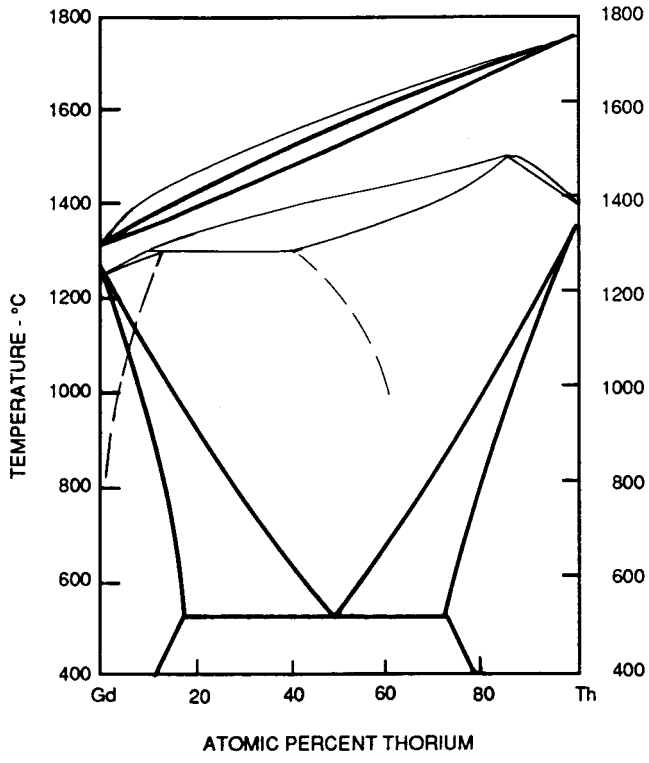

FIGURE 24. Calculated vs Experimental Gd-Th Diagram

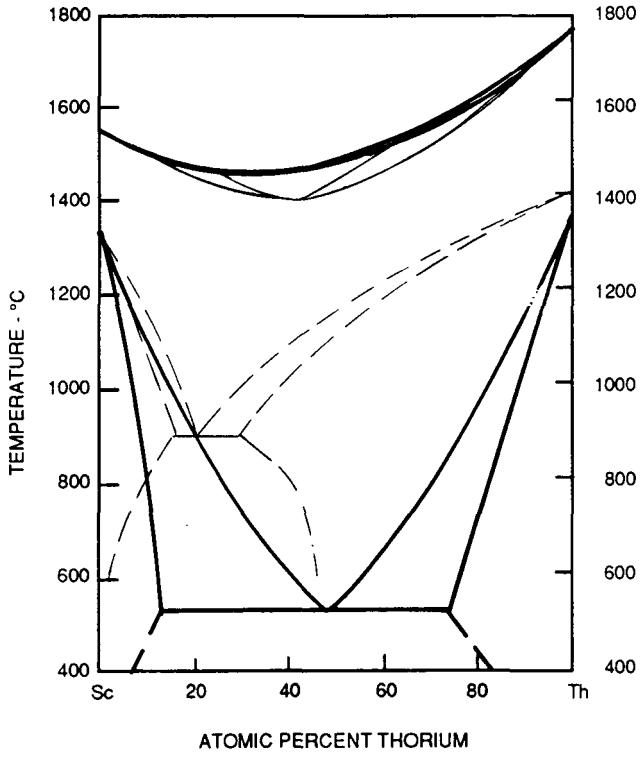

FIGURE 26. Calculated vs Experimental Sc-Th Diagram

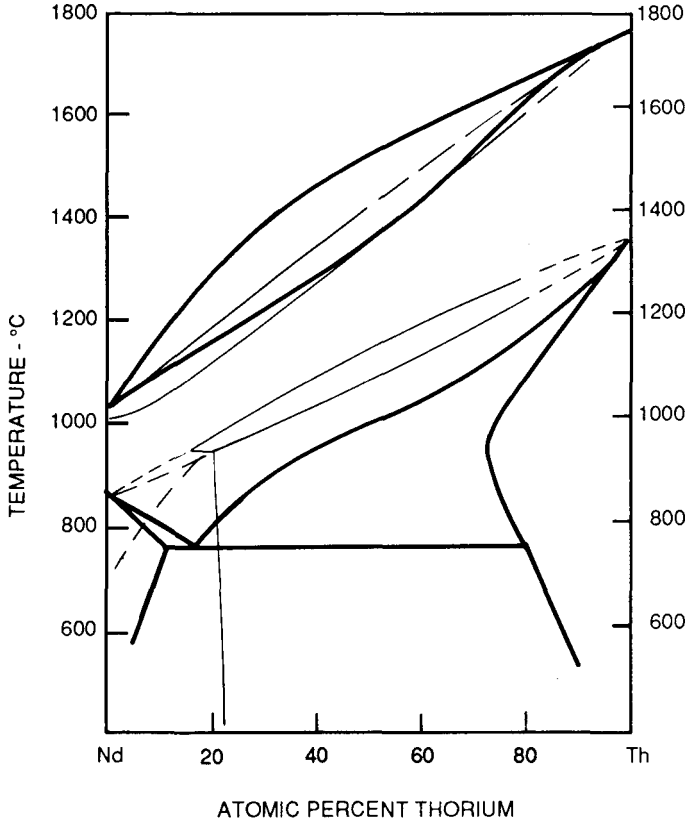

FIGURE 25. Calculated vs Experimental Nd-Th Diagram

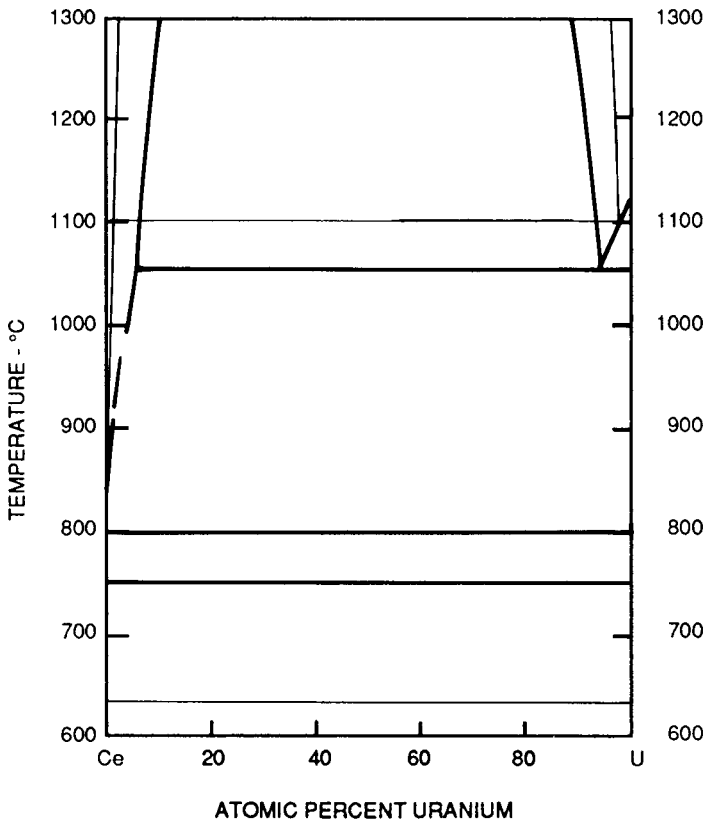

FIGURE 27. Calculated vs Experimental Ce-U Diagram

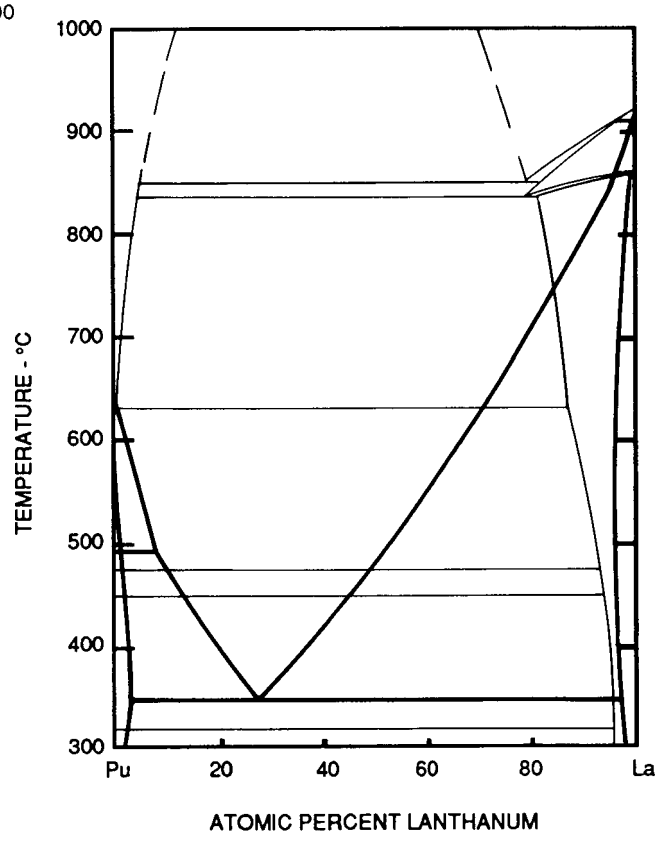

FIGURE 28. Calculated vs Experimental La-Pu Diagram

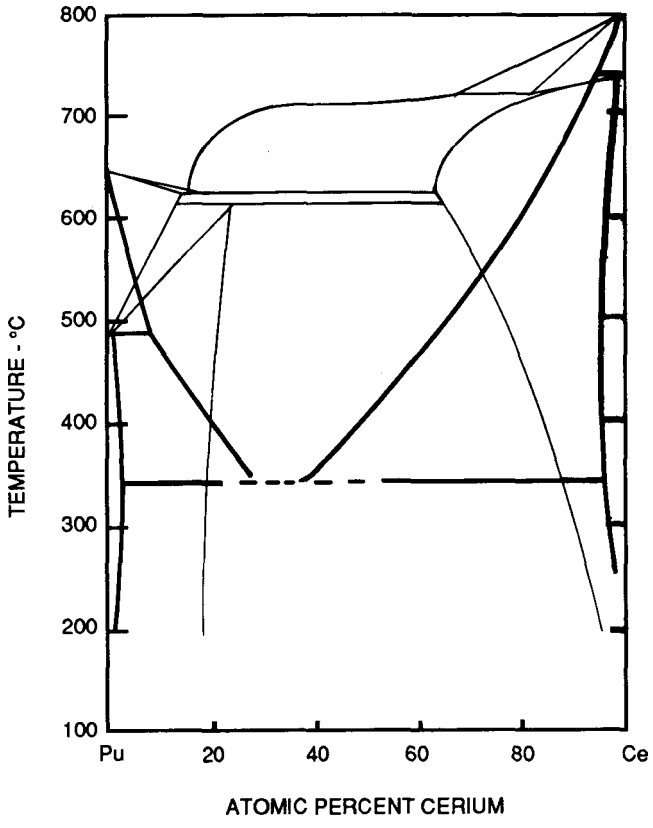

FIGURE 30. Calculated vs Experimental Ce-Pu Diagram

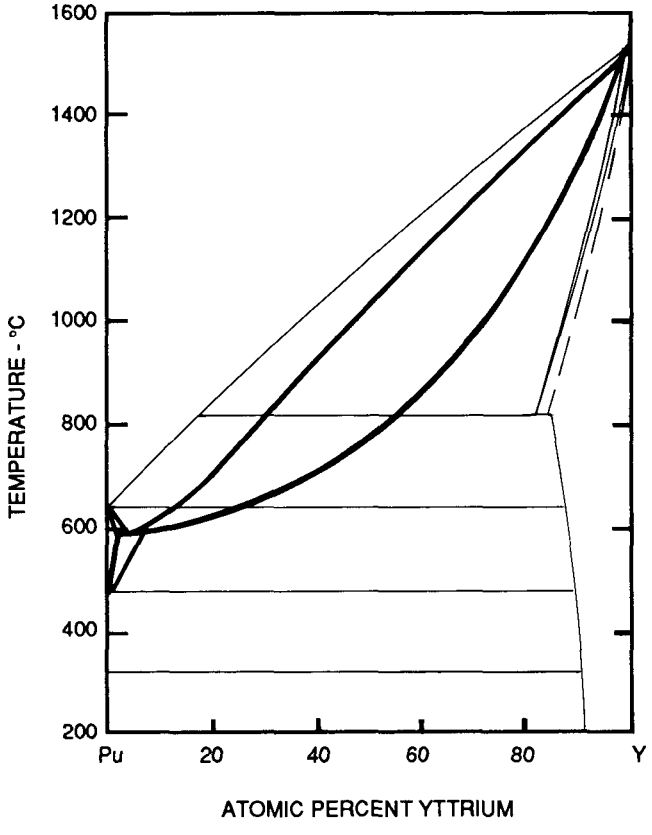

FIGURE 29. Calculated vs Experimental Pu-Y Diagram

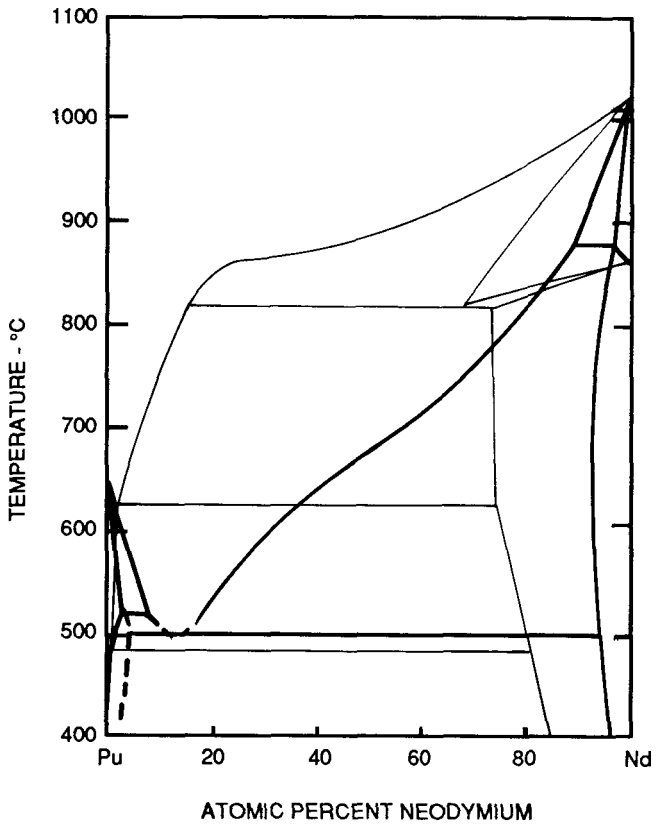

FIGURE 31. Calculated vs Experimental Nd-Pu Diagram

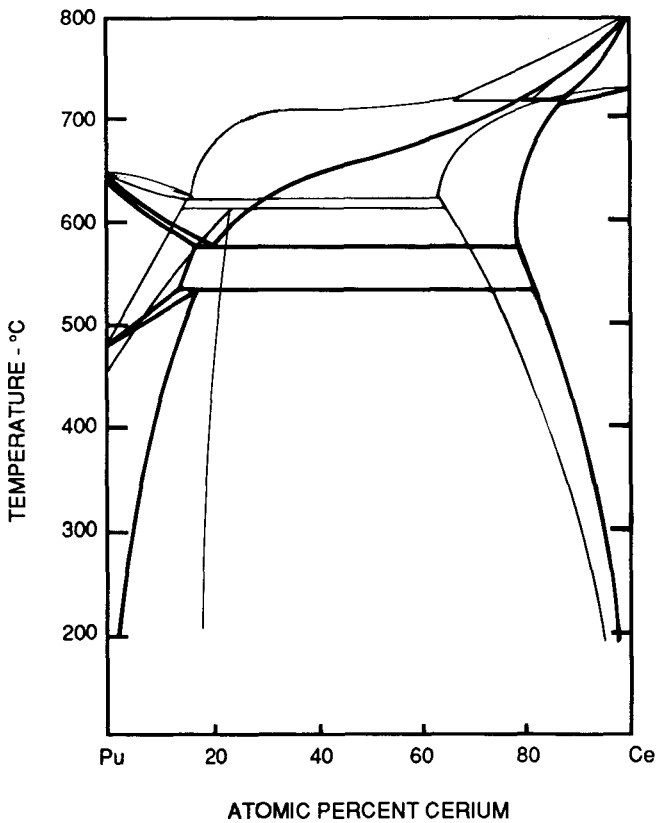

FIGURE 32. Calculated vs Experimental Ce-Pu Diagram

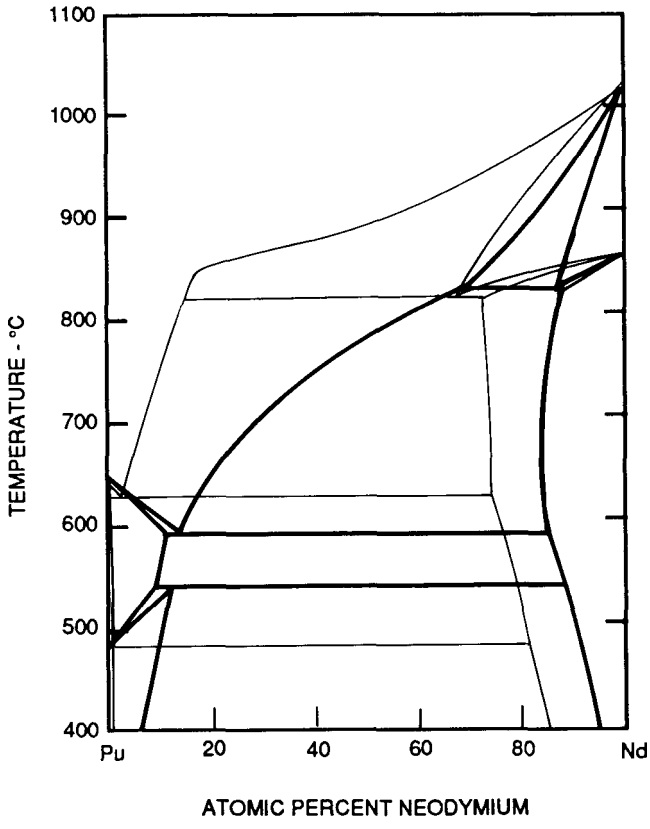

FIGURE 34. Calculated vs Experimental Nd-Pu Diagram

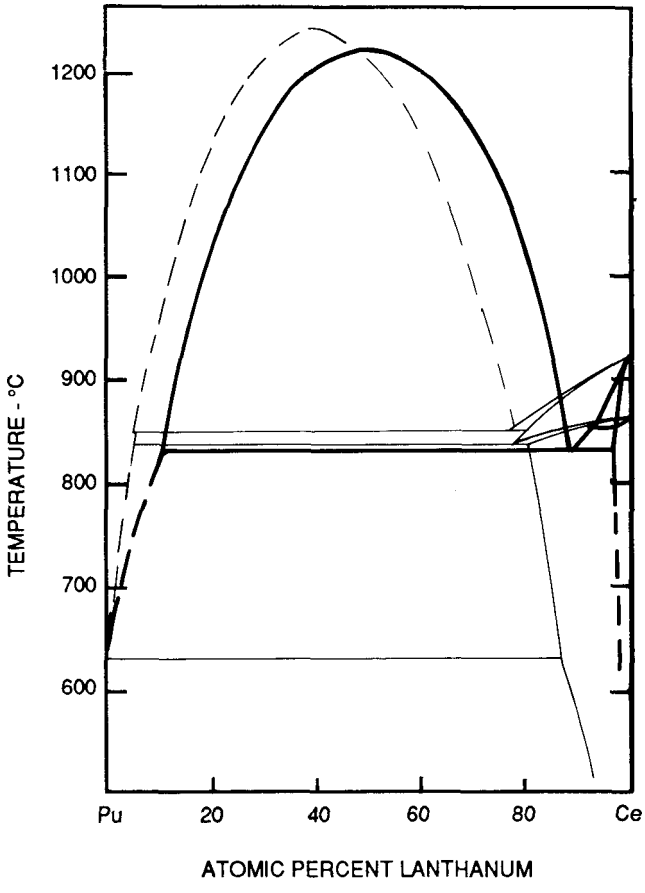

FIGURE 33. Calculated vs Experimental La-Pu Diagram

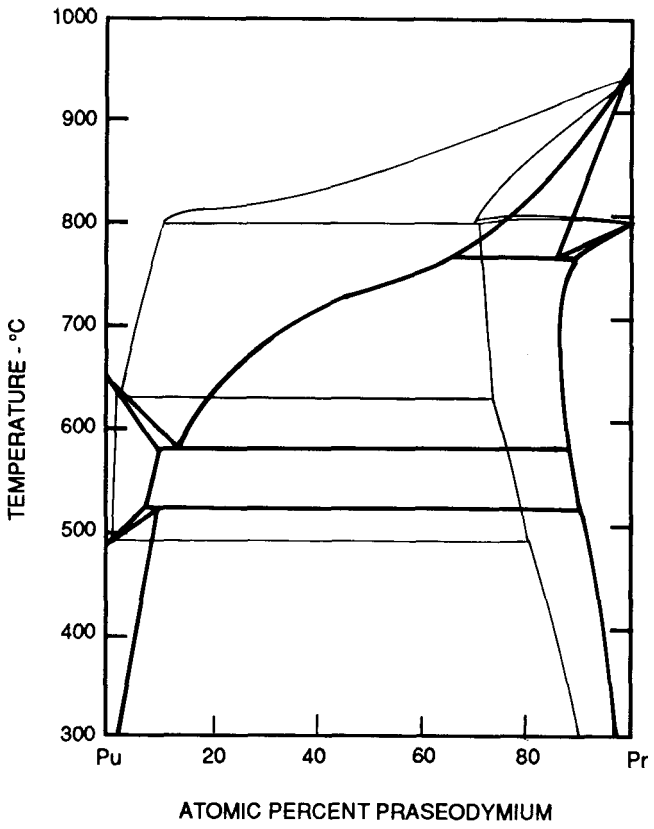

FIGURE 35. Calculated vs Experimental Pr-Pu Diagram

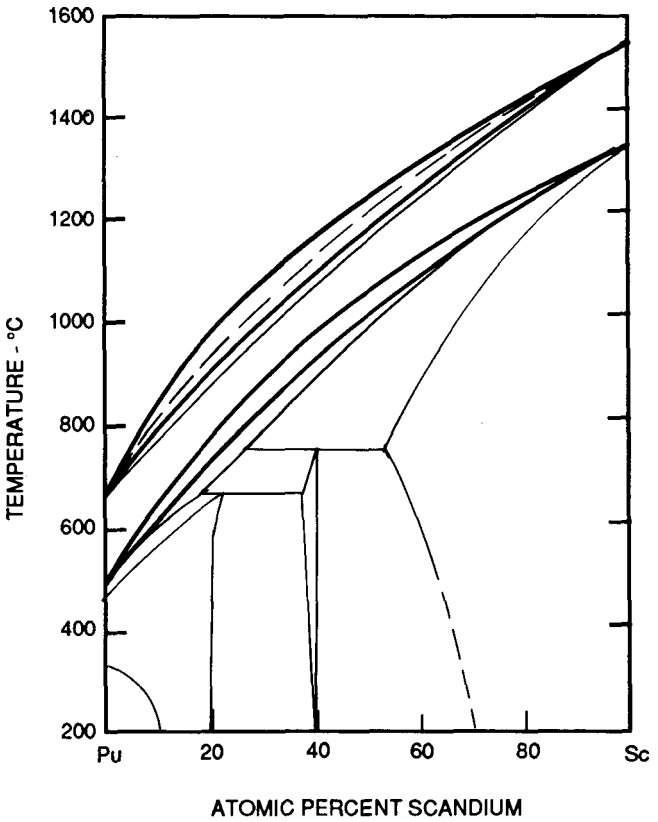

FIGURE 36. Calculated vs Experimental Pu-Sc Diagram

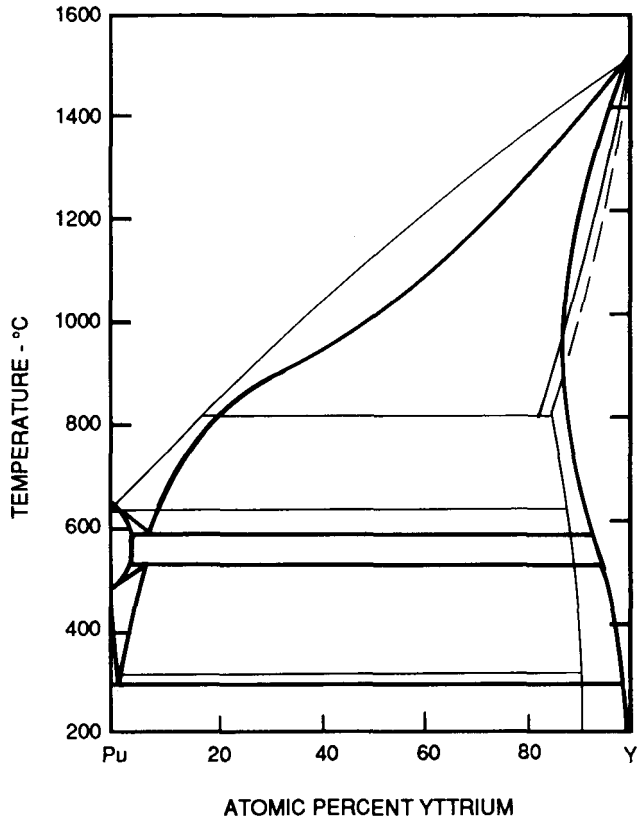

FIGURE 38. Calculated vs Experimental Pu-Y Diagram

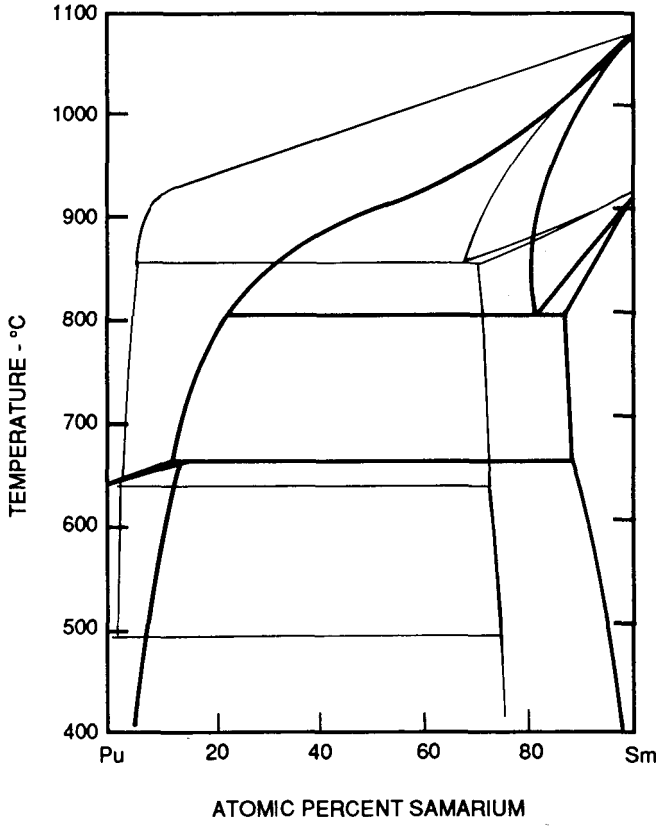

FIGURE 37. Calculated vs Experimental Pu-Sm Diagram

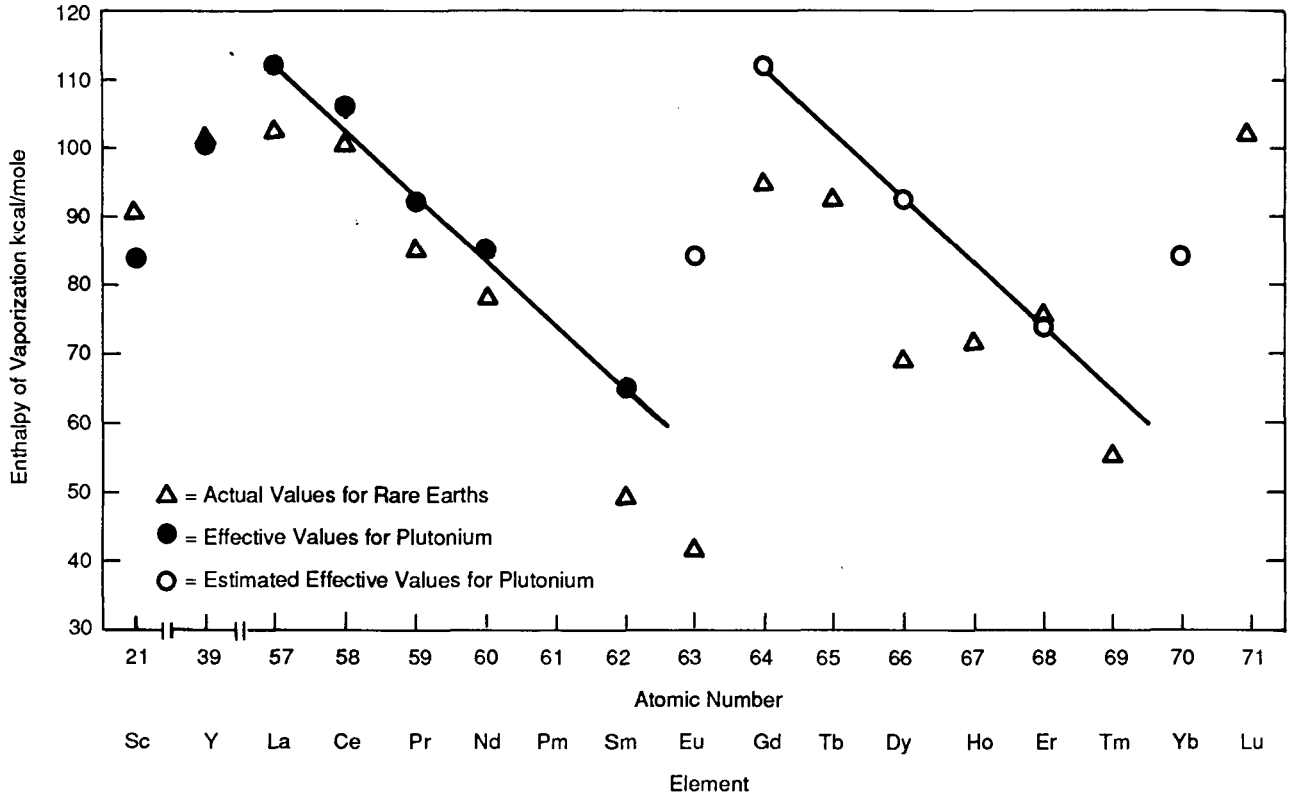

FIGURE 39. Values for Enthalpy of Vaporization of Rare Earths and Plutonium for Rare Earth-Plutonium Diagram Calculations

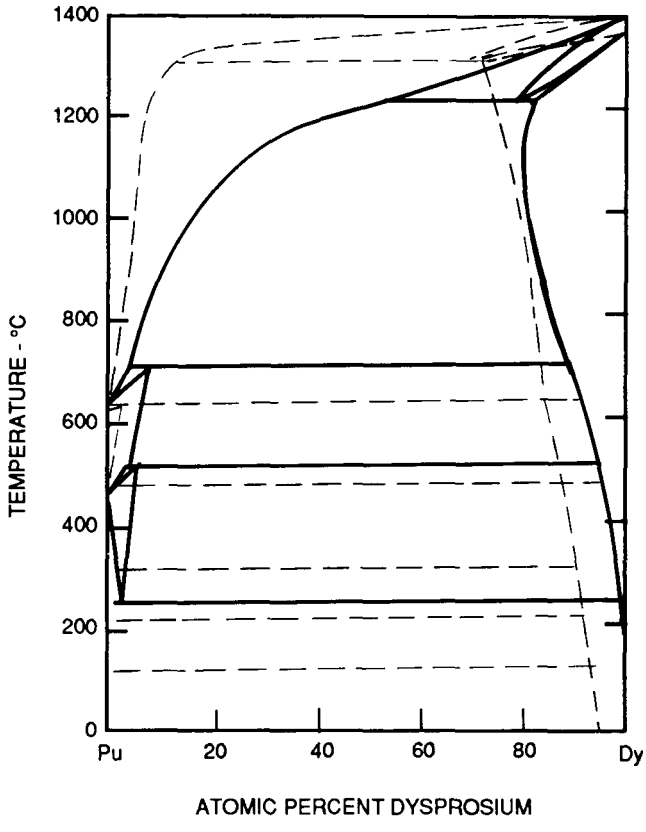

FIGURE 41. Calculated vs Estimated Dy-Pu Diagram

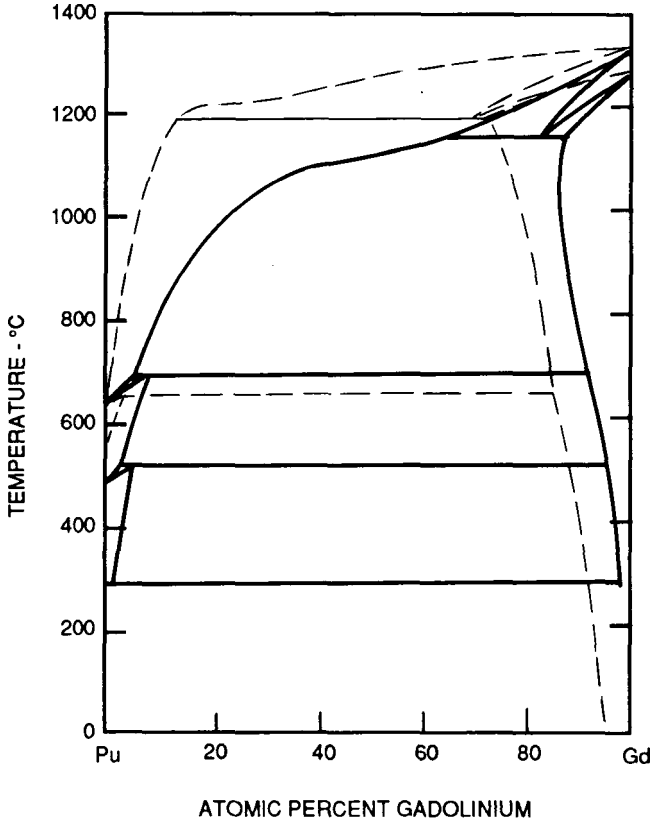

FIGURE 40. Calculated vs Estimated Gd-Pu Diagram

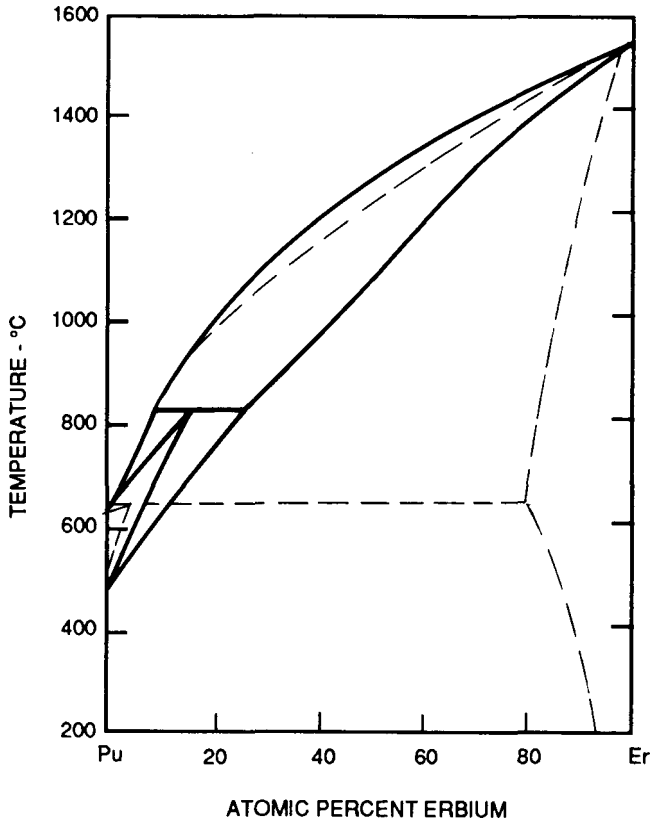

FIGURE 42. Calculated vs Estimated Er-Pu Diagram

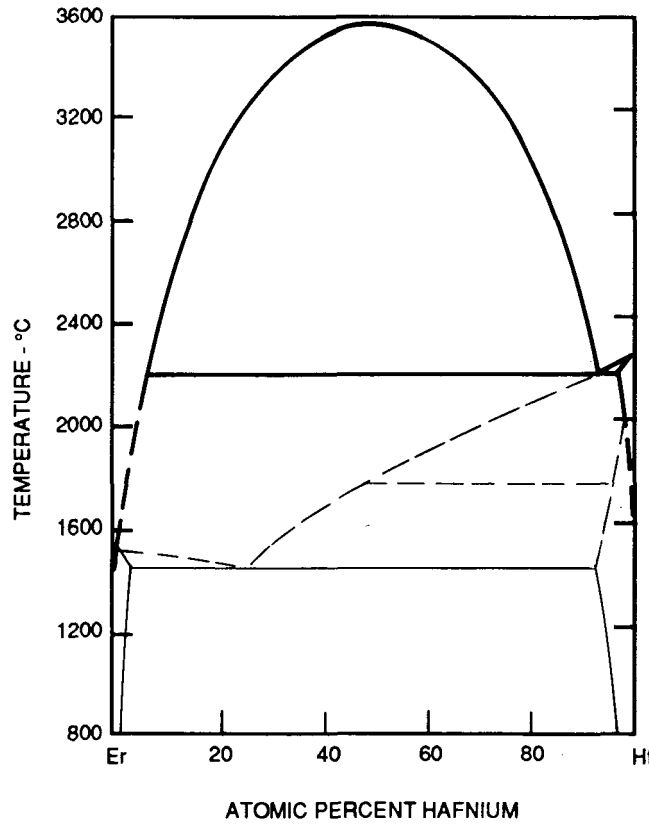

FIGURE 43. Calculated vs Experimental Er-Hf Diagram

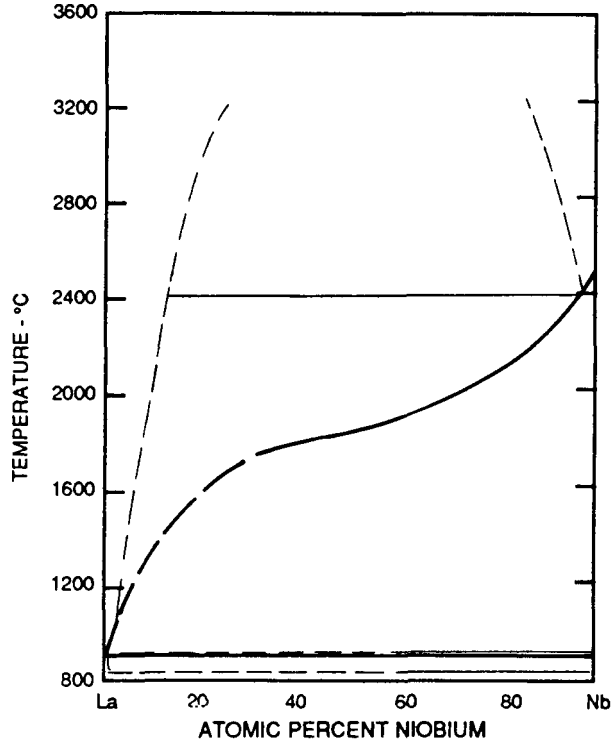

FIGURE 44. Calculated vs Estimated La-Nb Diagram

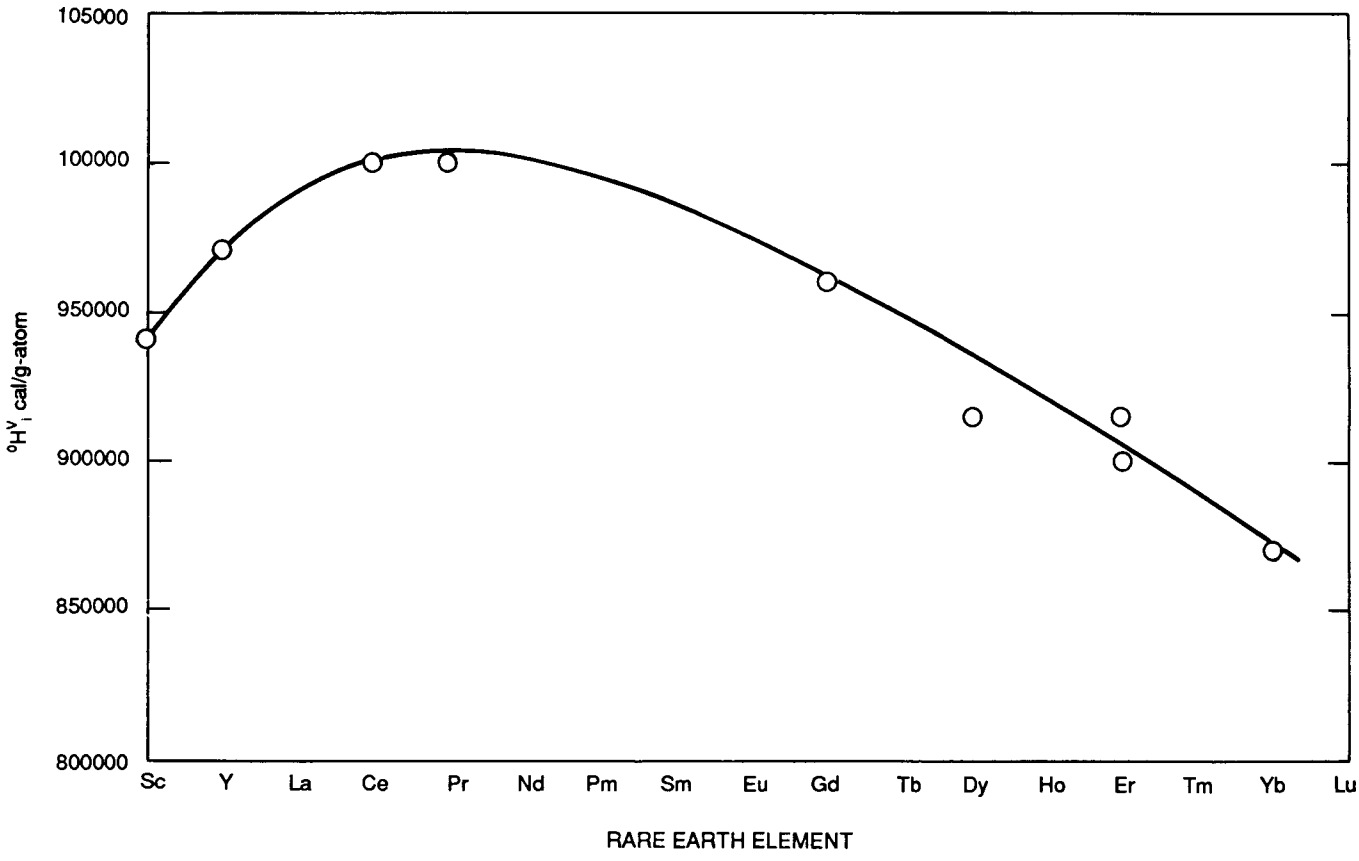

FIGURE 45. Empirically Determined Values for the Enthalpy of Vaporization $^{0}H_{i}^{V}$ for Rare Earth Elements with Zirconium and Hafnium

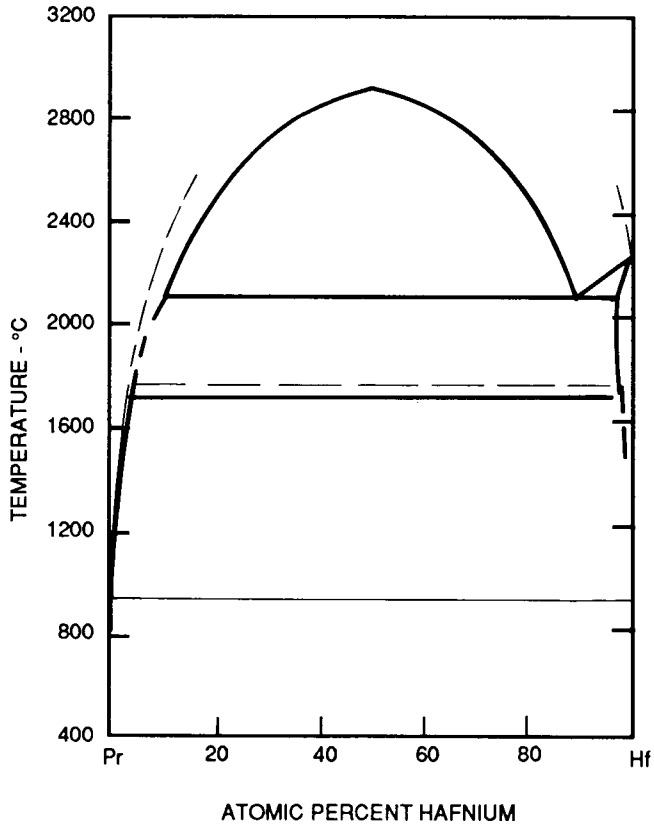

FIGURE 46. Calculated vs Estimated Hf-Pr Diagram

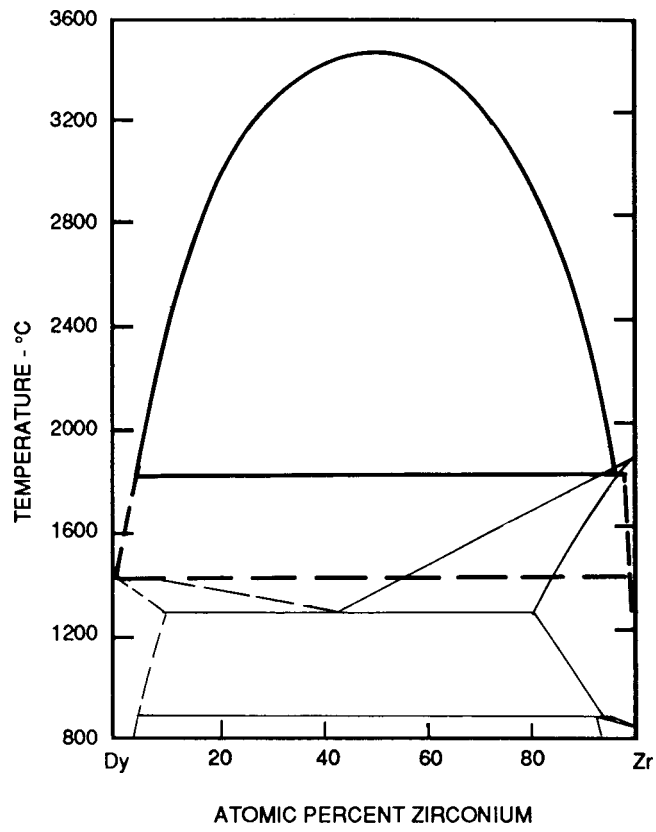

FIGURE 47. Calculated vs Experimental Dy-Zr Diagram

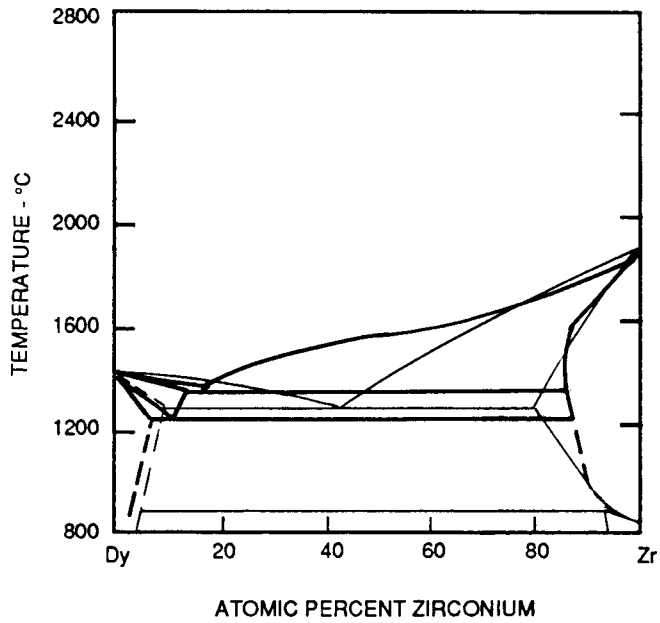

FIGURE 48. Calculated vs Experimental Dy-Zr Diagram using $^{o}H^{v}$ Value from Figure 45

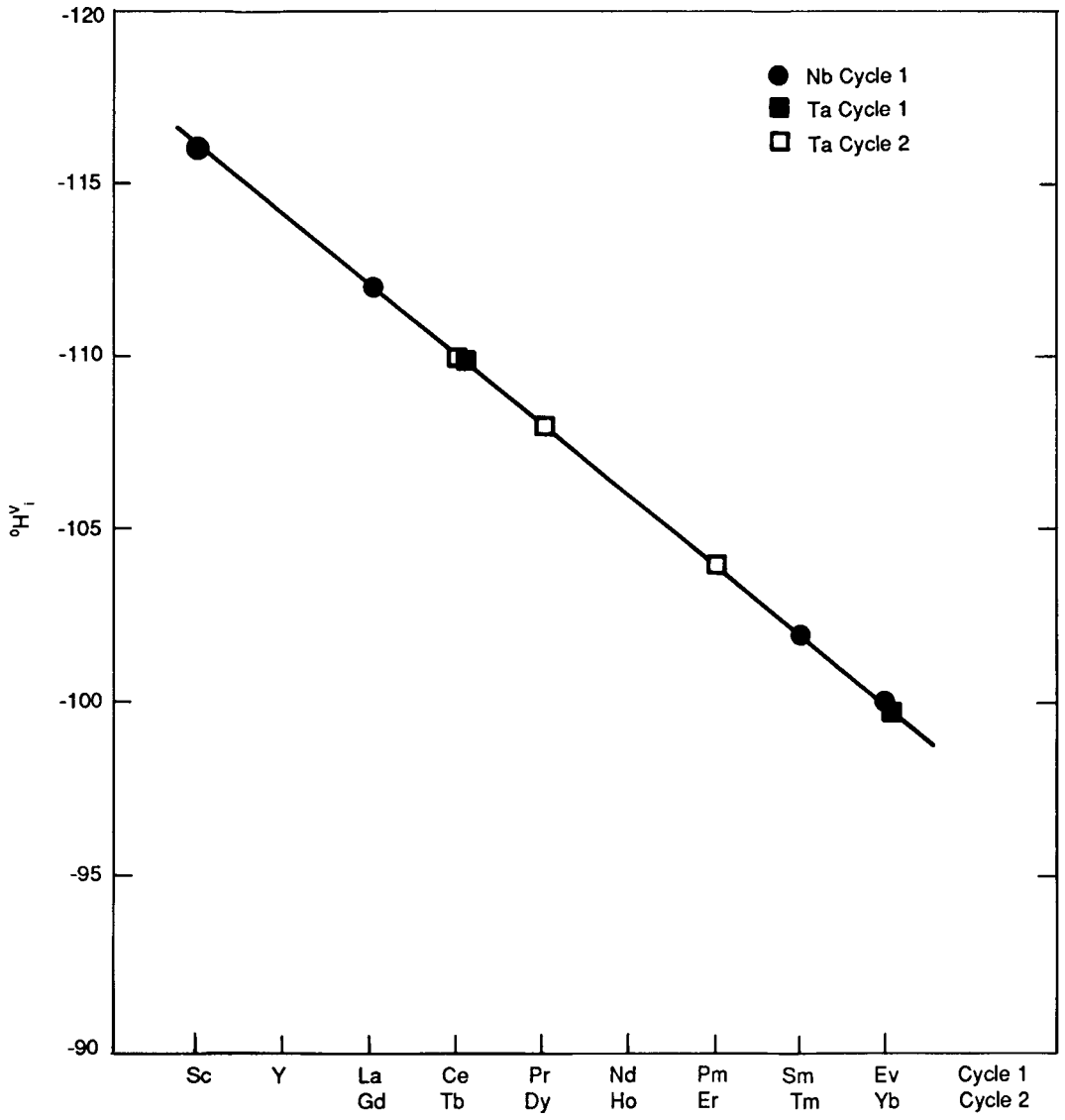

FIGURE 49. Empirically Determined Values for H_i^V for Rare Earth Diagrams with Niobium and Tantalum

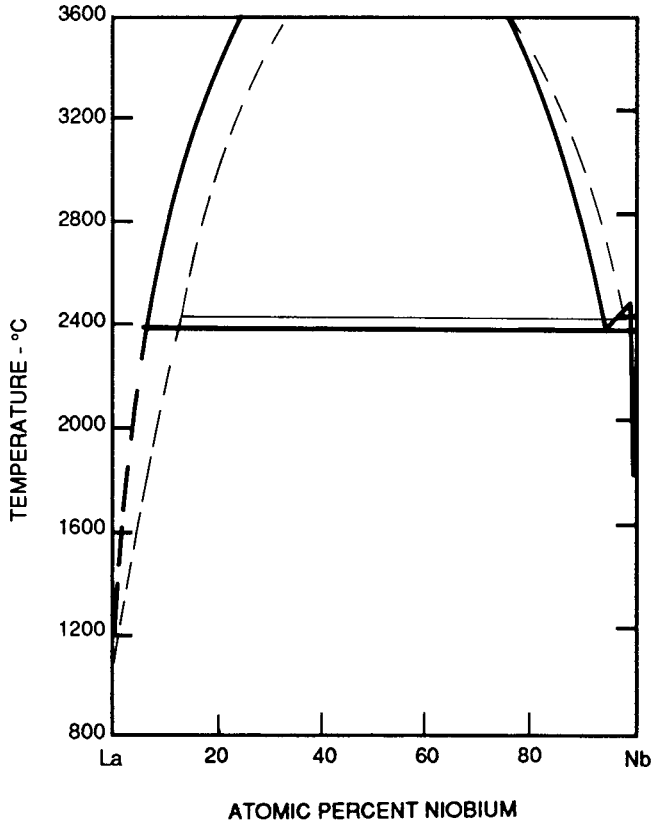

FIGURE 50. Calculated vs Estimated La-Nb Diagram

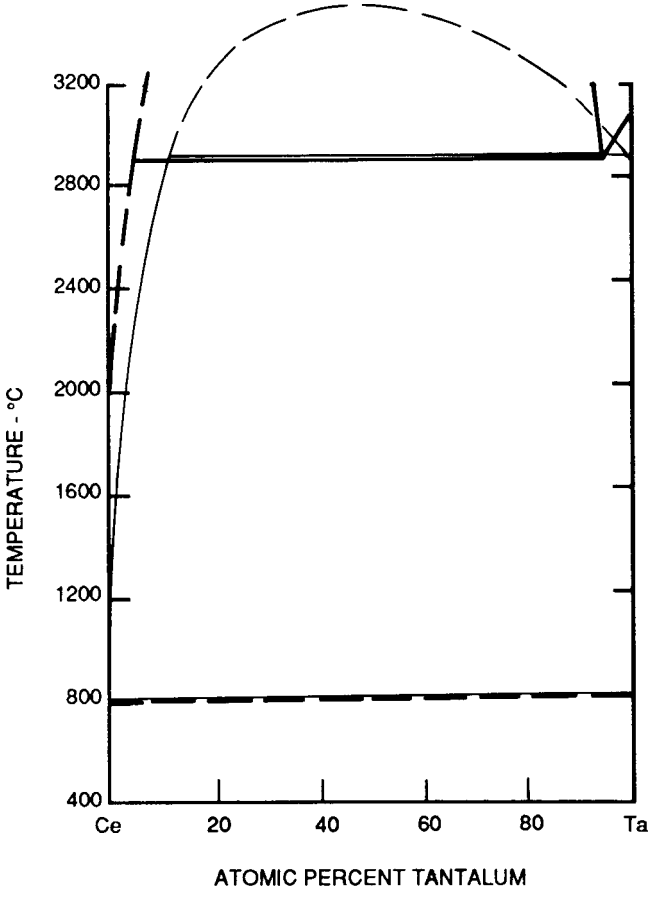

FIGURE 51. Calculated vs Estimated Ce-Ta Diagram

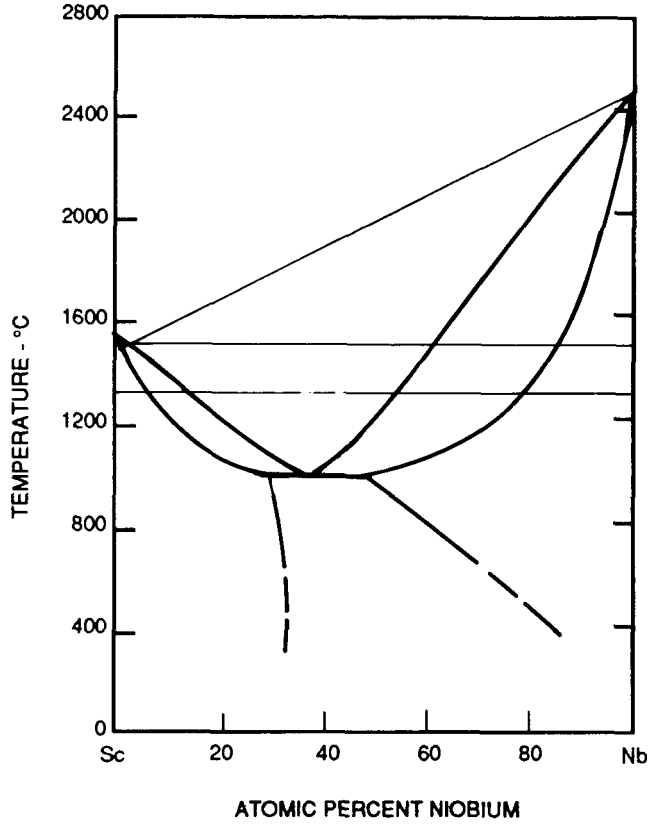

FIGURE 53. Calculated vs Experimental Nb-Sc Diagram

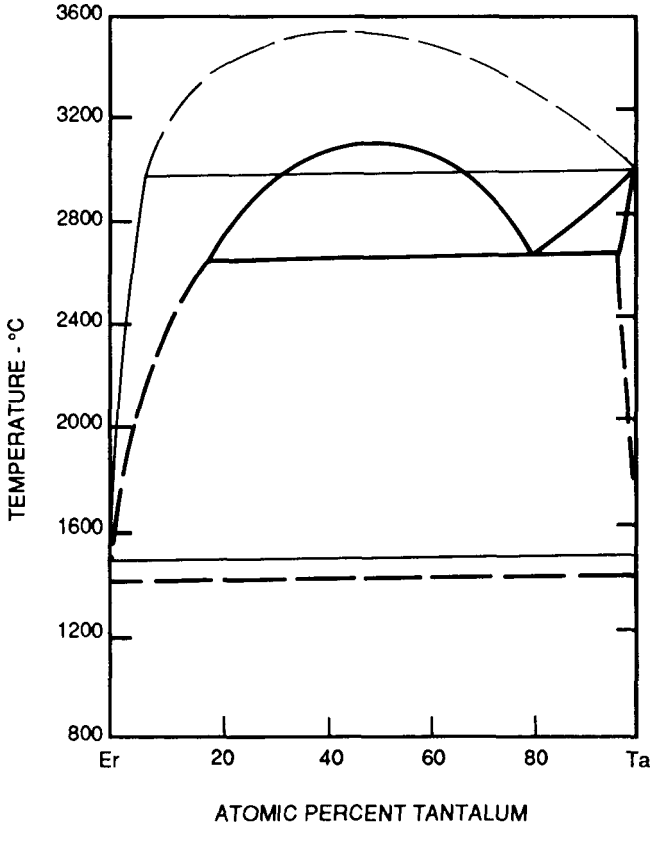

FIGURE 52. Calculated vs Estimated Er-Ta Diagram

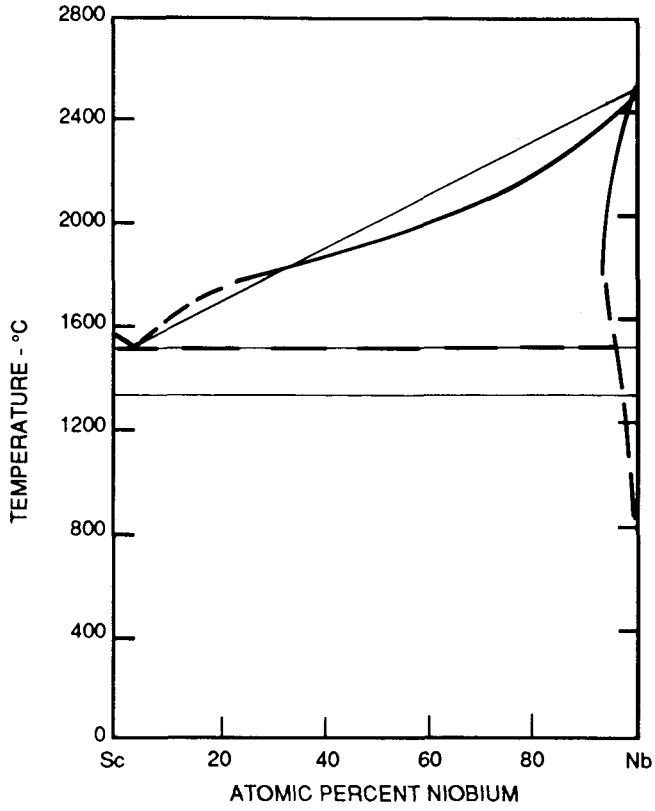

FIGURE 54. Calculated vs Experimental Nb-Sc Diagram, using Adjusted Value of ${}^{0}H^{V}$

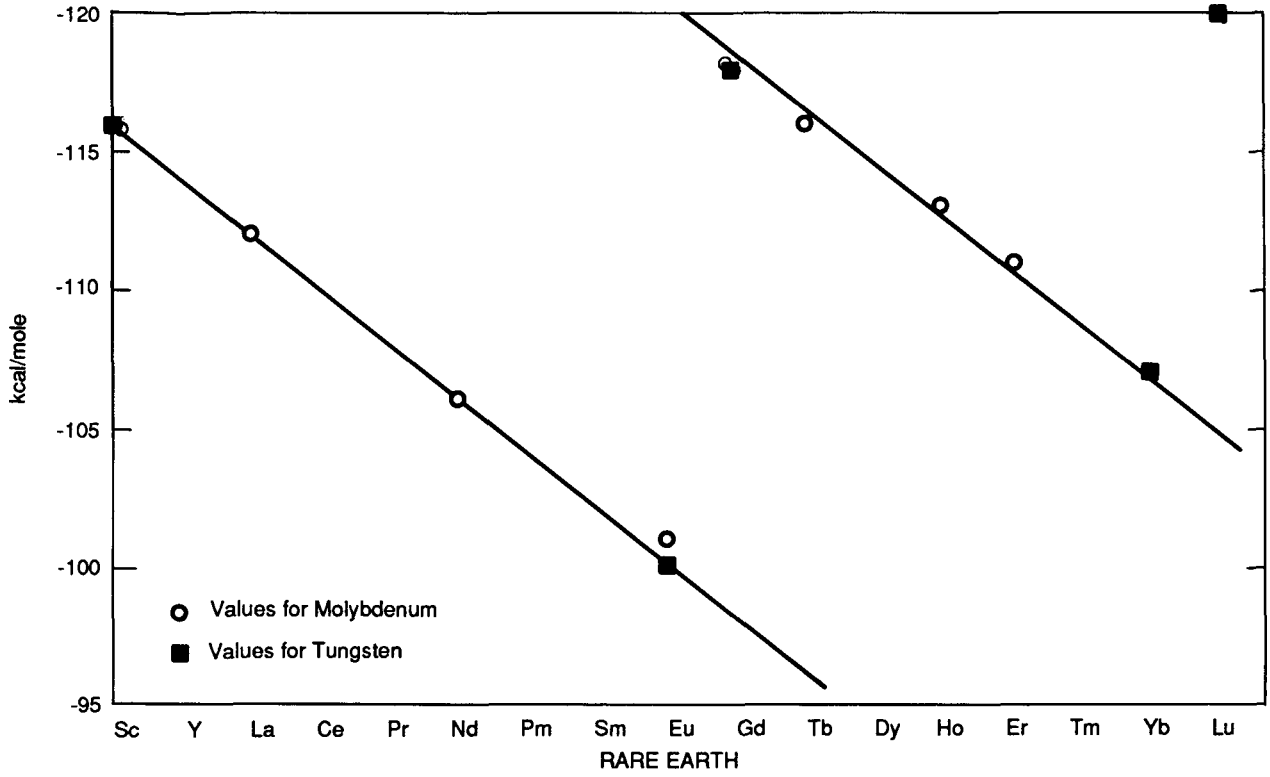

FIGURE 55. Empirically Determined Values of H_i^V for the Rare Earths with Molybdenum and Tungsten

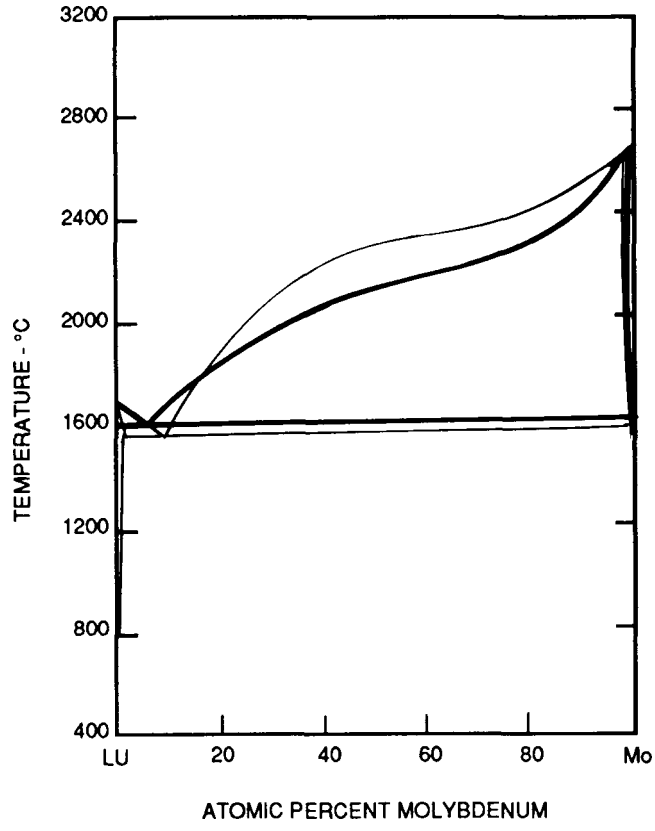

FIGURE 57. Calculated vs Experimental Lu-Mo Diagram

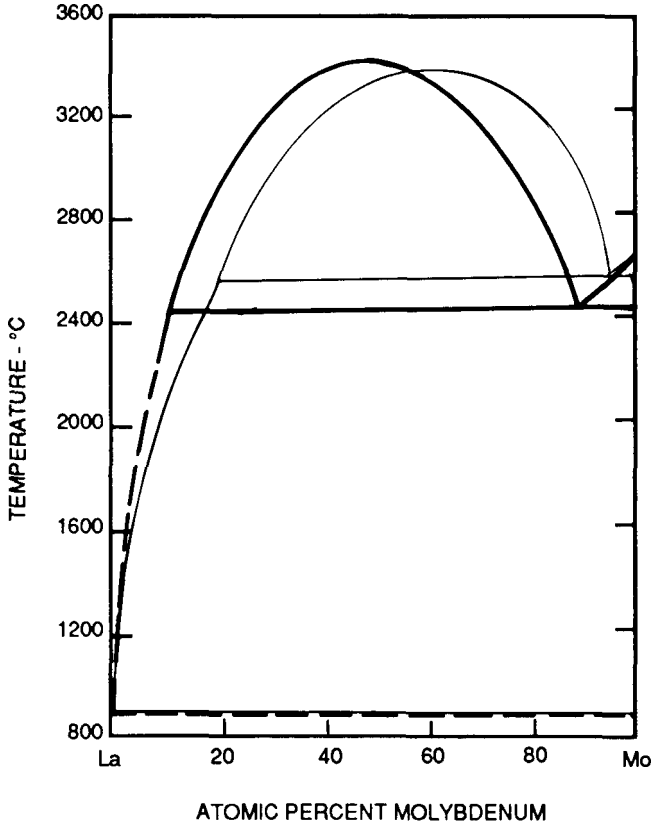

FIGURE 56. Calculated vs Experimental La-Mo Diagram

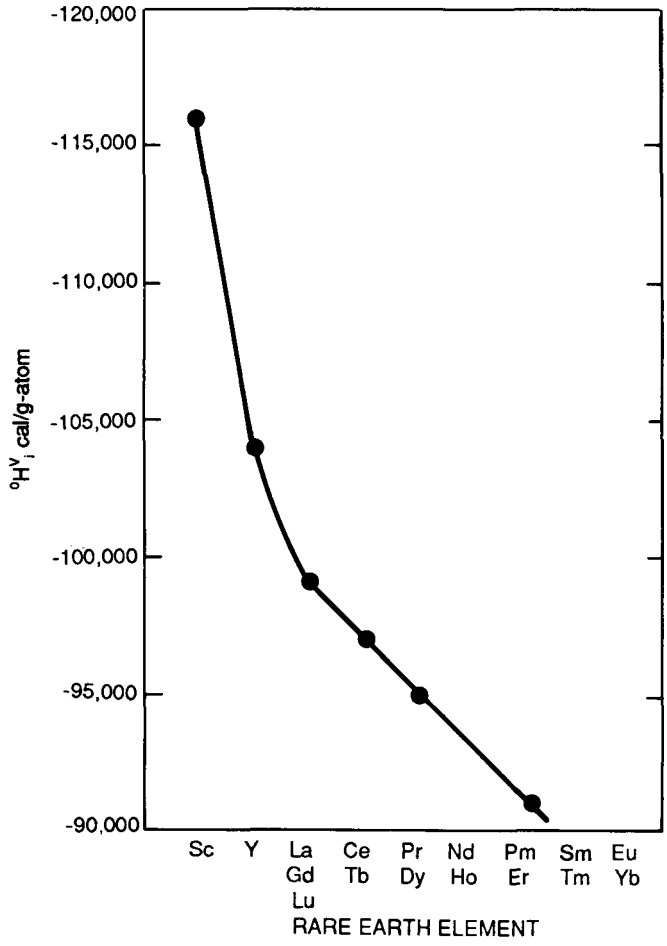

FIGURE 58. Empirically Determined Values of $^{0}H_{i}^{V}$ for the Rare Earths with Rhenium

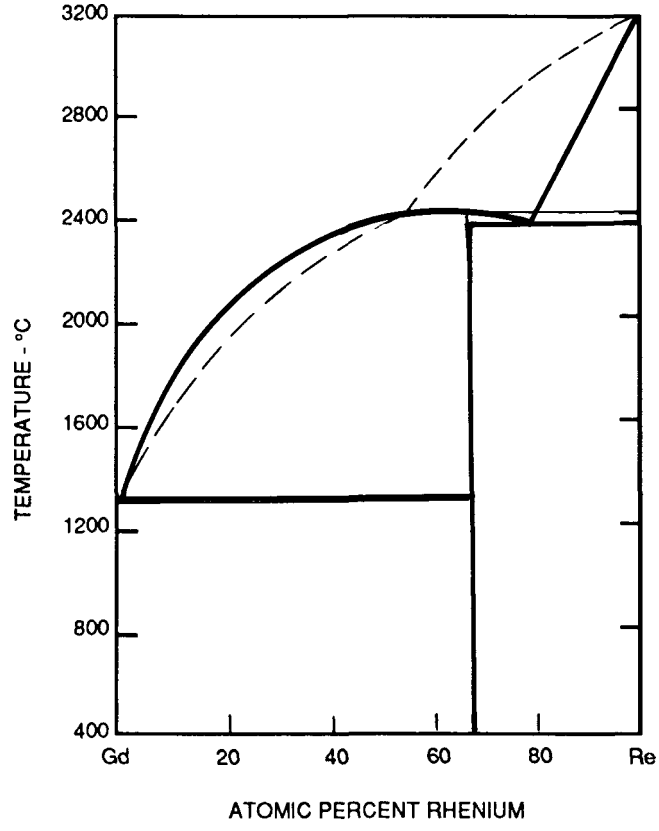

FIGURE 59. Calculated vs Estimated Gd-Re Diagram

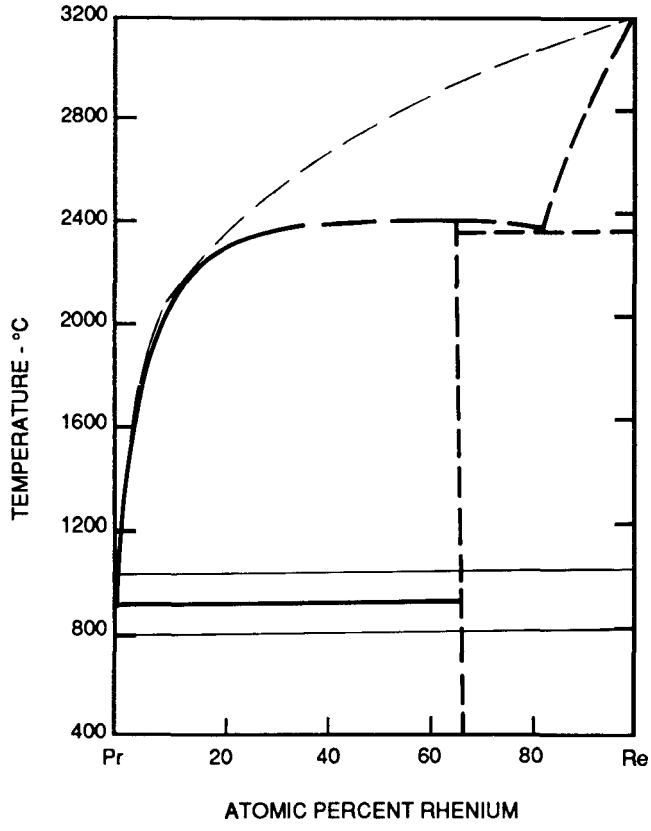

FIGURE 61. Calculated vs Estimated Pr-Re Diagram

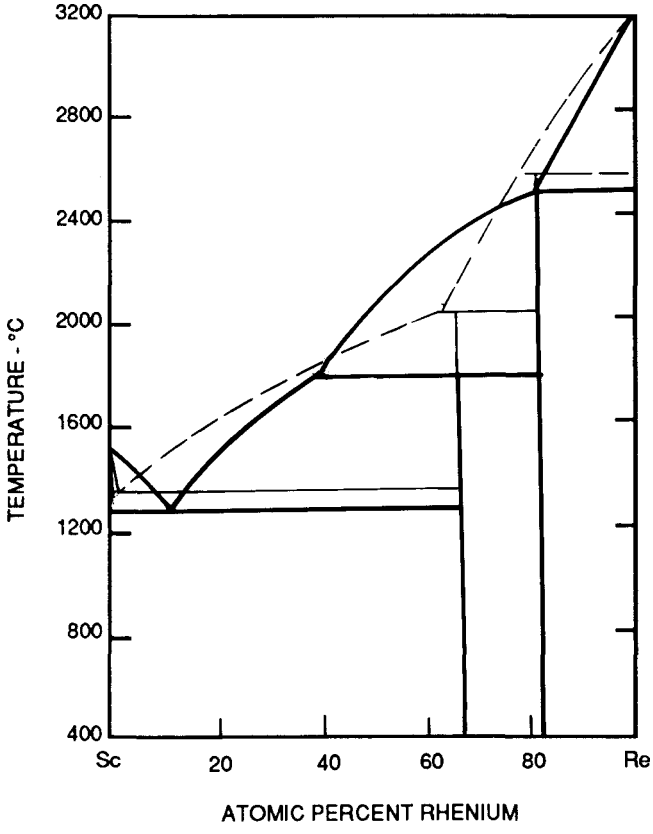

FIGURE 60. Calculated vs Estimated Re-Sc Diagram

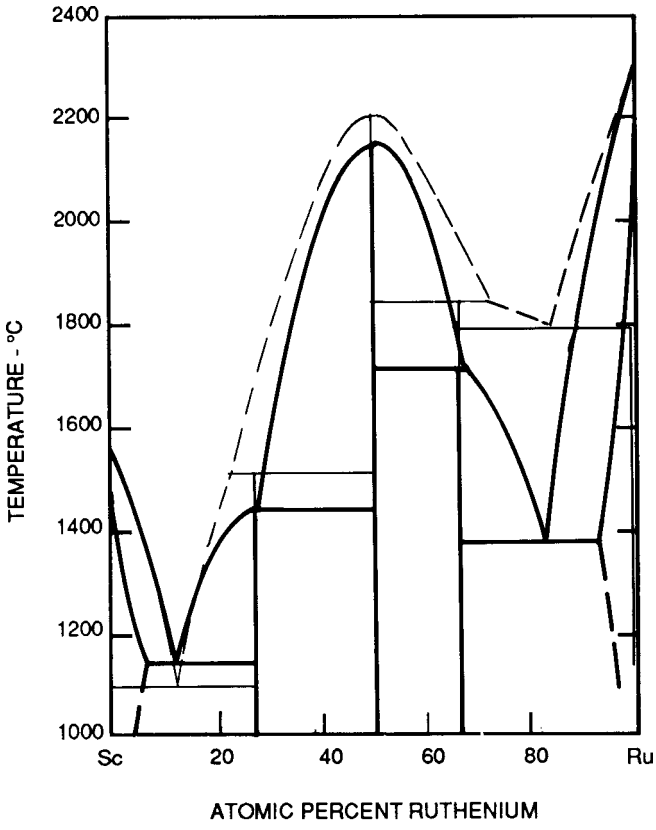

FIGURE 62. Calculated vs Estimated Ru-Sc Diagram

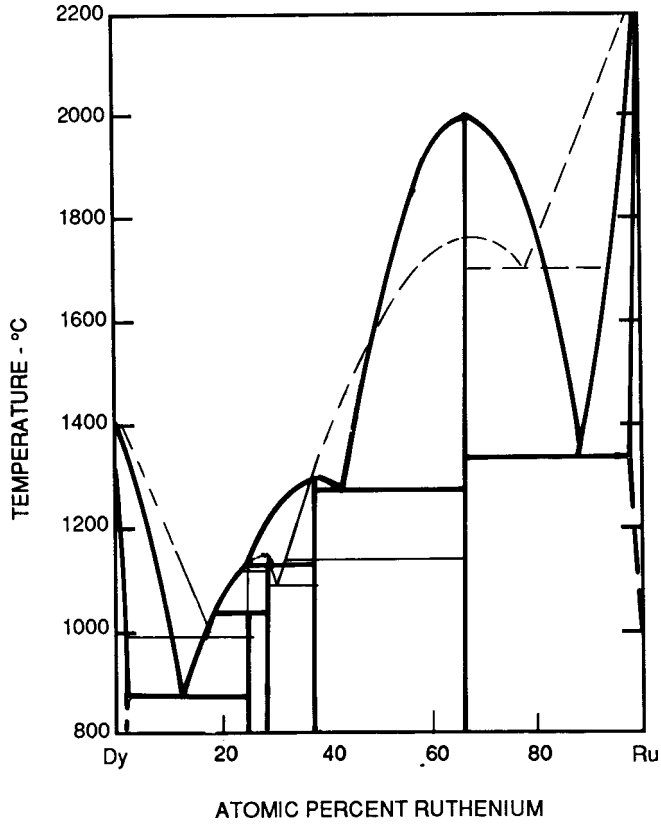

FIGURE 63. Calculated vs Estimated Dy-Ru Diagram

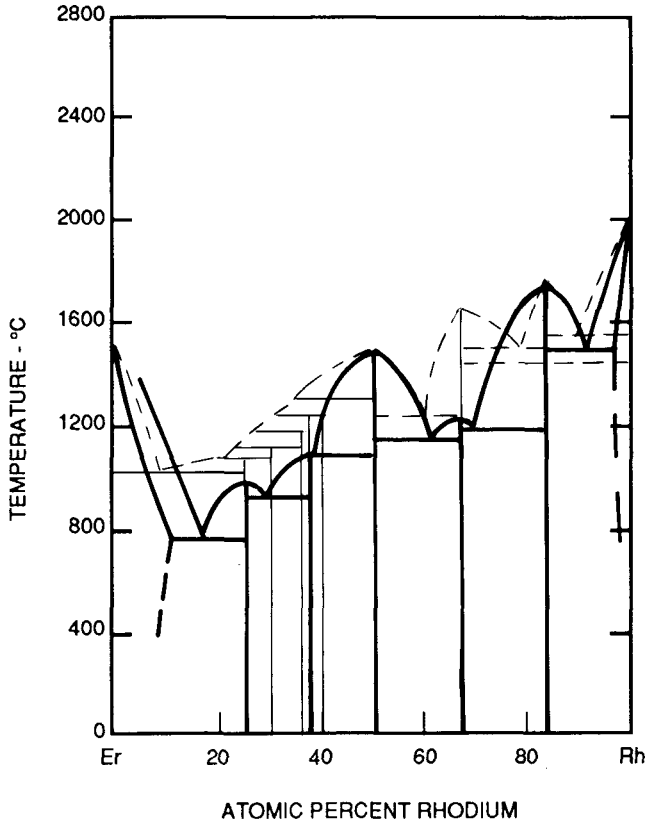

FIGURE 65. Calculated vs Estimated Er-Rh Diagram

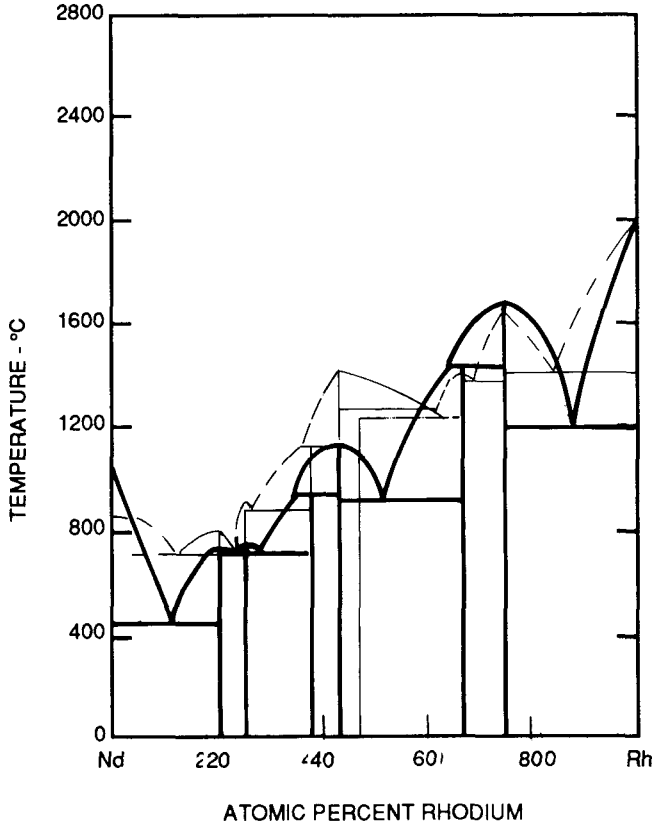

FIGURE 64. Calculated vs Estimated Nd-Rh Diagram

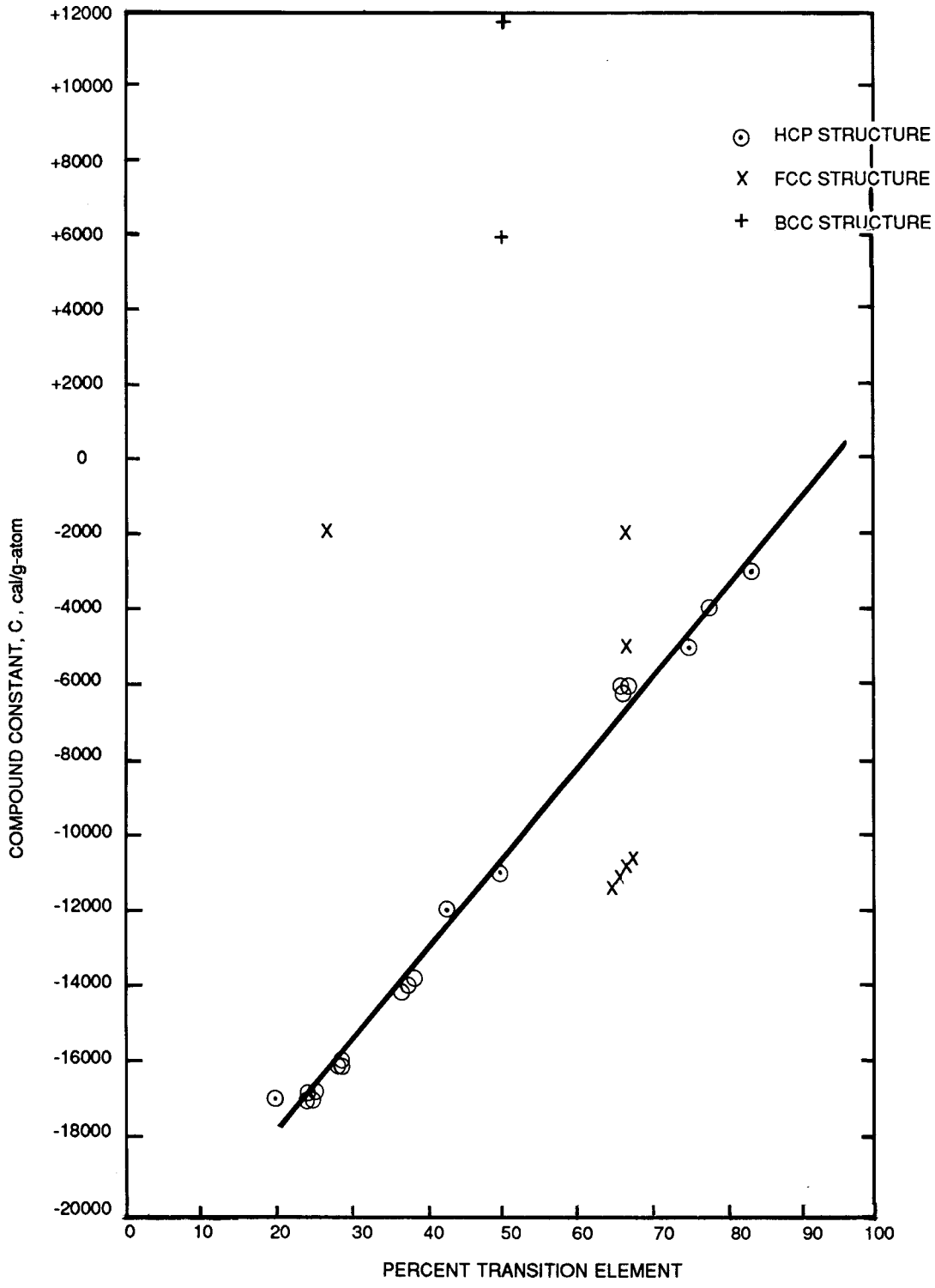

FIGURE 66. Empirically Determined Values for Constant used in Determining Liquidus Curves for Intermetallic Compounds for Diagrams Between Rare Earths and Ruthenium, Osmium, Rhodium, and Iridium

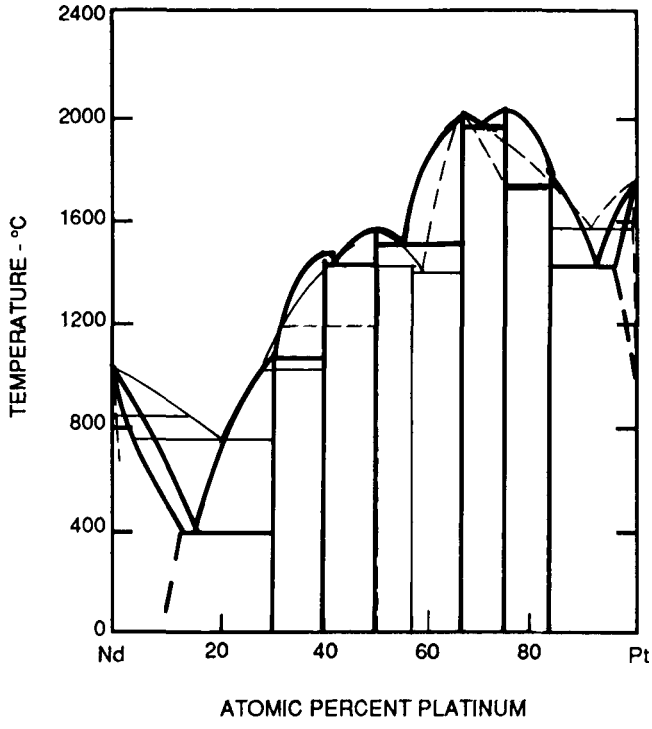

FIGURE 67. Calculated vs Experimental Nd-Pt Diagram

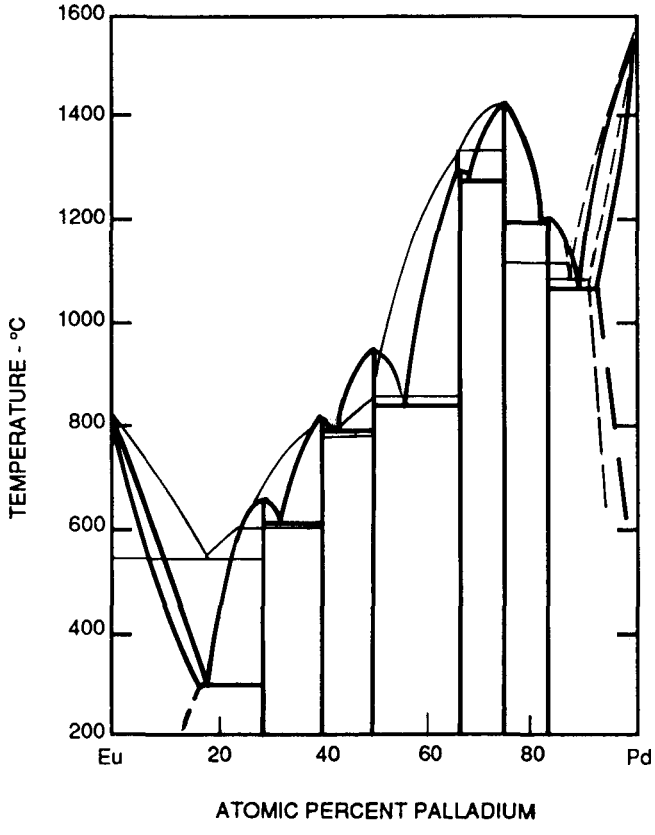

FIGURE 68. Calculated vs Experimental Eu-Pd Diagram

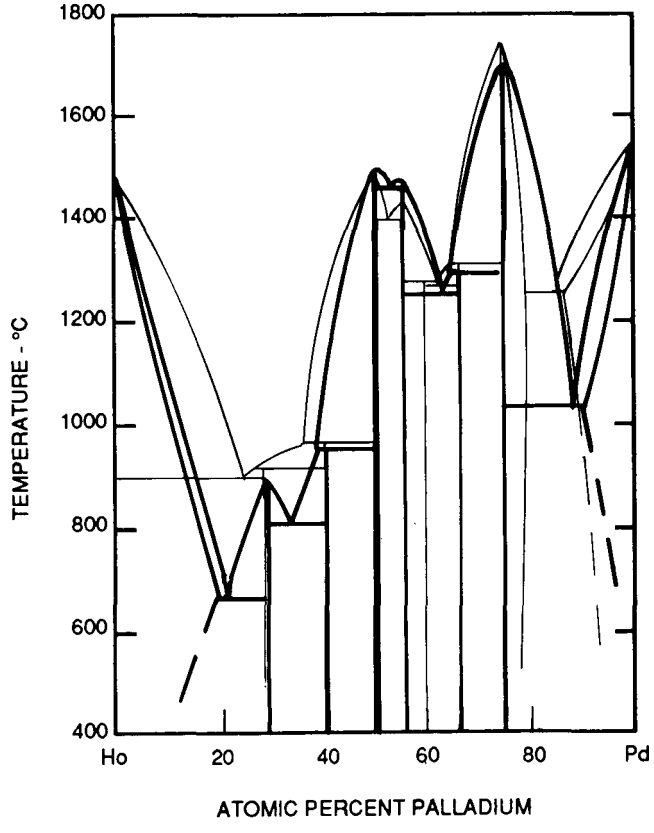

FIGURE 69. Calculated vs Experimental Ho-Pd Diagram

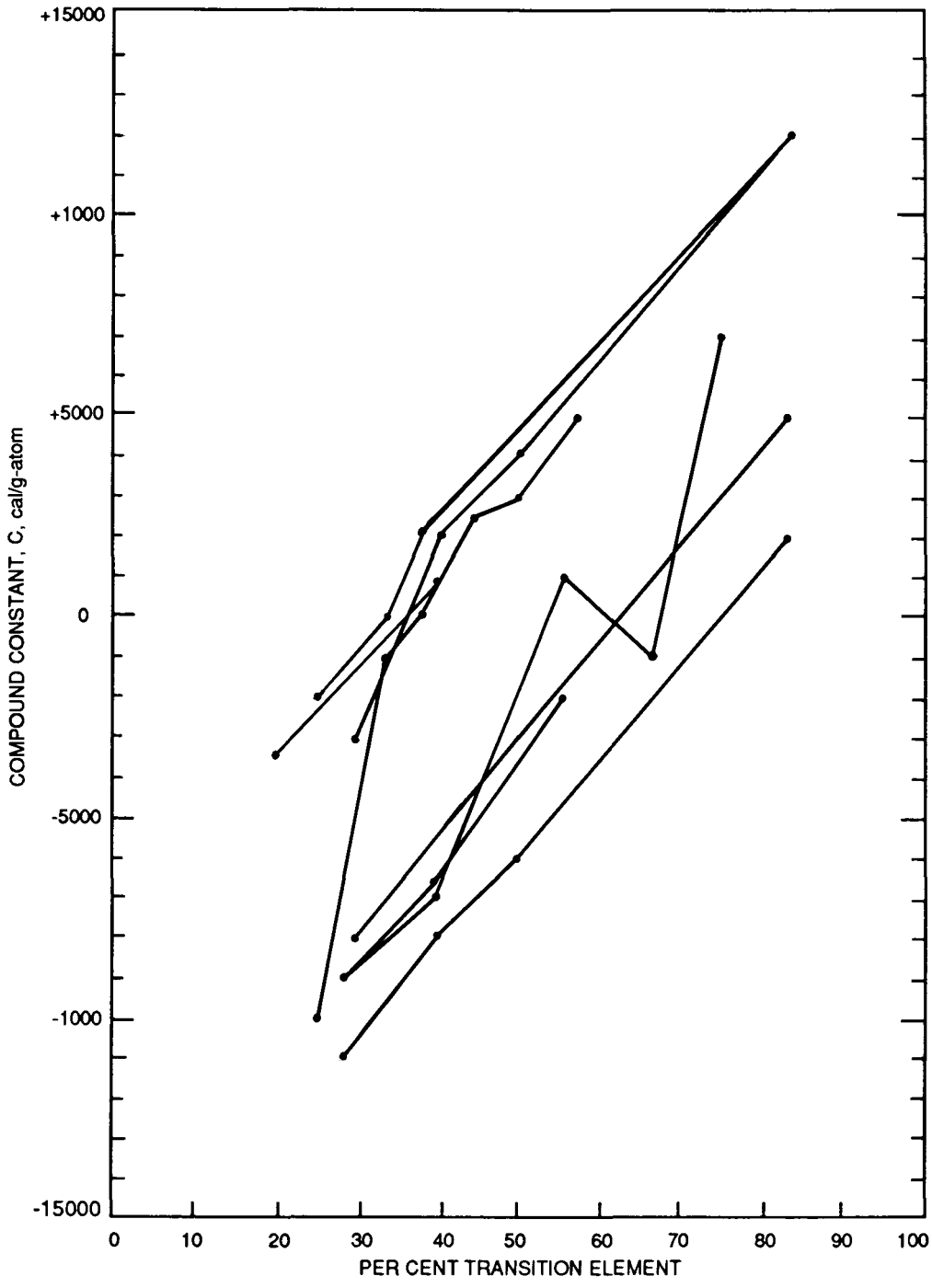

FIGURE 70. Empirically Determined Values for the Constant, C, for use with Palladium and Platinum - HCP Structure Compounds

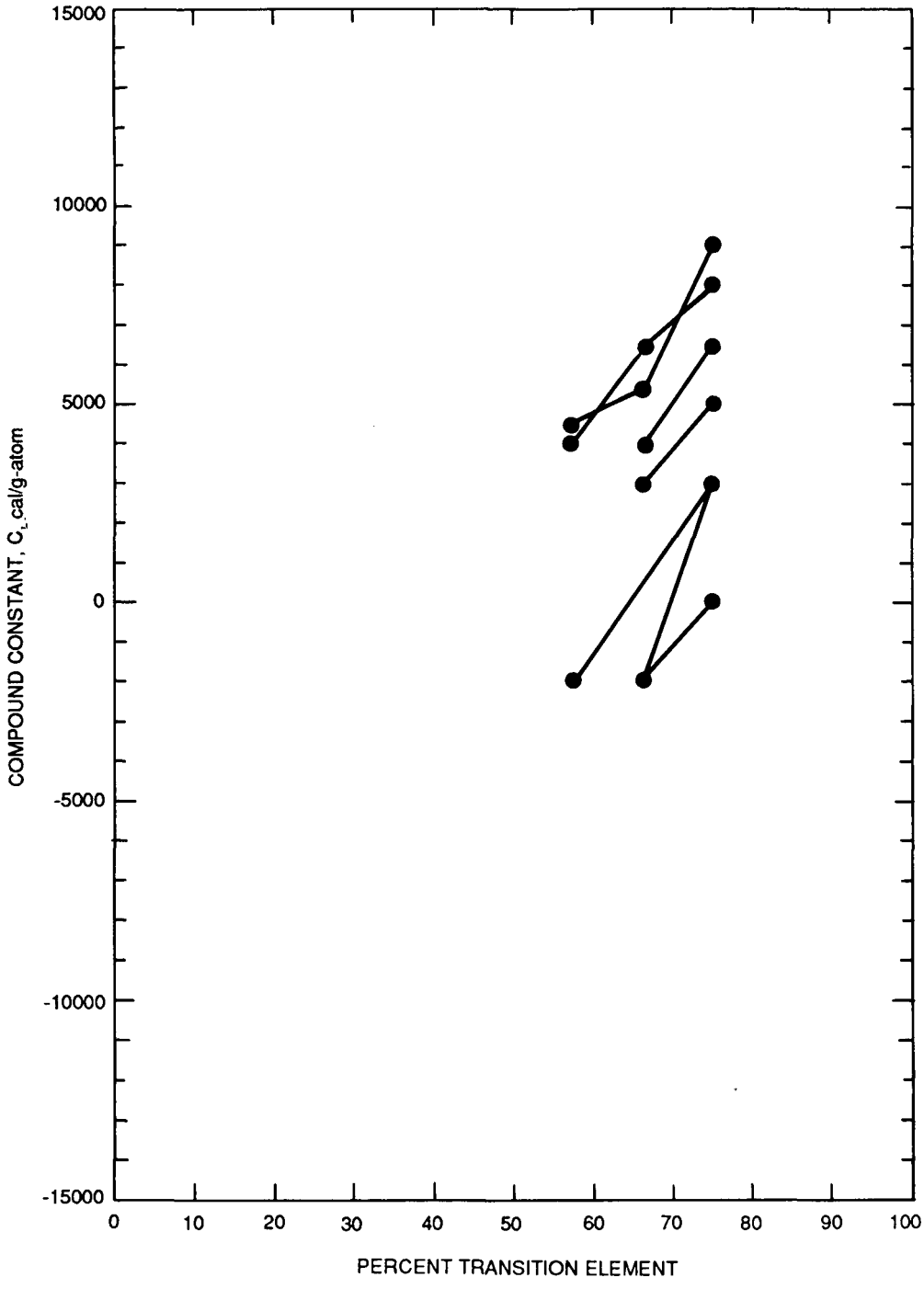

FIGURE 71. Empirically Determined Values for the Constant, C, for use with Palladium and Platinum - FCC Structure Compounds

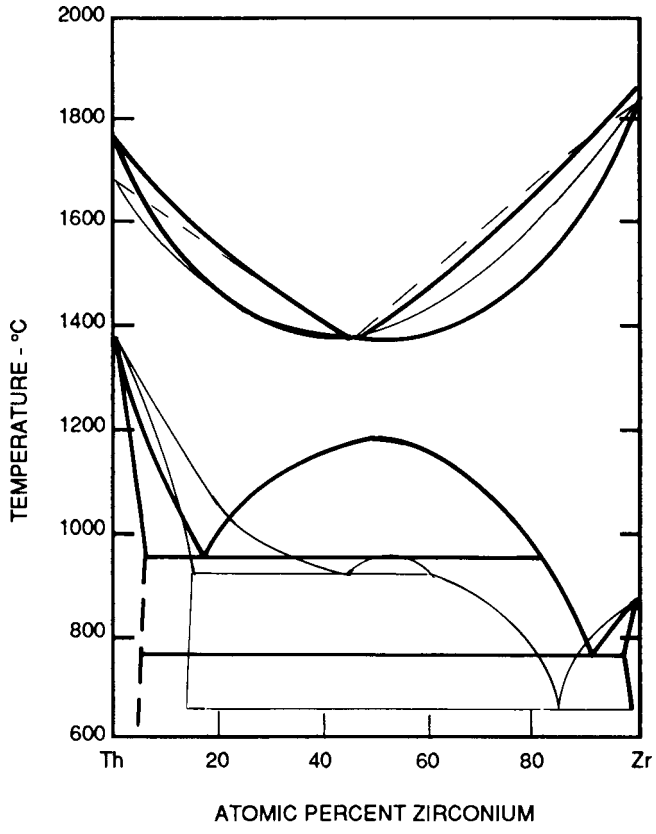

FIGURE 72. Calculated vs Experimental Th-Zr Diagram

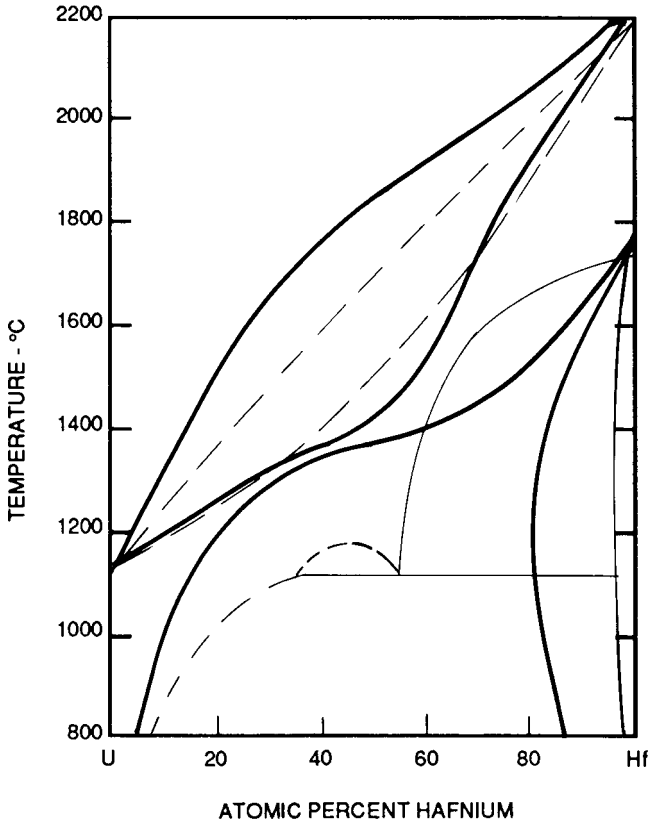

FIGURE 73. Calculated vs Experimental Hf-U Diagram

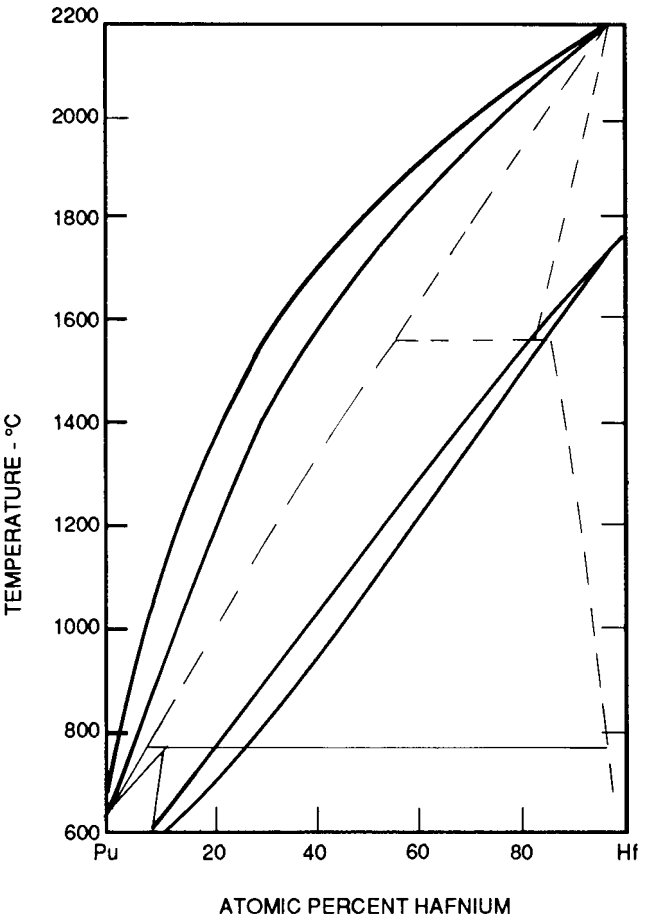

FIGURE 75. Calculated vs Estimated Hf-Pu Diagram

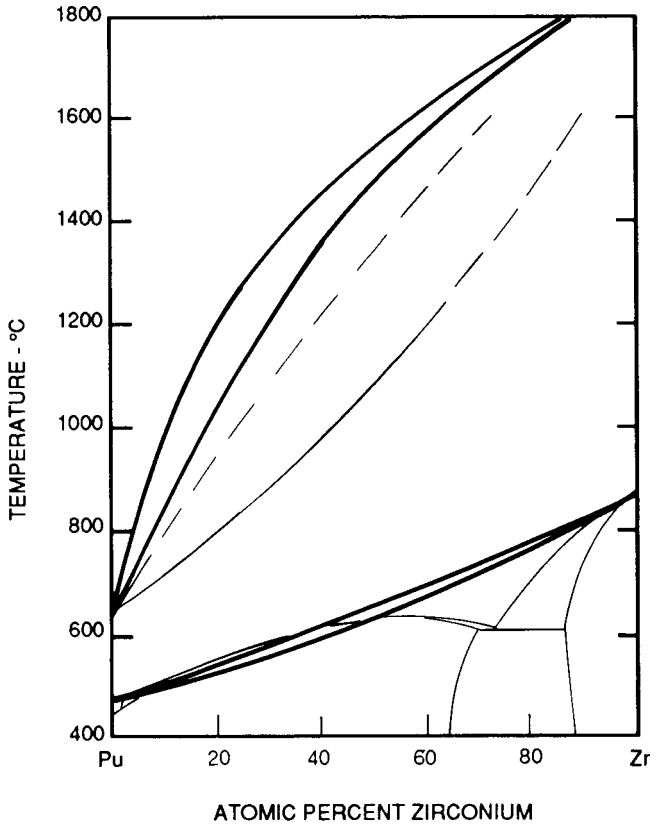

FIGURE 74. Calculated vs Experimental Pu-Zr Diagram

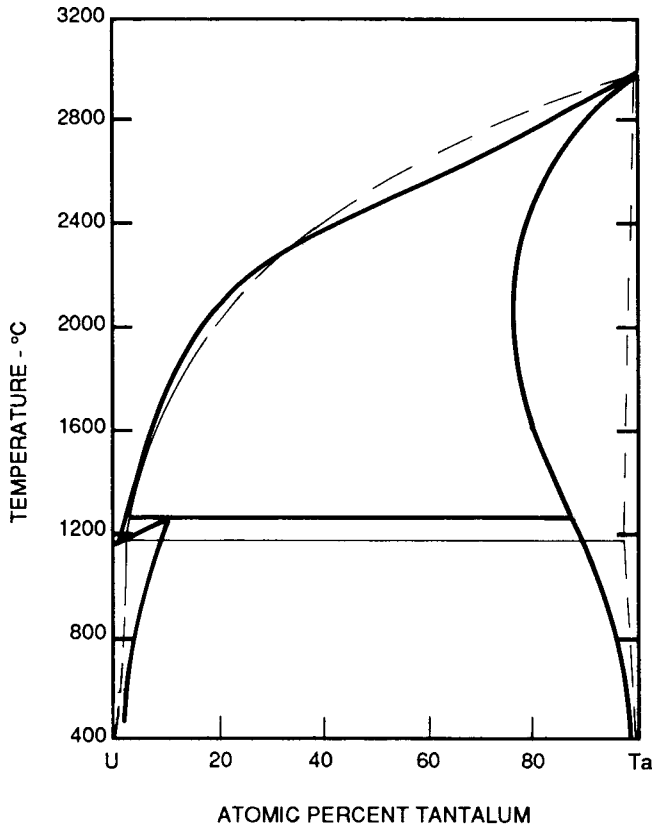

FIGURE 76. Calculated vs Estimated Ta-U Diagram

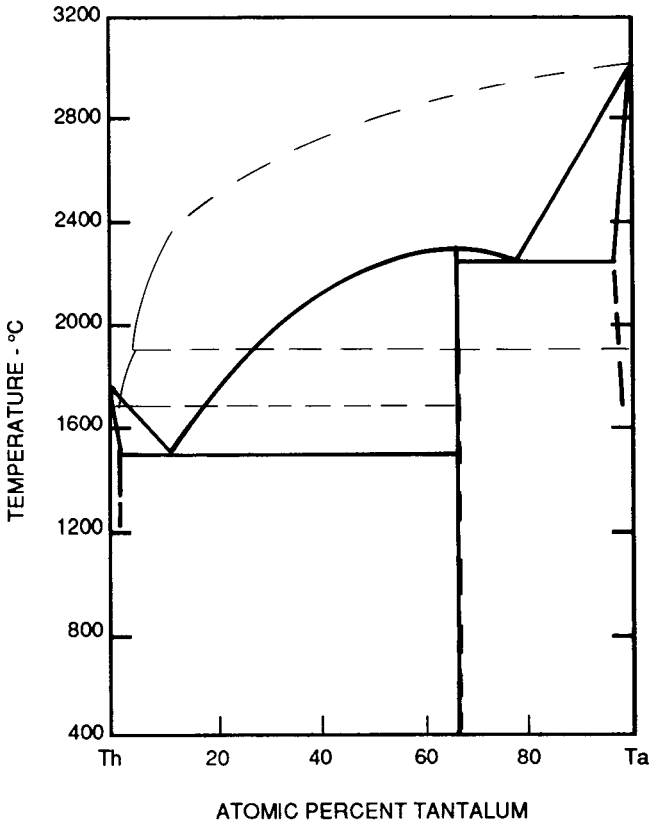

FIGURE 77. Calculated vs Estimated Ta-Th Diagram

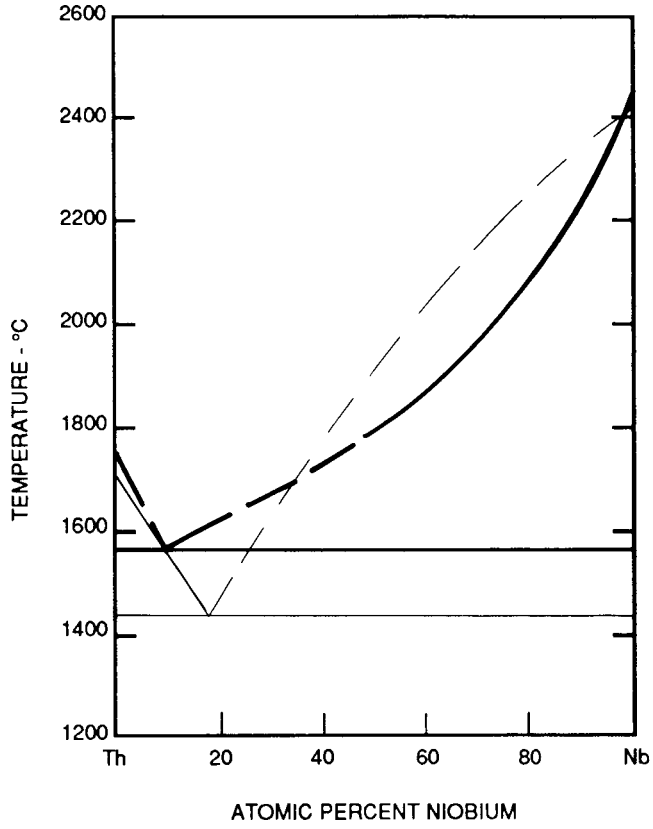

FIGURE 79. Calculated vs Estimated Nb-Th Diagram

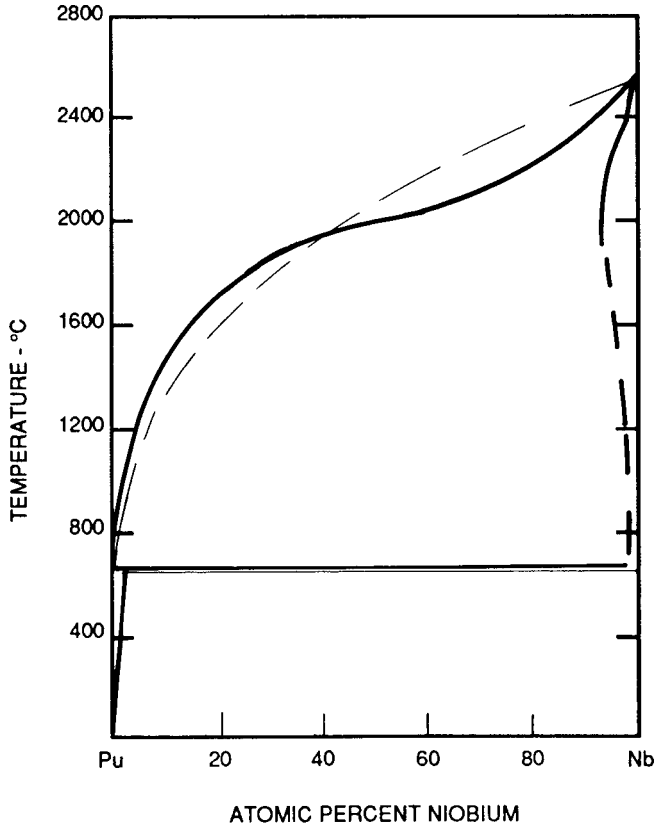

FIGURE 78. Calculated vs Estimated Nb-Pu Diagram

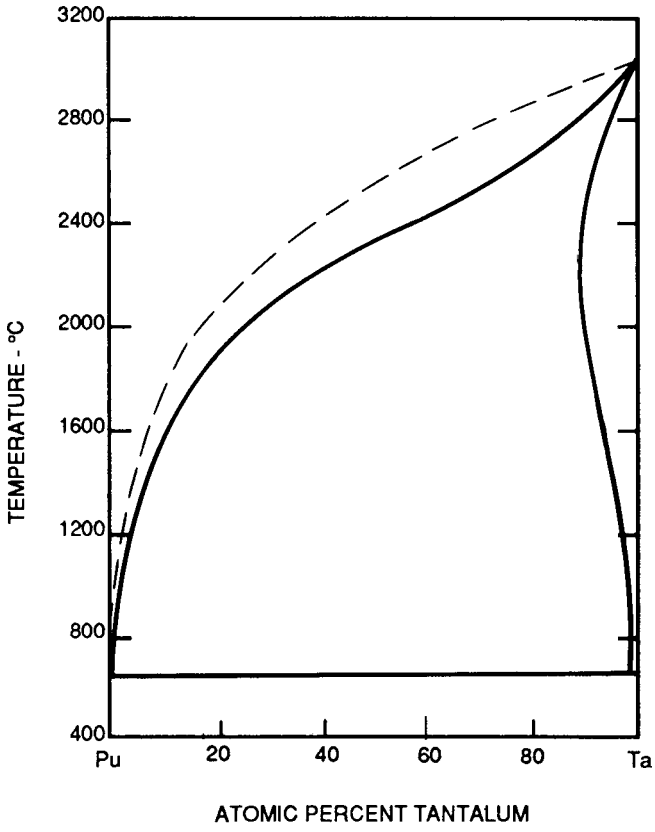

FIGURE 80. Calculated vs Estimated Pu-Ta Diagram

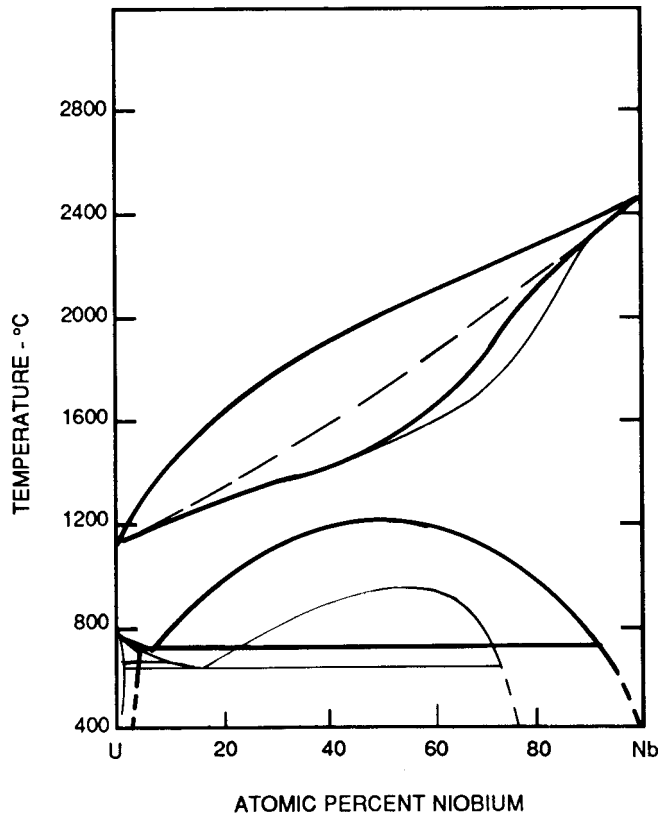

FIGURE 81. Calculated vs Experimental Nb-U Diagram

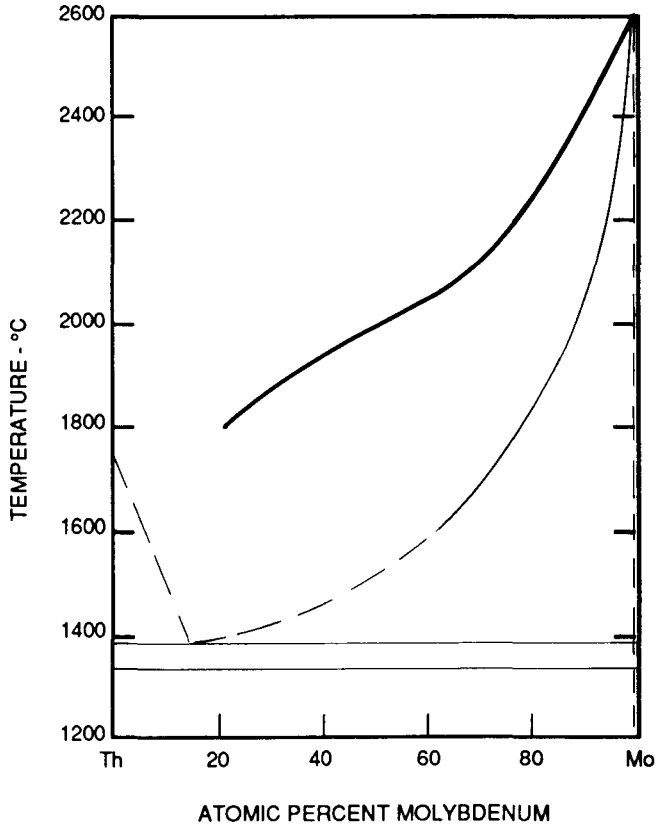

FIGURE 82. Calculated vs Experimental Mo-Th Diagram

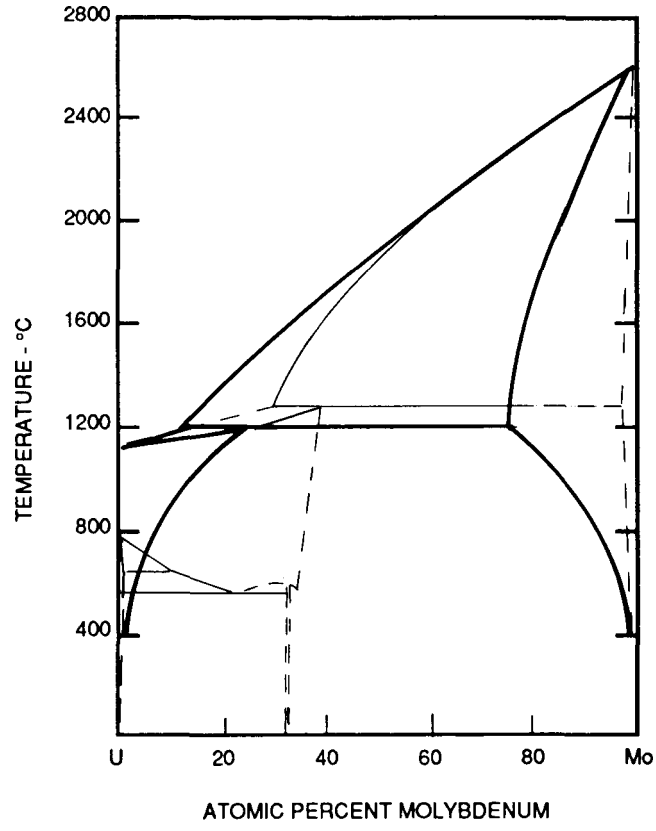

FIGURE 83. Calculated vs Experimental Mo-U Diagram

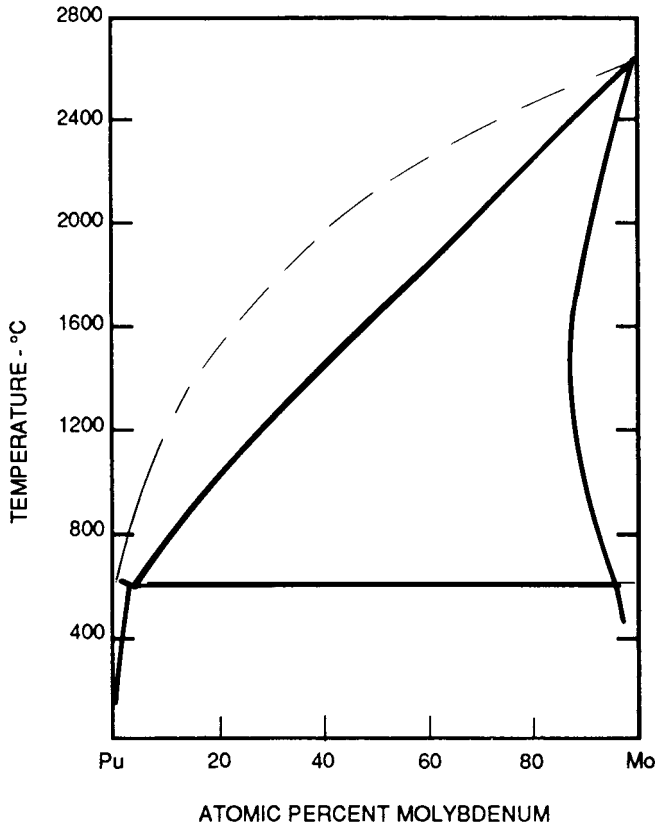

FIGURE 84. Calculated vs Estimated Mo-Pu Diagram

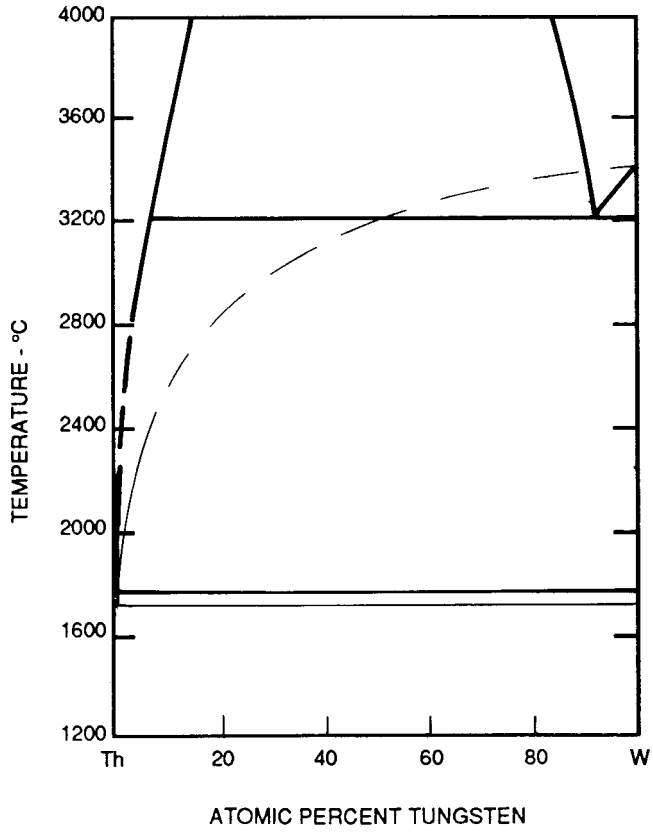

FIGURE 85. Calculated vs Estimated Th-W Diagram

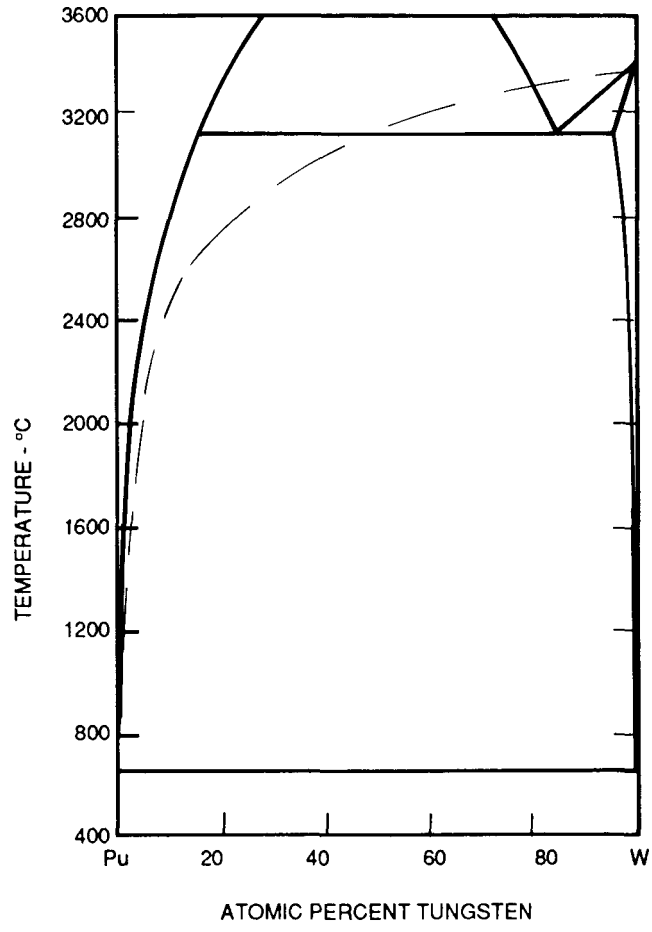

FIGURE 87. Calculated vs Estimated Pu-W Diagram

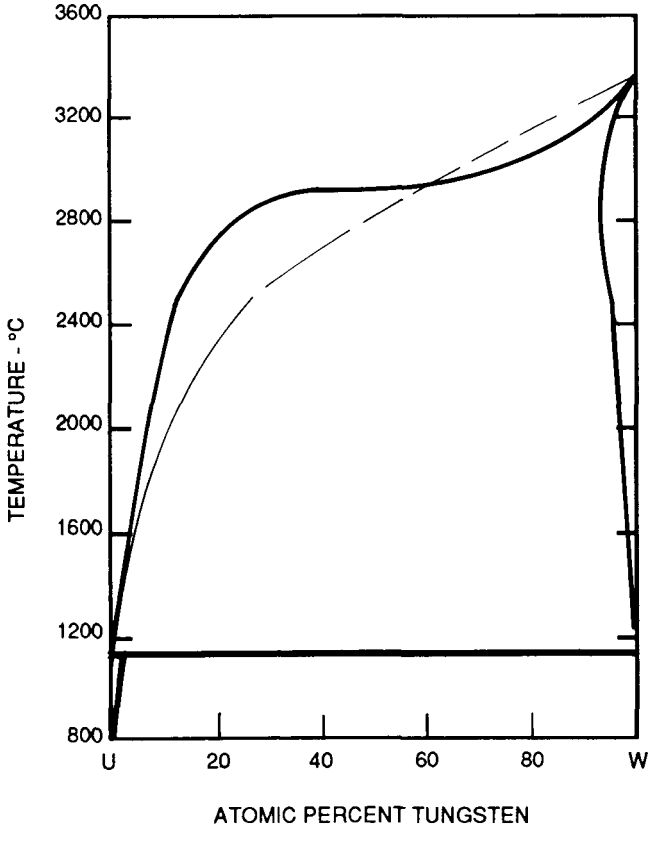

FIGURE 86. Calculated vs Experimental U-W Diagram

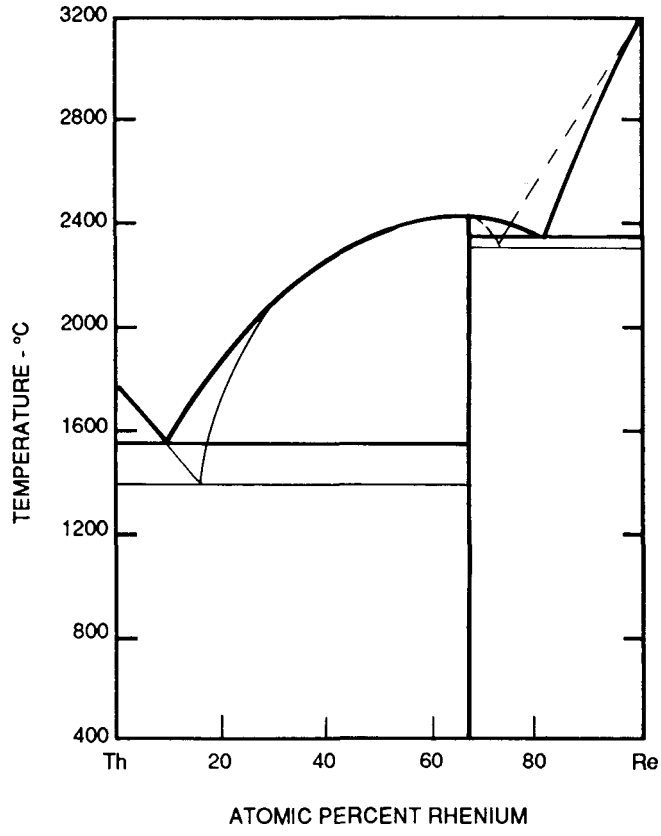

FIGURE 88. Calculated vs Experimental Re-Th Diagram

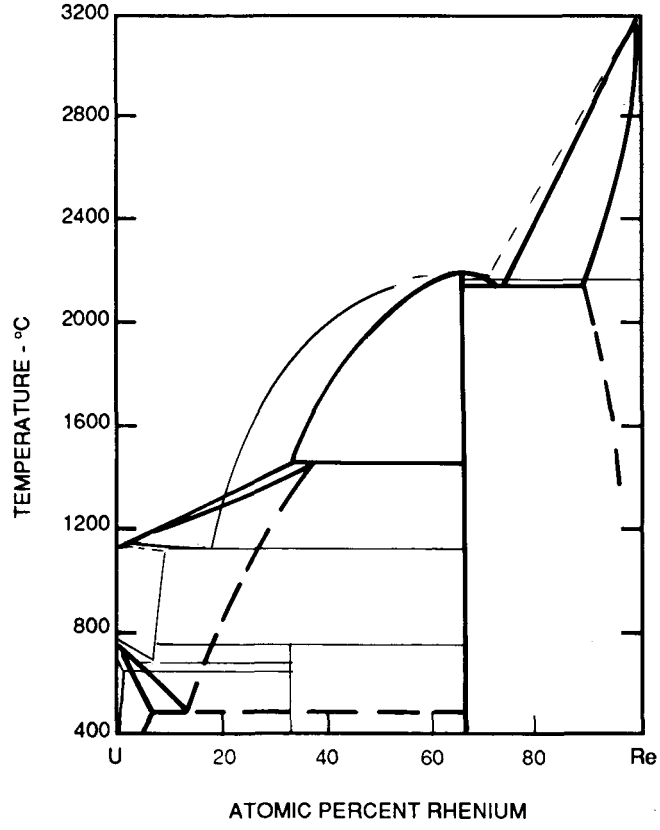

FIGURE 89. Calculated vs Experimental Re-U Diagram

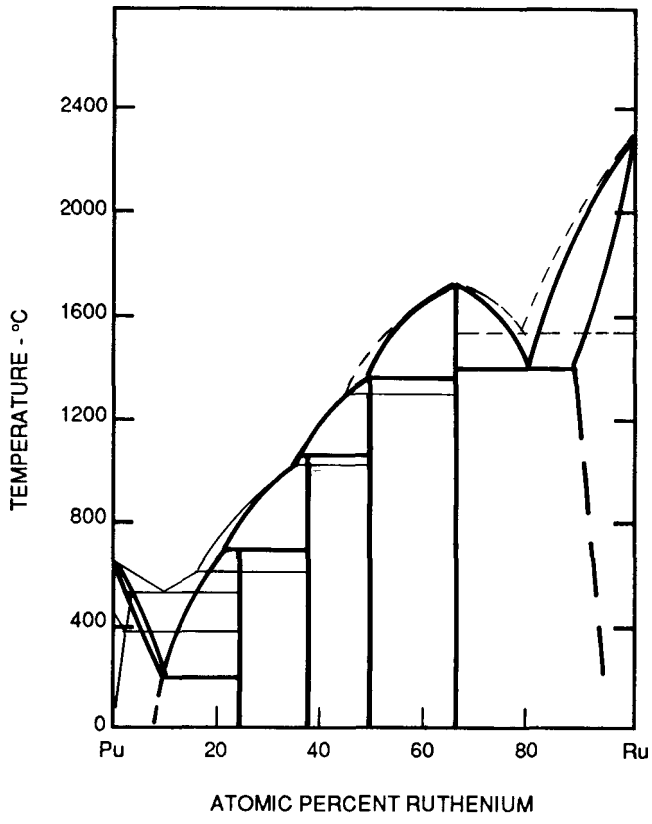

FIGURE 91. Calculated vs Experimental Pu-Ru Diagram

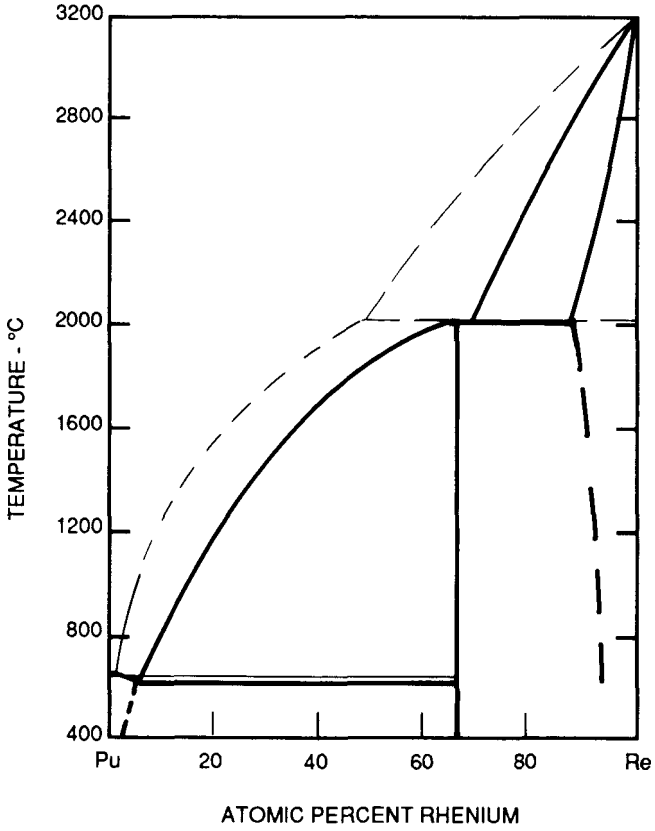

FIGURE 90. Calculated vs Estimated Pu-Re Diagram

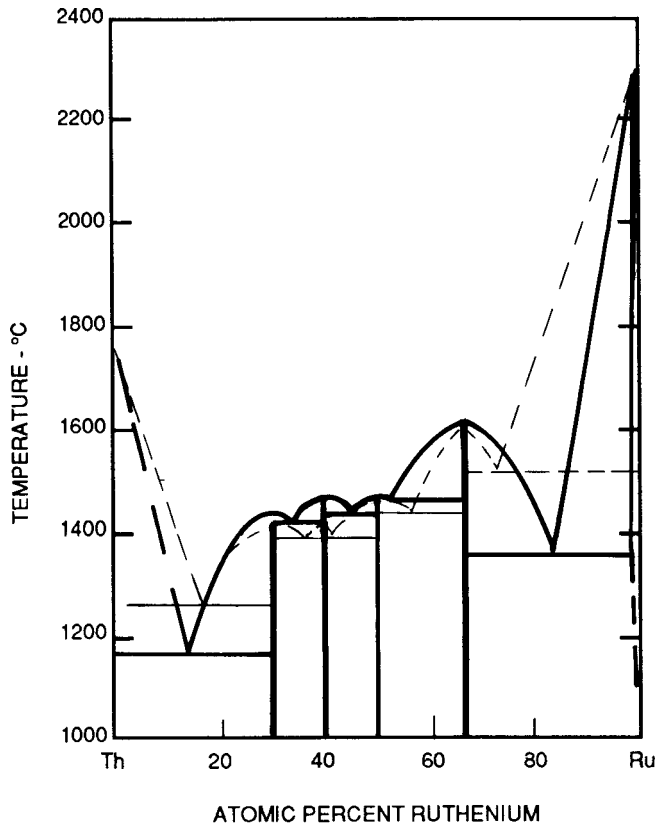

FIGURE 92. Calculated vs Estimated Ru-Th Diagram

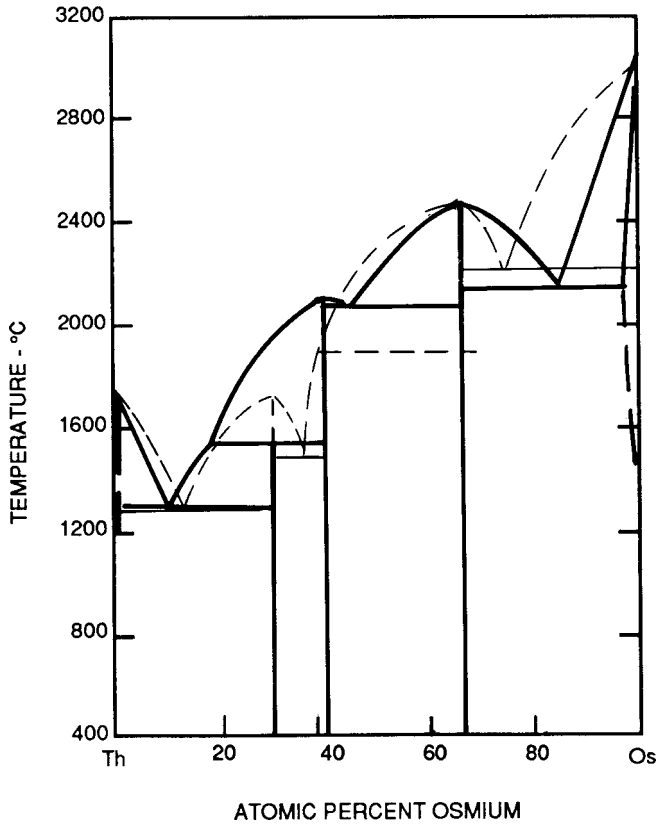

FIGURE 93. Calculated vs Estimated Os-Th Diagram

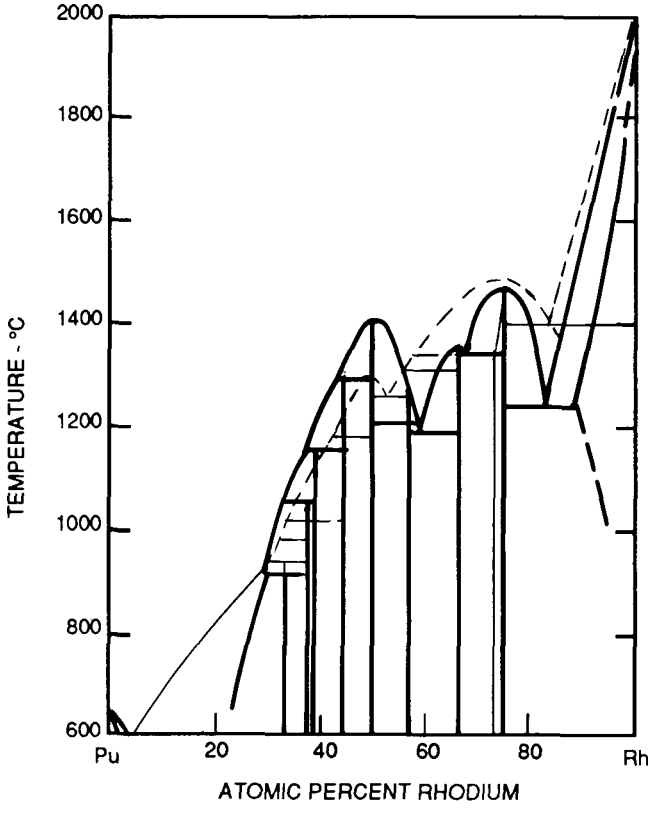

FIGURE 94. Calculated vs Estimated Pu-Rh Diagram

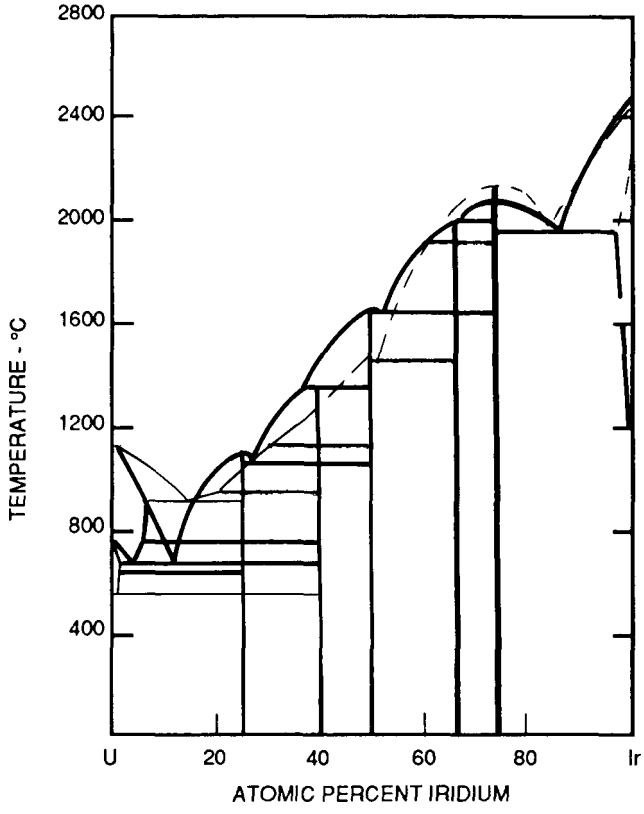

FIGURE 95. Calculated vs Experimental Ir-U Diagram

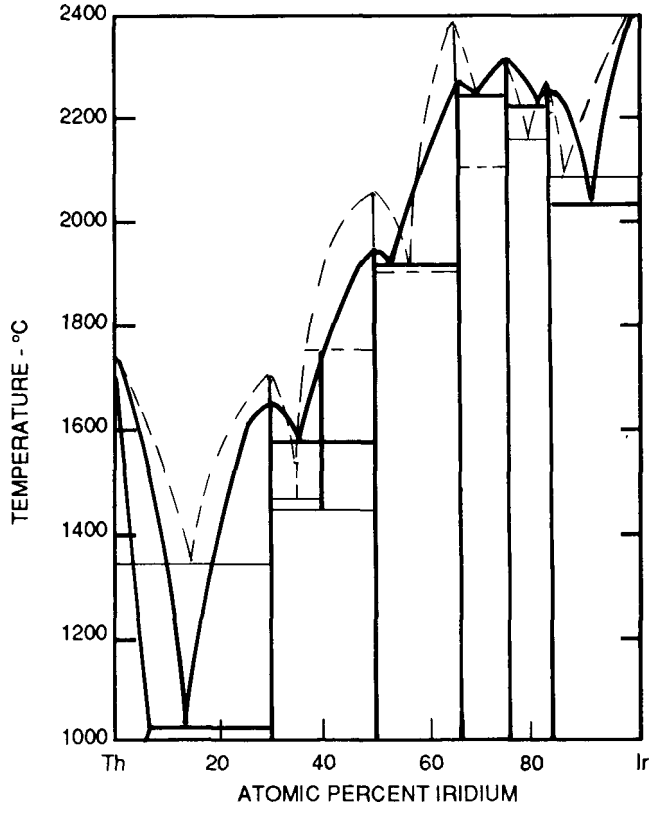

FIGURE 96. Calculated vs Estimated Ir-Th Diagram

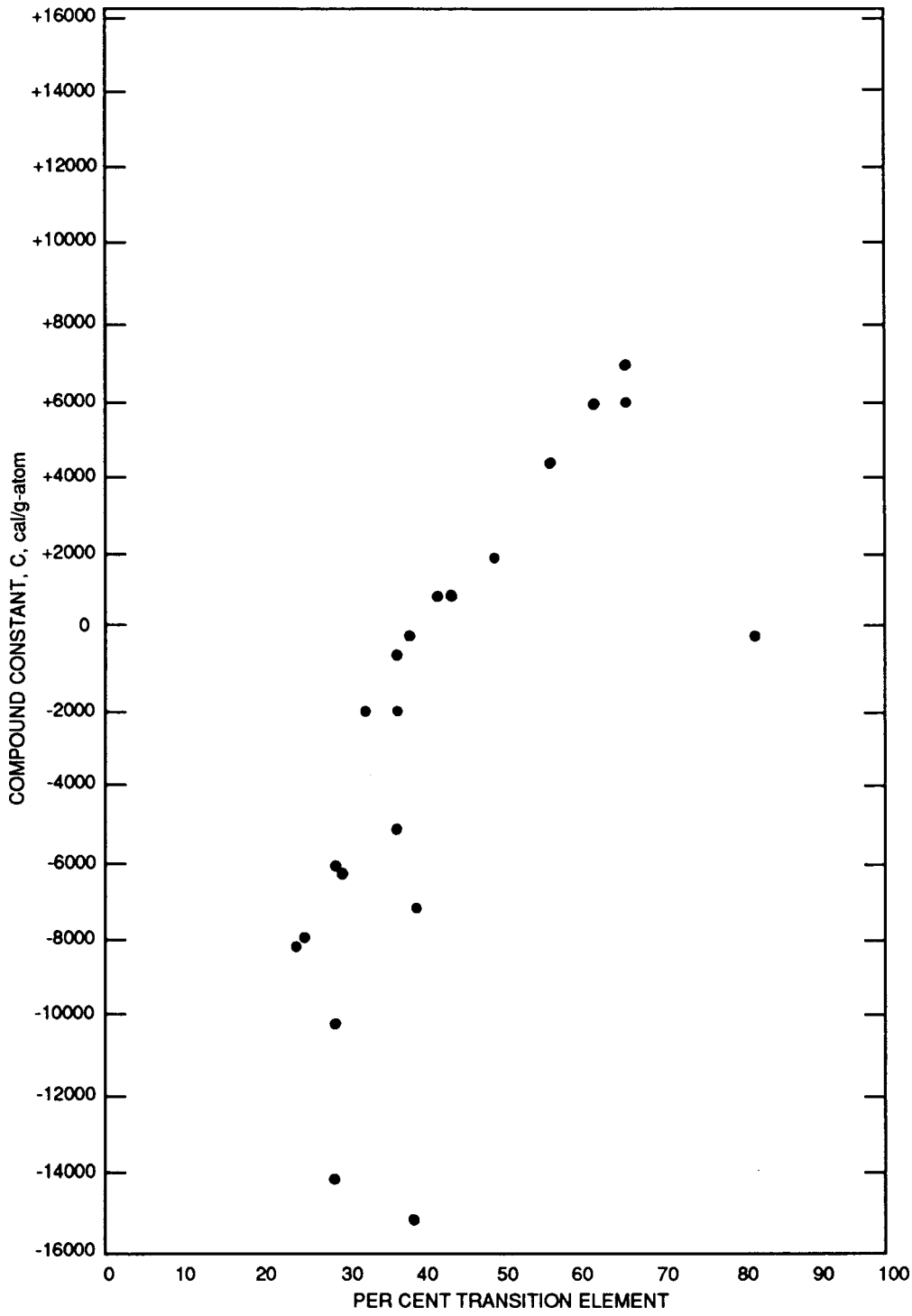

FIGURE 97. Empirically Determined Values for the Compound Constant, C, for use with Rhodium and Platinum-HCP Structure Compounds

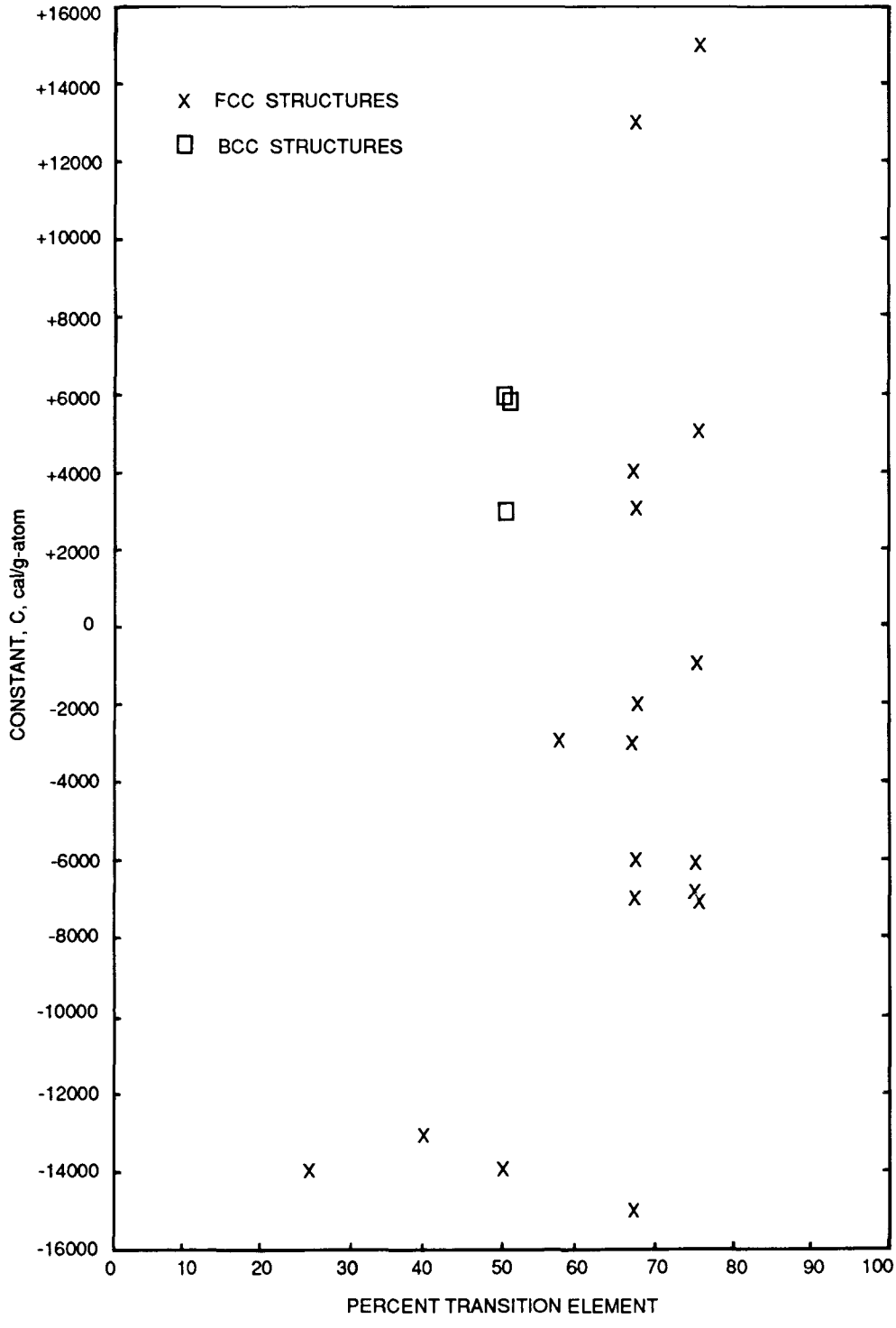

FIGURE 98. Empirically Determined Values for the Compound Constant, C, for use with Rhodium and Iridium-BCC and FCC Structure Compounds

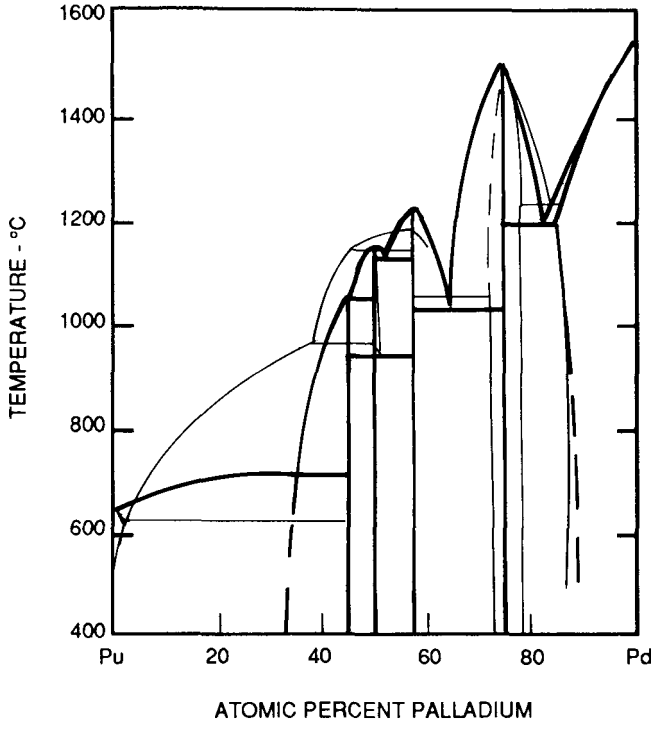

FIGURE 99. Calculated vs Experimental Pd-Pu Diagram

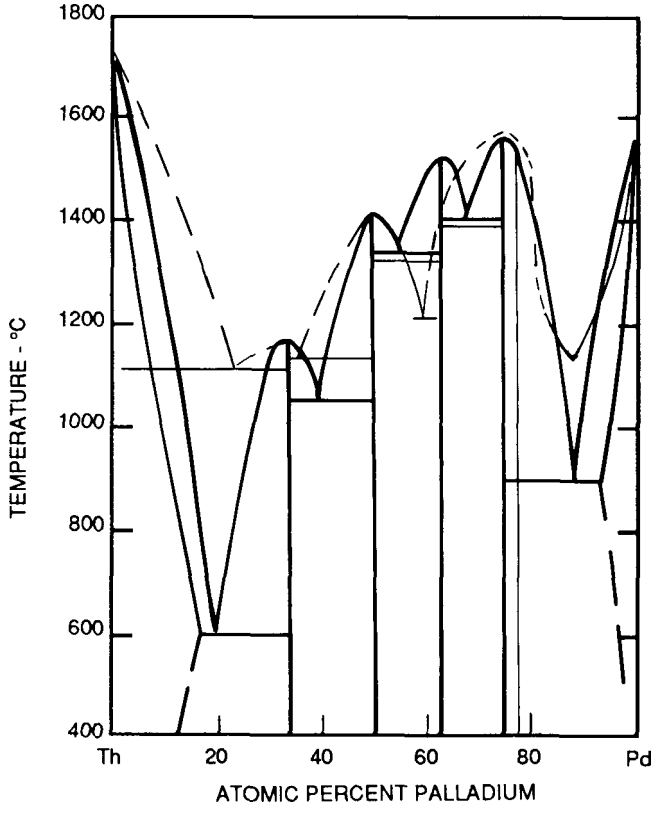

FIGURE 100. Calculated vs Estimated Pd-Th Diagram

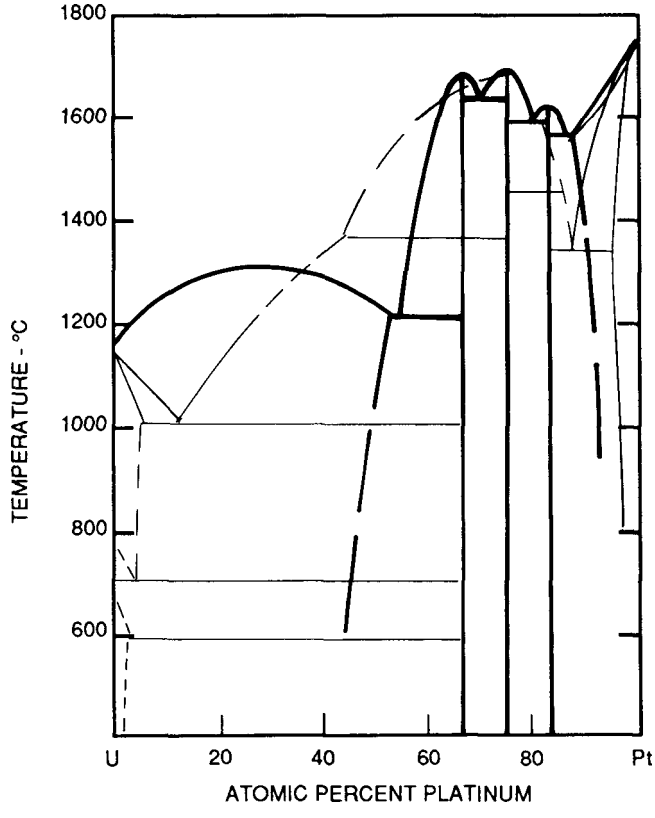

FIGURE 101. Calculated vs Experimental Pt-U Diagram

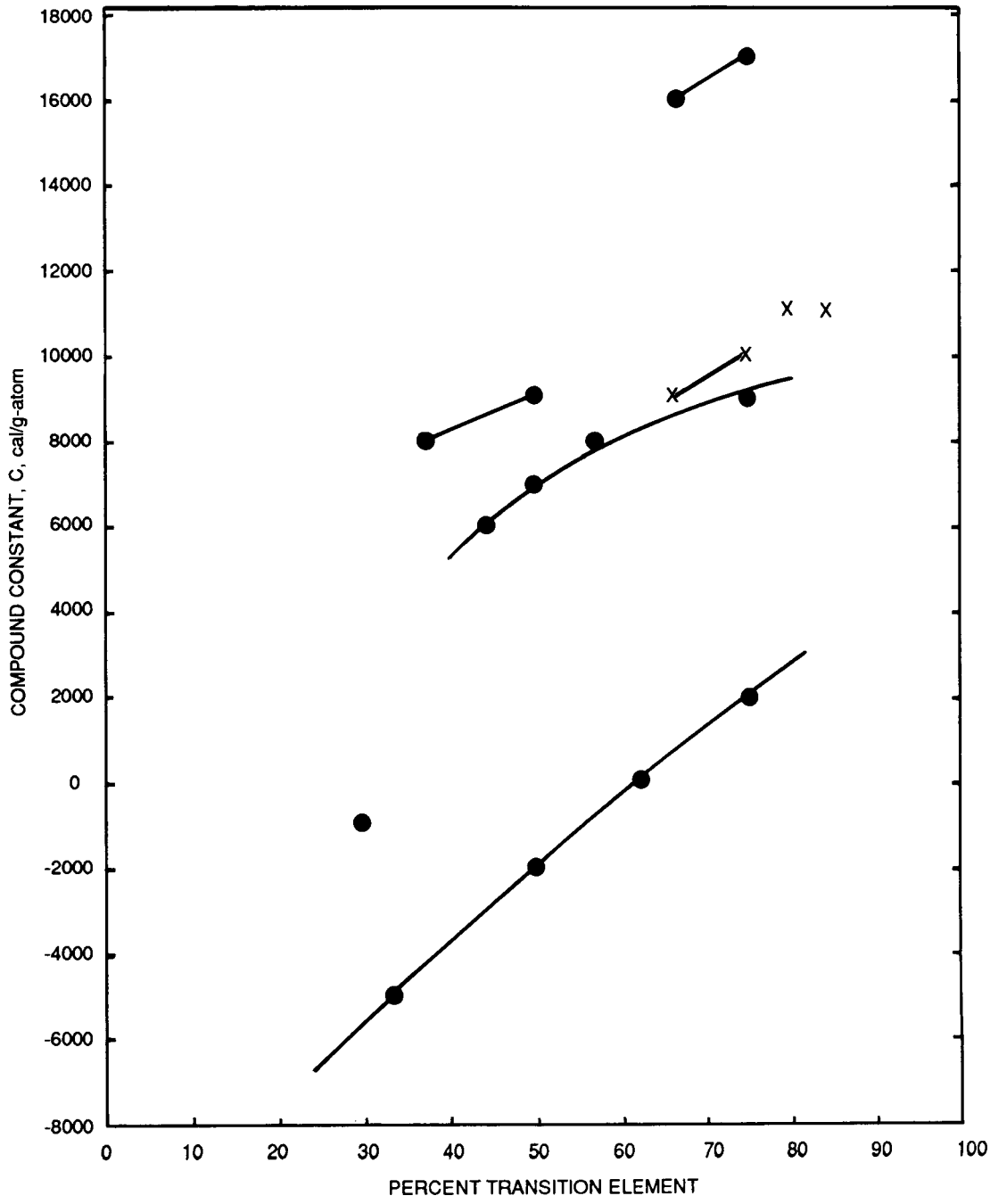

FIGURE 102. Empirically Determined Compound Constants for Actinides with Palladium and Platinum

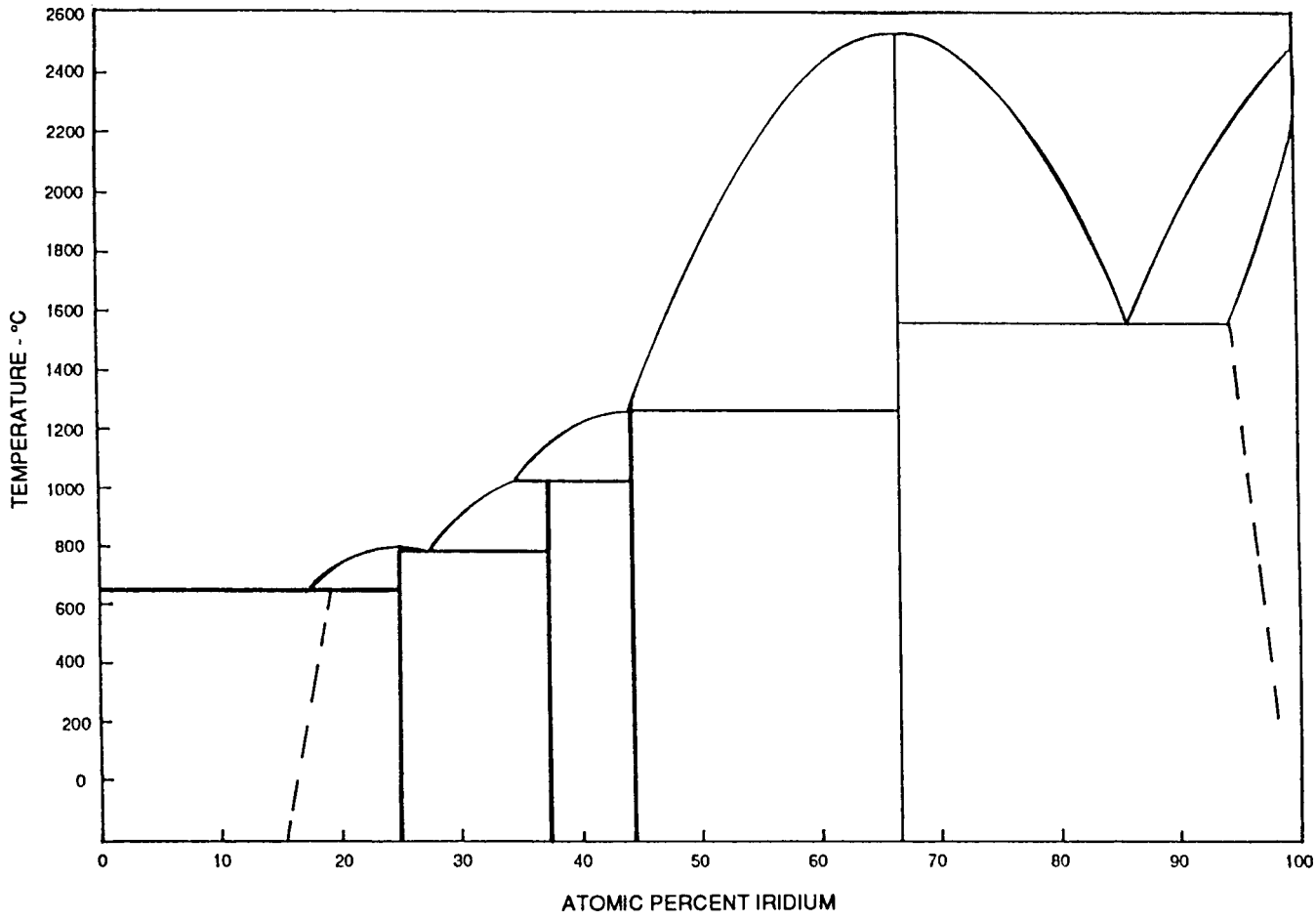

FIGURE 103. Calculated Ir-Pu Diagram

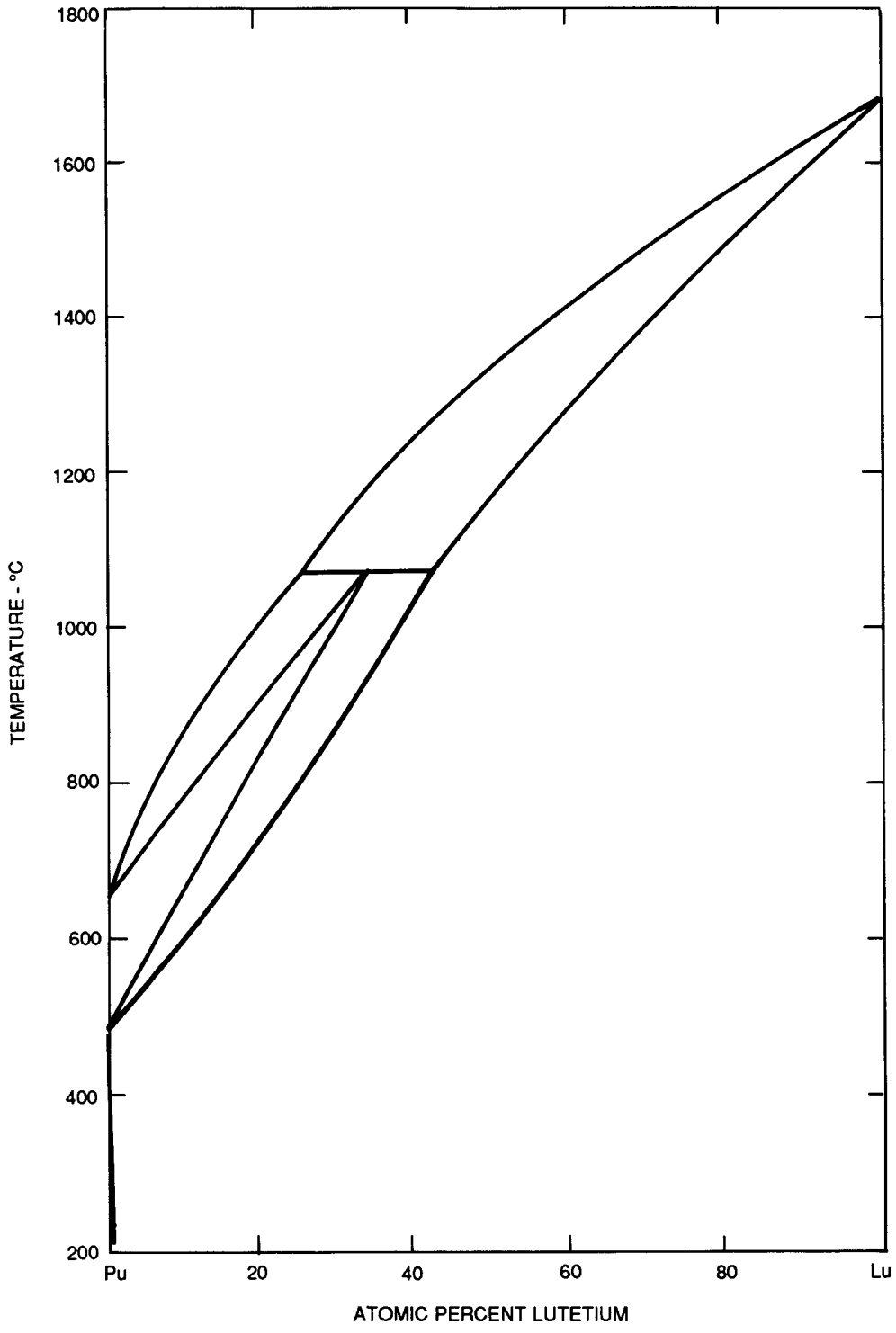

FIGURE 104. Calculated Lu-Pu Diagram

APPENDIX A. DETERMINATION OF STABILITY PARAMETERS

Stability parameters for some of the transformations for most of the rare earth and actinide elements were obtained from the compilation of Hultgren et al.[A1] From these, others were calculated directly from the relationships:

$$\Delta H^{1\rightarrow 3} = \Delta H^{1\rightarrow 2} + \Delta H^{2\rightarrow 3} \qquad \text{(Eq. A1)}$$

and

$$\Delta S^{1\rightarrow 3} = \Delta S^{1\rightarrow 2} + \Delta S^{2\rightarrow 3} \qquad \text{(Eq. A2)}$$

where the superscripts 1, 2, and 3, represent any of the phases of the element in question. In many cases, these calculations do not result in a complete set of stability parameters for a given element and other means are required. It is the purpose of this appendix to summarize the methods used for determining all of the stability parameters for the rare earth and actinide elements.

The stability parameters for the rare earths and actinides are presented in Table A1, and the footnotes describe the procedures used in their determination. Parameters obtained directly from Hultgren et al.[A1] or calculated by means of Equations A1 and A2 from these parameters account for approximately 50% of the parameters required. For the remainder of the parameters required, other means are necessary.

Plots were made of ΔH and ΔS for the ß→L and the ε→L transformations as a function of atomic number for the rare earths using parameters determined by Footnotes (a) and (b) in Table A1. These plots are shown in Figures A1 and A2, respectively. From these figures, unknown parameters can be determined by interpolation. This procedure is based on the observation of Gschneidner[A2] that the rare earth properties are systematic, in most cases, so that interpolations are possible. Values estimated by this method are indicated with a (c), and values determined by a combination of (a), (b), and (c) are indicated by a (d). Values determined by a combination of (a) and (c) are indicated by (g).

Very few data are available for the α→L transformation, but available data are given in Figure A3. A linear relationship is also assumed for this transformation, and this is rationalized on the basis that the ß→L and ε→L versus atomic number data are linear, so that the α→L versus atomic number data could be expected to be linear also. Values estimated by interpolation from this figure are indicated by (e), and values determined by combining (a), (b), and (e) are indicated by (f).

Scandium and yttrium present special cases of the rare earths. These elements, while not in the third long period with the rare earths, have a valence of three and are similar to the rare earths chemically and metallurgically. Parameters for these elements were estimated from plots of ΔH and ΔS for the α→ε transformation as a function of atomic number for the first and second long periods.[A3] These plots are given in Figure A4. Values estimated from these plots are indicated by (h), and values determined by a combination of (a), (b), and (h) are indicated by (i).

A different approach was necessary for europium and ytterbium which are divalent metals. The methods described above originally resulted in the lattice stability parameters given in Table A2. These values indicate that neither of these elements would solidify to the body-centered cubic phase, in direct conflict with experiment. For europium, both the ε→L (1204 °C) and the α→L (851 °C) transformations would occur at higher temperatures than the observed ß→L transformation (817 °C); for ytterbium only, the ε→L transformation would occur at a higher temperature (1625 °C) than the observed ß→L transformation (823 °C).

For these transformations, the entropy (ΔS) values were determined by interpolation of Figures A2 and A3. A transformation temperature was then assumed and the enthalpy (ΔH) value was calculated. For the α→L transformation in europium, a temperature near but below the ß→L

Table A1. Lattice Stability Parameters (Free Energy Differences) for the Rare Earths and Actinides

Element	$\Delta F(\beta \rightarrow L)$	$\Delta F(\varepsilon \rightarrow L)$	$\Delta F(\alpha \rightarrow L)$	$\Delta F(\beta \rightarrow \varepsilon)$	$\Delta F(\alpha \rightarrow \varepsilon)$	$\Delta F(\alpha \rightarrow \beta)$
Sc	3369 – 1.86T	4327 – 2.46T	3377 – 2.41T	–958 + 0.60T	–950 + 0.05T	8 – 0.55T
	T = 1538 (a)	T = 1486 (b)	T = 1128 (i)	T = 1324 (a)	T = 18727 (h)	T = –258 (i)
Y	2724 – 1.51T	3917 – 2.19T	2967 – 2.14T	–1193 + 0.68T	–950 + 0.05T	243 – 0.63T
	T = 1531 (a)	T = 1516 (b)	T = 1113 (i)	T = 1481 (a)	T = 18727 (h)	T = 113 (i)
La	1481 – 1.24T	2314 – 2.06T	2227 – 1.90T	–833 + 0.82T	–87 + 0.16T	746 – 0.66T
	T = 921 (a)	T = 850 (b)	T = 899 (b)	T = 743 (b)	T = 271 (a)	T = 857 (a)
Ce	1305 – 1.22T	2150 – 2.10T	2020 – 1.93T	–845 + 0.88T	–130 + 0.17T	715 – 0.71T
	T = 797 (a)	T = 751 (c)	T = 774 (b)	T = 687 (d)	T = 492 (d)	T = 726 (a)
Pr	1646 – 1.36T	2403 – 2.07T	2230 – 1.94T	–757 + 0.71T	–173 + 0.13T	584 – 0.58T
	T = 937 (a)	T = 888 (b)	T = 876 (e)	T = 793 (a)	T = 1058 (f)	T = 734 (f)
Nd	1707 – 1.32T	2431 – 1.96T	2232 – 1.95T	–724 + 0.64T	–199 + 0.01T	525 – 0.63T
	T = 1020 (a)	T = 967 (b)	T = 872 (e)	T = 858 (a)	T = 19627 (f)	T = 560 (f)
Sm	2060 – 1.53T	2804 – 2.16T	2235 – 1.98T	–744 + 0.63T	–569 + 0.18T	175 – 0.45T
	T = 1073 (a)	T = 1025 (b)	T = 856 (e)	T = 908 (a)	T = 2888 (f)	T = 116 (f)
Eu	2202 – 2.02T	2091 – 2.15T	2215 – 1.99T	111 + 0.13T	64 + 0.16T	–47 + 0.03T
	T = 817 (a)	T = 700 (j)	T = 810 (k)	(l)	(m)	T = 1293 (f)
Gd	2403 – 1.52T	3338 – 2.13T	2239 – 2.00T	–935 + 0.61T	–1099 + 0.13T	–164 – 0.48T
	T = 1308 (a)	T = 1294 (b)	T = 846 (e)	T = 1260 (a)	T = 8181 (f)	(f)
Tb	2580 – 1.59T	3780 – 2.36T	2240 – 2.01T	–1200 + 0.77T	–1540 + 0.35T	–340 – 0.42T
	T = 1350 (a)	T = 1329 (b)	T = 841 (e)	T = 1285 (a)	T = 4127 (f)	(f)

TABLE A1. (Continued)

Element	ΔF(β→L)	ΔF(ε→L)	ΔF(α→L)	ΔF(β→ε)	ΔF(α→ε)	ΔF(α→β)
Dy	2643 – 1.57	3638 – 2.18	2242 – 2.02T	–995 + 0.61T	–1396 + 0.16T	–401 – 0.45T
	T = 1410 (a)	T = 1396 (b)	T = 837 (e)	T = 1358 (a)	T = 8452 (f)	(f)
Ho	2911 – 1.67T	4122 – 2.33T	2244 – 2.04T	–1211 + 0.66T	–1878 + 0.29T	–667 – 0.37T
	T = 1470 (a)	T = 1496 (b)	T = 827 (e)	T = 1561 (a)	T = 6203 (f)	(f)
Er	3000 – 1.78T	4757 – 2.65T	2245 – 2.05T	–1757 + 0.87T	–2512 + 0.65T	–755 – 0.27T
	T = 1412 (c)	T = 1522 (a)	T = 822 (e)	T = 1746 (g)	T = 3592 (f)	(f)
Tm	3160 –1.83T	4025 – 2.22T	2246 – 2.06T	–865 + 0.39T	–1779 + 0.16T	–914 – 0.23T
	T = 1454 (c)	T = 1540 (a)	T = 817 (e)	T = 1945 (g)	T = 10846 (f)	(f)
Yb	1830 – 1.67T	2430 – 2.33T	2248 – 2.07T	–600 + 0.67T	–182 + 0.26T	418 – 0.40T
	T = 823 (a)	T = 770 (o)	T = 813 (b)	T = 623 (p)	T = 427 (q)	T = 772 (a)
Lu	3467 – 1.923T	4457 – 2.30T	2250 – 2.08T	–990 + 0.37T	–2207 + 0.22T	–1217 – 0.15T
	T = 1530 (c)	T = 1665 (a)	T = 808 (e)	T = 2403 (g)	T = 9759 (f)	(f)
Th	3853 – 1.90T	3100 – 2.25T	4507 – 2.30T	753 – 0.35T	1407 – 0.05T	654 – 0.40T
	T = 1755 (a)	T = 1105 (t)	T = 1686 (b)	T = 1878 (u)	T = 27867 (u)	T = 1362 (a)
U	2036 – 1.45T	3840 – 3.25T	3173 – 2.54T	–1804 + 1.80T	–667 + 0.71T	1137 – 1.09T
	T = 1131 (a)	T = 908 (b)	T = 976 (b)	T = 729 (b)	T = 666 (a)	T = 770 (a)
Np	1240 – 1.36T	3840 – 5.27T	2500 – 2.85T	–2600 + 3.91T	–1340 + 2.42T	1260 – 1.49T
	T = 639 (r)	T = 456 (s)	T = 604 (s)	T = 392 (s)	T = 281 (r)	T = 573 (r)
Pu	680 – 0.74T	1119 – 1.32T	1141 – 1.35T	–439 + 0.58T	22 – 0.03T	461 – 0.61T
	T = 646 (a)	T = 575 (b)	T = 570 (b)	T = 484 (a)	T = 460 (a)	T = 483 (b)

(a) Data from Ref. A1
(b) Calculated from Hultgren data and Equations 1 and 2
(c) Estimated by interpolation of B→L and E→L vs Z plots
(d) Calculated from a, b, and c
(e) Estimated from interpolation of A→L vs Z plot
(f) Calculated from a, b, and e
(g) Calculated from a and c
(h) Estimated from ΔH and ΔS vs Z plots for first and second long periods
(i) Calculated from a, b, and h
(j) ΔS value determined from plot of ΔS vs Z and $T_{tr}(\varepsilon \rightarrow L)$ = 700 °C
(k) ΔS value determined from plot of ΔS vs Z and $T_{tr}(\alpha \rightarrow L)$ = 810 °C
(l) Calculated from a and j
(m) Calculated from j and k
(n) Calculated from a and k
(o) ΔS value determined from plot of ΔS vs Z and $T_{tr}(\varepsilon \rightarrow L)$ = 770 °C
(p) Calculated from a and o
(q) Calculated from b and o
(r) From Ref. A4
(s) Calculated from j
(t) Estimated from E→L vs Z plot for actinides
(u) Calculated from a, b, and l

Table A2. Original Values Calculated for Lattice Stability Parameters for Europium and Ytterbium

Element	$\Delta F(\beta \rightarrow L)$	$\Delta F(\varepsilon \rightarrow L)$	$\Delta F(\alpha \rightarrow L)$	$\Delta F(\beta \rightarrow \varepsilon)$	$\Delta F(\alpha \rightarrow \varepsilon)$	$\Delta F(\alpha \rightarrow \beta)$
Eu	2202 – 2.02T	3220 – 2.18T	2237 – 1.99T	−1018 + 0.16T	−983 + 0.19T	−35 + 0.03T
	t = 817 (a)	t = 1204 (c)	t = 851 (e)	t = 6090 (g)	t = 4901 (f)	t = 894 (f)
Yb	1830 – 1.67T	4575 – 2.14T	2248 – 2.07T	−2745 + 0.74T	−2327 + 0.34T	418 – 0.40T
	t = 823 (a)	t = 1625 (c)	t = 813 (b)	t = 3436 (d)	t = 6571 (d)	t = 772 (a)

T = temperature in °K
t = temperature in °C

(a) Data from Hultgren et al. (6)
(b) Calculated from Hultgren data and Equations A1 and A2
(c) Estimated from interpolation of $\beta \rightarrow L$ and $\varepsilon \rightarrow L$ vs Z plots
(d) Calculated from a, b, and c
(e) Estimated from interpolation of $\alpha \rightarrow L$ vs Z plot
(f) Calculated from a, b, and e
(g) Calculated from a and c

transformation was chosen, and this value was arbitrarily set at 810 °C. This was done to make europium follow the values for ytterbium.

For the $\varepsilon \rightarrow L$ transformation for both elements, a temperature was chosen below the $\alpha \rightarrow L$ transformation. Trial and error resulted in temperatures of 700 and 770 °C for europium and ytterbium, respectively, which still gave reasonable values for the unknown solid-state transformations. This is a very arbitrary method and results in values that may be suspect, but no other reasonable method could be devised.

Parameters for the actinides were obtained in similar fashion. For uranium and plutonium, values were obtained from Hultgren et al.[A1] and unknown values were obtained by using Equations A1 and A2. Neptunium data were obtained from Rechtien and Nelson.[A4] Data for three transformations were obtained from Hultgren et al. [A1] For the remainder of the transformations, a plot of ΔH and ΔS for the $\varepsilon \rightarrow L$ transformation in the actinides was used. This plot is given in Figure A5. From this plot, values for thorium were estimated and used to calculate the $\beta \rightarrow \varepsilon$ and $\alpha \rightarrow \varepsilon$ transformations.

Values obtained by interpolation of entropy data in Figures A2 and A3 are indicated by Footnotes (j) and (k), respectively. From these values, the parameters for the remaining solid-state transformations were calculated as indicated in Footnotes (l), (m), and (n).

REFERENCES

A1. R. Hultgren et al., "Selected Values of the Thermodynamic Properties of the Elements," *ASM*, Metals Park, OH.

A2. K. A. Gschneidner Jr. and F. W. Calderwood, "Use of Systematics for the Evaluation of Rare Earth Phase Diagrams and Crystallographic Data," *Bulletin of Alloy Phase Diagrams, 4(2)*, pp 129-31, 1983.

A3. L. Kaufman and H. Bernstein, *Computer Calculation of Phase Diagrams*, Academic Press, New York, NY, 1970.

A4. J. J. Rechtein and R. D. Nelson, "Phase Transformations in Uranium, Plutonium, and Neptunium," *Met. Trans., 4*, pp 2755-2765, 1973.

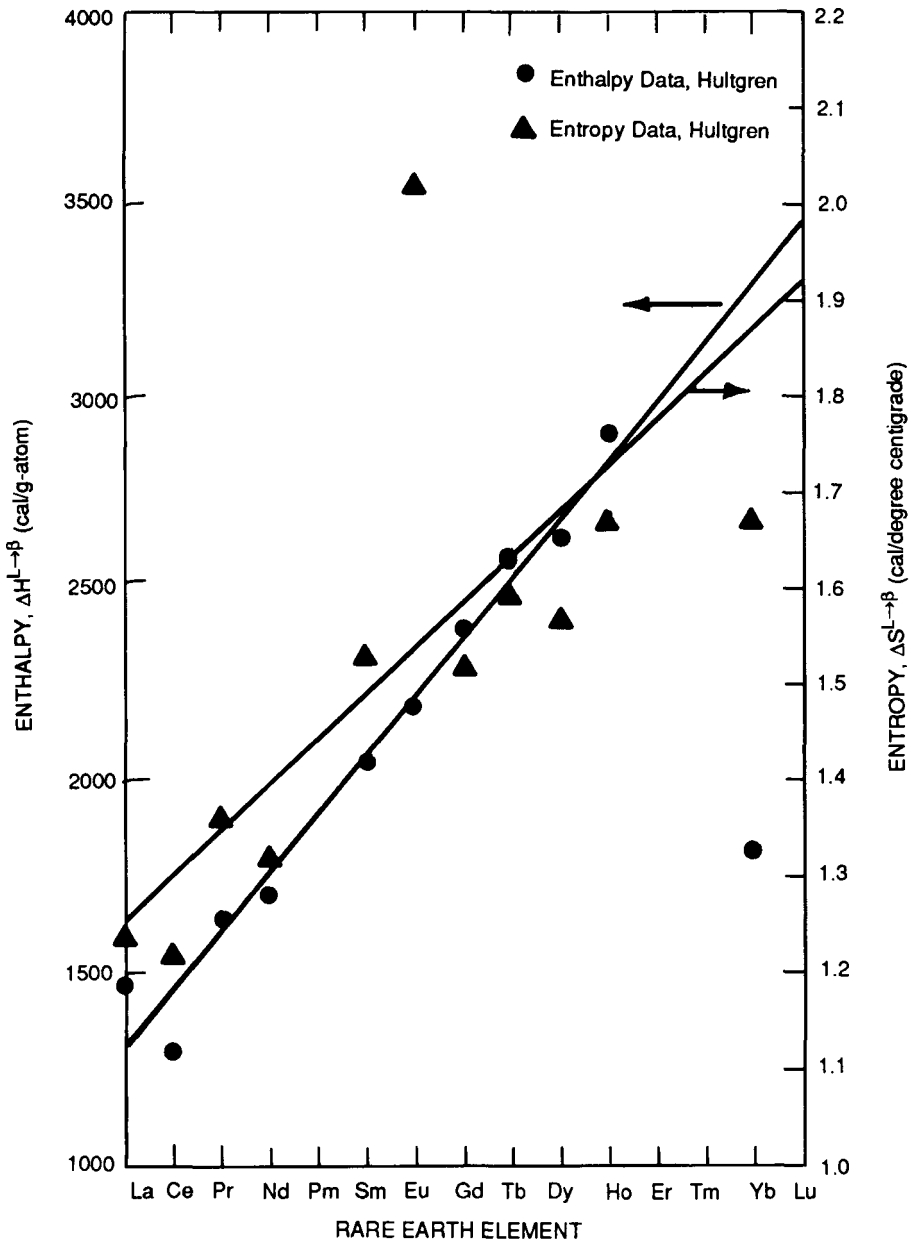

FIGURE A1. Enthalpy and Entropy Values for the L→B Transformation; from Hultgren (Ref. 6)

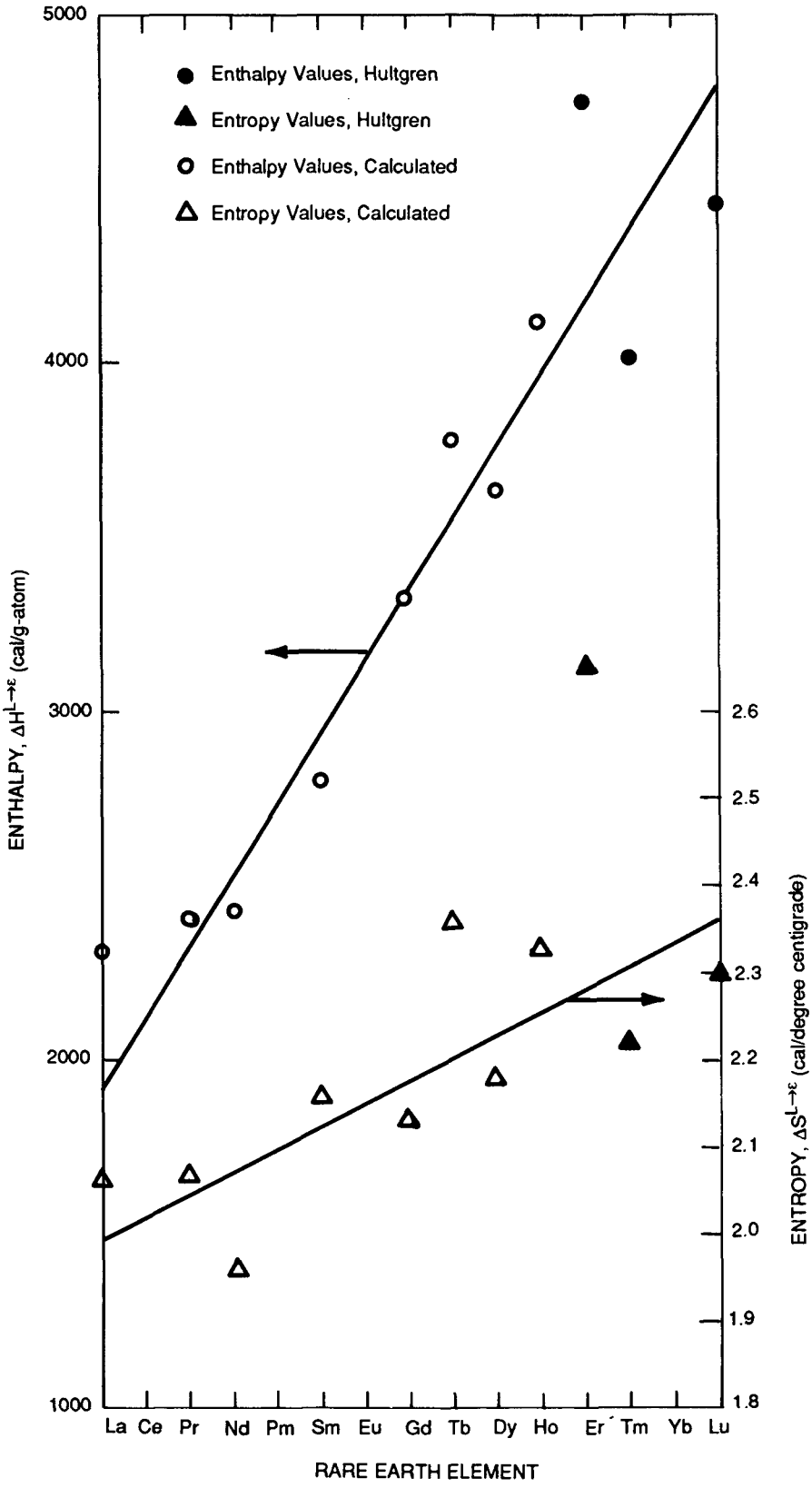

FIGURE A2. Enthalpy and Entropy Values for the L→ε Transformation

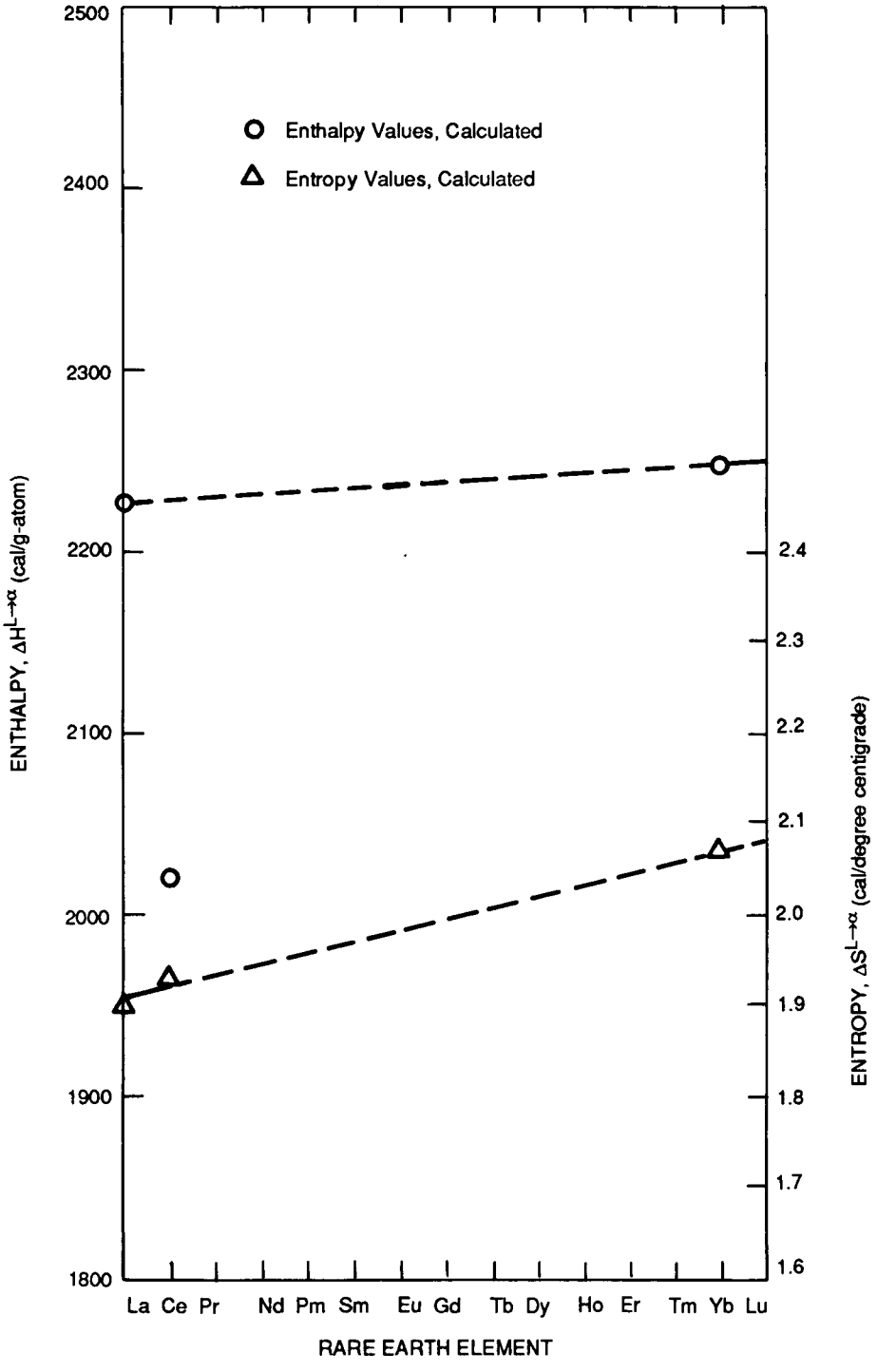

FIGURE A3. Enthalpy and Entropy Values for the L→α Transformation

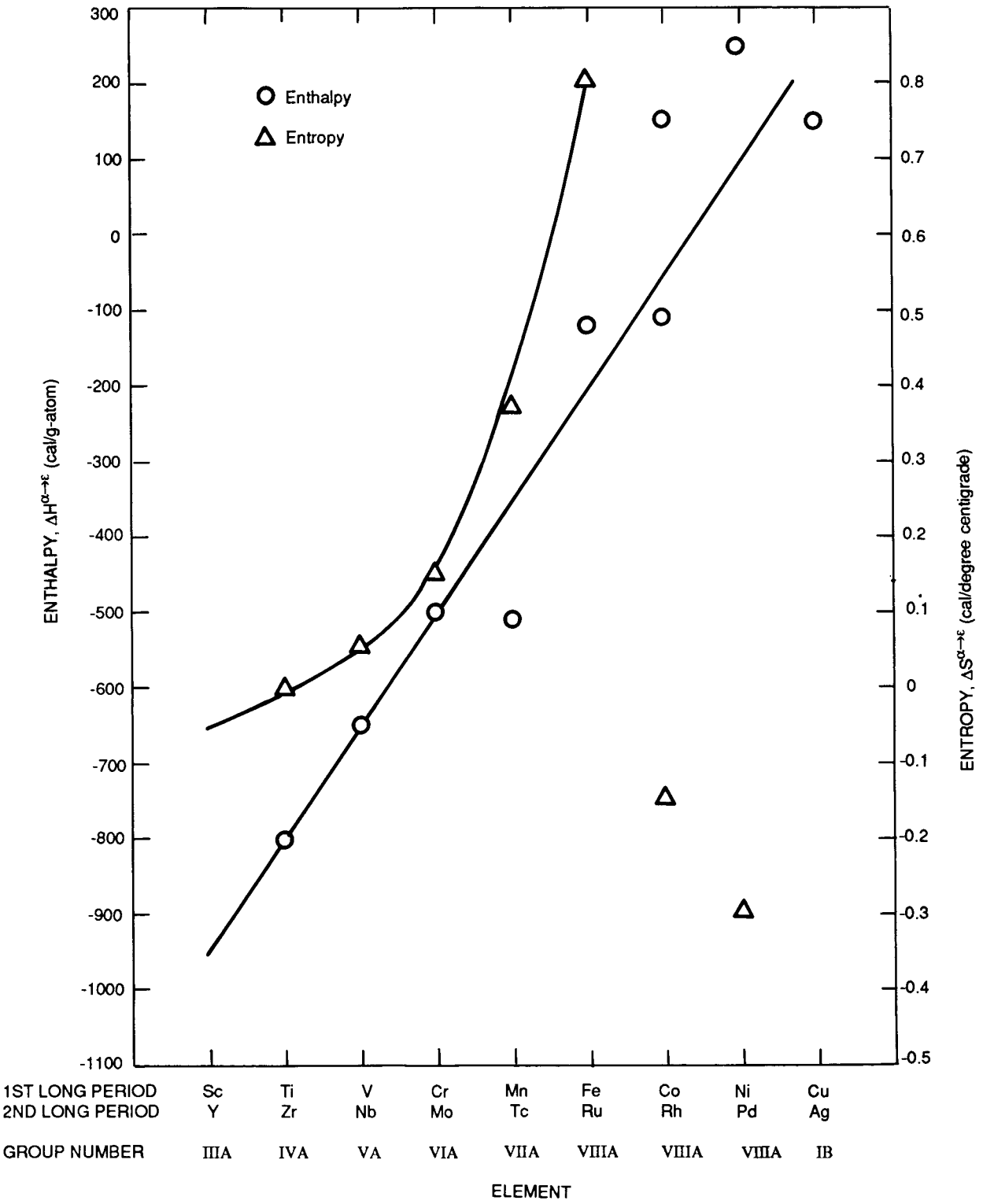

FIGURE A4. Enthalpy and Entropy Values for the $\alpha \rightarrow \varepsilon$ Transformation; from Kaufman (Ref. 1)

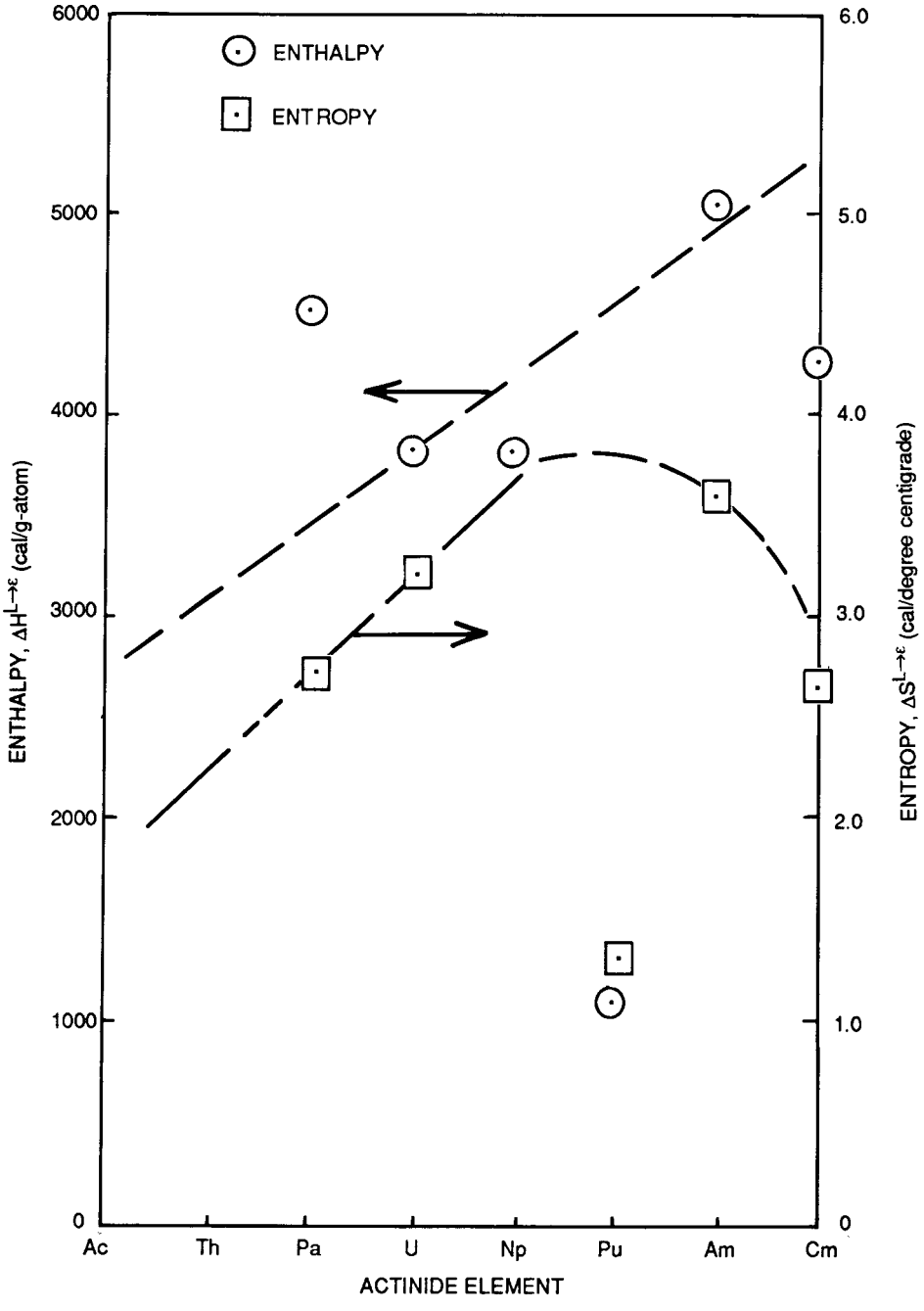

FIGURE A5. Enthalpy and Entropy
Values for the L→ε Transformation

APPENDIX B. DETERMINATION OF ATOMIC VOLUME FOR ALL PHASES

Values for the atomic volume for each phase of the rare earth elements and the actinide elements are given in Table B1. The method used for each value is indicated in the footnotes. In determining these values, the following assumptions were made:

1. The $\varepsilon \rightarrow \alpha$ transformation on cooling involves a 0.5% contraction.

2. The $\beta \rightarrow \varepsilon$ transformation on cooling involves a 1% contraction.

3. The $L \rightarrow \beta$ transformation involves a 2.5% contraction.

These assumptions were invoked whenever literature data were not available or for hypothetical phases. Whenever possible, atomic volumes were calculated from density values,[B1] and the volumes for other phases were determined on the basis of the above assumptions. Atomic volumes for high temperature phases were calculated, when necessary, from lower temperature phase values, the coefficient of volume expansion,[B1] and the volume changes based on the above assumptions.

For five rare earth elements and one actinide element, an empirical method was found to be necessary. For these elements (cerium, dysprosium, lanthanum, scandium, yttrium, and plutonium), the original values determined for the atomic volume for each phase produced calculated diagrams that deviated considerably from experimentally determined diagrams. The atomic volumes determined originally are summarized in Table B2. Interaction parameters calculated from these values for cerium, dysprosium, lanthanum, scandium, and yttrium with selected rare earths are given in Table B3, and diagrams calculated from these parameters are presented in Figures B1-B3. Calculated diagrams are represented by thick lines while literature diagrams are represented by thin lines. The calculated diagrams show considerable deviation from the experimentally determined diagrams. For each of the systems given in Figures B1-B3, the atomic volumes were varied until a diagram was calculated that was more aligned with the experimentally determined diagram. The resulting diagrams are presented in Figures B4-B6 and in the text of this report. Atomic volumes determined by this method are presented in Table B1. These values were used in all subsequent calculations of systems containing the element. Thus, only one system was used for the empirical determination of atomic volumes for these elements, and "curve fitting" was kept to a minimum.

For cerium and scandium, the value for the liquid phase was used as the reference, and values for the other phases were calculated by means of the relationship:

$$\frac{V_{S1}}{V_{L1}} = \frac{V_{S3}}{V_{L3}} \qquad \text{(Eq. B1)}$$

where V_{S1} and V_{L1} are the altered atomic volumes for the solid phase and the liquid phase respectively, and V_{S3} and V_{L3} are the volumes for the solid phase and the liquid given in Table B2. Thus, V_{S1} and V_{L1} were changed proportionately until the liquidus was satisfactory. In this way, the relative changes for each phase remained the same as the original changes. In the case of dysprosium only, V_{ε} and V_{β} were changed; for yttrium, only V_{ε} was changed to produce more acceptable results.

Europium and ytterbium are divalent metals in the pure state; but in alloys, they can become trivalent.[B5,6] With the rare earths and actinides, the use of atomic volumes for the divalent metals gives calculated diagrams showing good agreement with the literature diagrams. However, when calculations were attempted with elements of Groups VIA-VIIIA, poor results were obtained. However, when using an estimated value for the atomic volume of the trivalent atom given by Teatum et al.,[B3] calculated diagrams were found

TABLE B1. Enthalpy of Formation and Atomic Volumes for the Rare Earths and Actinides

Element	H_{vap} (cal/mole) (a)	V_L (cm^3/mole)	V_β (cm^3/mole)	V_ε (cm^3/mole)	V_α (cm^3/mole)
Sc	-90,320	17.33 (h)	16.81 (h)	16.00 (h)	15.92 (h)
Y	-101,500	21.53 (i)	21.01 (f)	20.49 (j)	19.79 (j)
La	-103,000	22.30 (k)	22.22 (k)	21.58 (k)	21.43 (k)
Ce	-101,000	22.50 (l)	22.42 (l)	22.47 (l)	22.20 (l)
Pr	-85,000	21.32 (b)	21.22 (b)	20.80 (b)	20.70 (c)
Nd	-78,300	21.62 (b)	21.21 (b)	20.58 (b)	20.48 (c)
Sm	-65,000 (m)	21.17 (d)	20.32 (b)	20.46 (b)	20.00 (b)
Eu	-41,900	32.92 (d)	28.98 (b)	28.69 (g)	28.55 (c)
		22.49 (v)	19.80 (u)	19.60 (v)	19.50 (v)
Gd	-95,000	20.59 (d)	20.16 (b)	19.90 (b)	19.80 (c)
Tb	-92,900	20.22 (d)	19.57 (b)	19.31 (b)	19.21 (b)
Dy	-69,400	19.84 (d)	19.40 (j)	18.70 (j)	18.91 (c)
Ho	-71,900	21.12 (d)	18.94 (c)	18.75 (b)	18.66 (c)
Er	-75,800	21.22 (d)	18.63 (e)	18.45 (b)	18.36 (c)
Tm	-55,500	20.54 (d)	18.30 (e)	18.12 (b)	18.03 (c)
Yb	-36,350	27.50 (b)	26.38 (b)	25.07 (b)	24.84 (b)
		19.90 (v)	19.09 (v)	18.15 (v)	17.98 (u)
Lu	-102,200	19.31 (d)	18.83 (f)	17.78 (b)	17.69 (c)
Th	-137,500	22.10 (b)	20.99 (b)	20.58 (q)	20.18 (b)
U	-125,000	13.91 (p)	13.61 (f)	13.51 (s)	13.40 (r)
Np	-110,000	13.62 (n)	13.33 (n)	13.24 (o)	13.11 (o)
Pu	-84,100	14.72 (n)	14.95 (n)	15.24 (n)	15.30 (n)

(a) Data from Ref. B1
(b) From Ref. B2
(c) Estimated from 0.5% contraction
(d) Estimated from room temperature density, coefficient of thermal expansion, and ΔV melting
(e) Estimate from 1% expansion from ε phase
(f) Estimated from CTE + 1% expansion upon transformation
(g) Calculated from Ref. B2 + CTE + 1% ΔVtr
(h) Determined empirically from Nd-Sc diagram
(i) Estimated from CTE and 2.5% expansion upon melting
(j) Determined empirically from Dy-Y diagram
(k) Determined empirically from La-Tb diagram
(l) Determined empirically from Ce-La Diagram
(m) Determined empirically from Lu-Sm diagram
(n) Determined empirically from Np-Pu diagram
(o) Calculated from (h) and ΔVtr
(p) Estimated from CTE and 2.5% expansion upon melting
(q) Estimated from average of α and β phases
(r) From Ref. B3 + CTE
(s) Estimated from 0.5% expansion
(t) From Ref. B4
(u) Ref. B3.
(v) Estimated from (u) + Equation B1

TABLE B2. Original Values for Atomic Volumes for Selected Rare Earths and Plutonium

Element	V_L (cm^3/mole)	V_β (cm^3/mole)	V_ε (cm^3/mole)	V_α (cm^3/mole)
Sc	16.29 (k)	15.80 (f)	15.04 (b)	14.96 (c)
Y	21.53 (k)	21.01 (f)	19.89 (b)	19.79 (c)
La	23.35 (b)	23.27 (b)	22.60 (b)	22.44 (b)
Ce	20.98 (b)	20.91 (b)	20.95 (b)	20.70 (b)
Dy	19.84 (d)	18.98 (b)	19.00 (b)	18.91 (c)
Pu	14.38 (p)	14.60 (q)	14.89 (r)	14.95 (s)

(b) From Ref. B2
(c) Estimated from 0.5% contraction
(d) Estimated from room temperature density, coefficient of thermal expansion, and V melting
(f) Estimated from CTE + 1% expansion upon transformation
(k) Estimated from CTE and 2.5% expansion upon melting
(p) From Ref. B3
(q) Calculated from p and 1.5% expansion upon freezing (Ref. B3)
(r) Calculated from q + 2% expansion upon cooling (Ref. B3)
(s) Calculated from r and 0.4% expansion upon cooling (Ref. B3)

TABLE B3. Interaction Parameters Calculated from the Original Values for Atomic Volumes

System	L	B	E	A
Dy-Y	1124	1393	1179	1178
Nd-Sc	2320	4546	4840	4847
Ce-La	117	414	267	287
La-Tb	24	802	667	651

TABLE B4. Atomic Volumes and Interaction Parameters for Np-Pu Diagram before Empirical Determination

Phase	Atomic Volume (cm^3/mole)	Interaction Parameter
Liquid, L	14.38	1507
BCC, B	14.60	1722
HCP, E	14.89	1865
FCC, A	14.95	1955

to represent the literature diagrams more accurately. The values given by Teatum et al.[B3] are 19.80 and 17.98 cm^3/mole for body-centered cubic Eu and face-centered cubic Yb, respectively. Using these values as reference, a relationship similar to Equation B1 was used to calculate the values for the other phases. These values are given in Table B1 in the second line of values for europium and ytterbium.

For samarium, the literature value for the enthalpy of vaporization was found to be low. When the literature value of -49,400 cal/mole was used, a monotectic diagram was calculated for the Lu-Sm system. The enthalpy of vaporization was varied until a reasonable representation of the estimated diagram was calculated. By this empirical means, a value of -65,000 cal/mole was determined. This value was used in all diagrams between samarium and other rare earths and actinides.

For the actinide systems, values for the atomic volumes were determined using the Np-Pu system as the reference. The values initially determined for plutonium are presented in Table B4, along with the interaction parameters calculated for each phase. These values produced the calculated diagram shown in Figure B7. In this case, the atomic volumes were increased to raise the temperature of the minimum in the liquidus and in the $\beta \rightarrow \alpha$ transformation solvus lines. As in the case of cerium and scandium, values for the solid phases were determined by means of Equation B1. The diagram calculated from the empirically determined values for the atomic volume and shown in Table B1 is given in Figure B8.

Values for the atomic volumes for Np were estimated from the volume change upon transformation for uranium. This action was taken because no data for neptunium was found, and the crystal structure of the various phases are identical.

REFERENCES

B1. R. Hultgren et al., *Selected Values of the Thermodynamic Properties of the Elements*, ASM, Metals Park, OH.

B2. *ASM Metals Handbook, Ninth Edition, 2, Properties and Selection: Nonferrous Alloys and Pure Metals*, pp 714-833, ASM, Metals Park, OH, 1979.

B3. E. T. Teatum, K. A. Gschneidner, and J. T. Waber, *Compilation of Calculated Data Useful in Predicting Metallurgical Behavior of the Elements in Binary Alloy Systems*, LA-4003, Los Alamos Scientific Laboratory, Los Alamos, NM, December 1968.

B4. "Properties and Selection of Metals," *ASM Metals Handbook, 8th Ed., 1,* ASM, Metals Park, OH.

B5. K. A. Gschneidner Jr., "On the Valences of Europium and Ytterbium in Compounds," *J. Less-Common Metals, 17*, pp 13-24, 1969.

B6. A. R. Miedema, "On the Valence State of Europium in Alloys," *J. Less- Common Metals, 46*, pp 167-173, 1976.

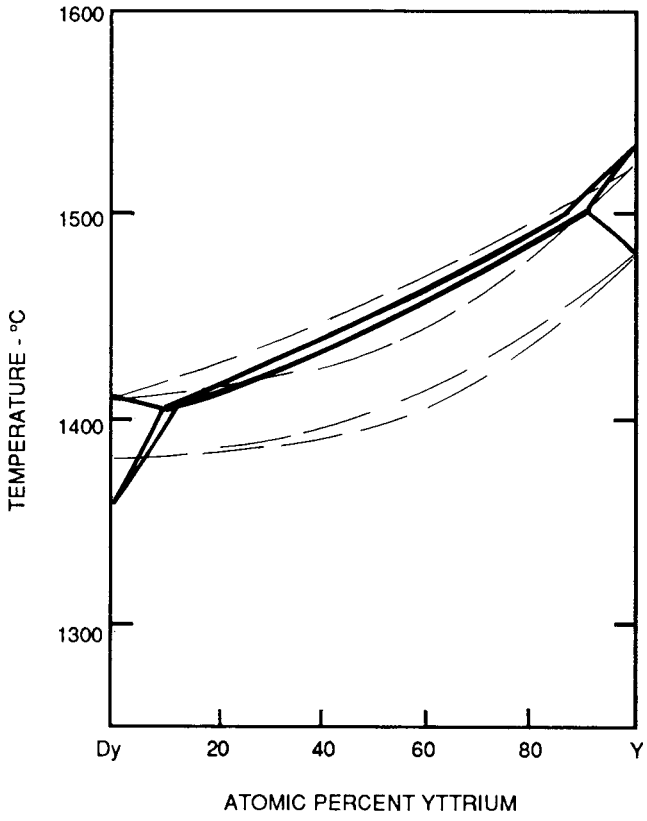

FIGURE B1. Calculated vs Estimated Dy-Y Diagram Based on Original Values for Atomic Volumes

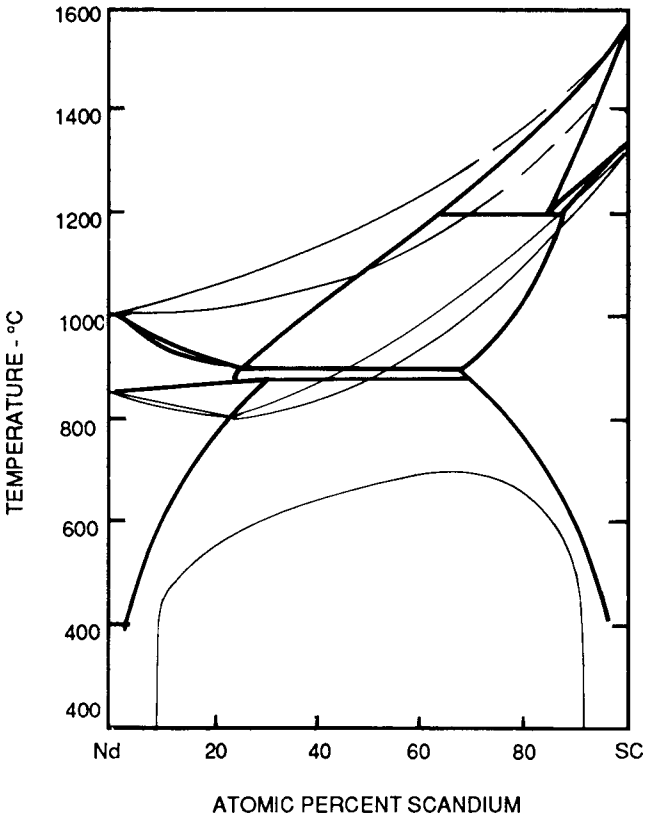

FIGURE B2. Calculated vs Experimental Nd-Sc Diagram Based on Original Values for Atomic Volumes

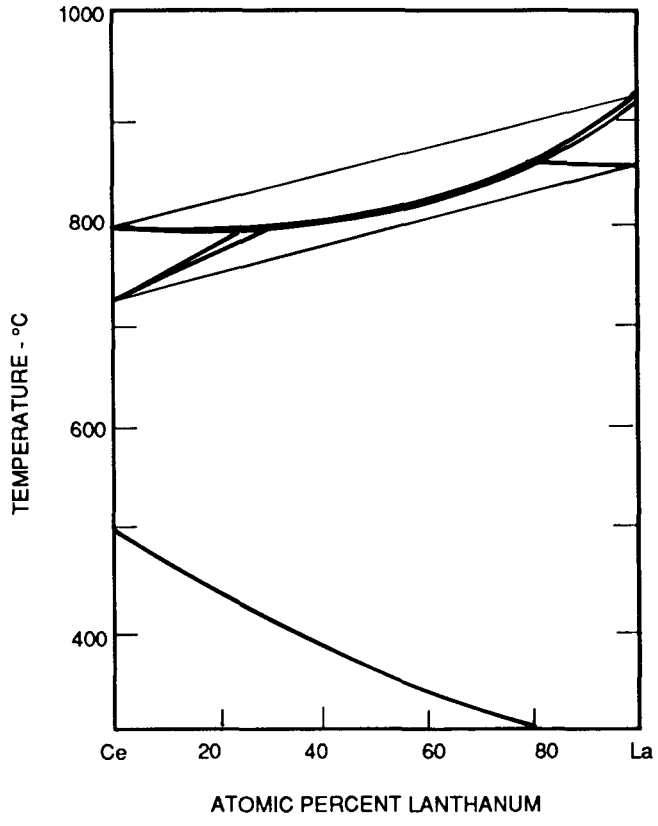

FIGURE B3. Calculated vs Experimental Ce-La Diagram Based on Original Values for Atomic Volumes

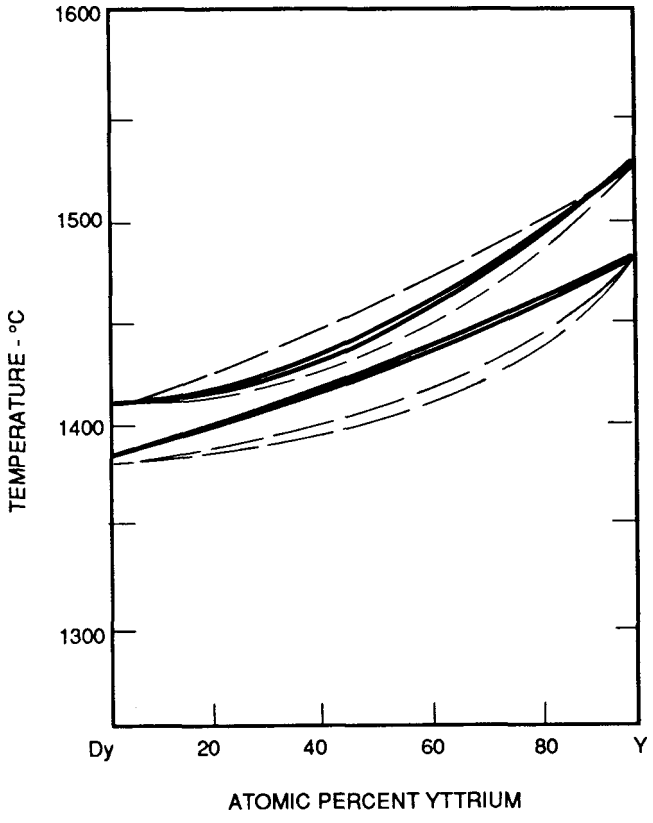

FIGURE B4. Calculated vs Estimated Dy-Y Diagram Based on Empirically Determined Atomic Values

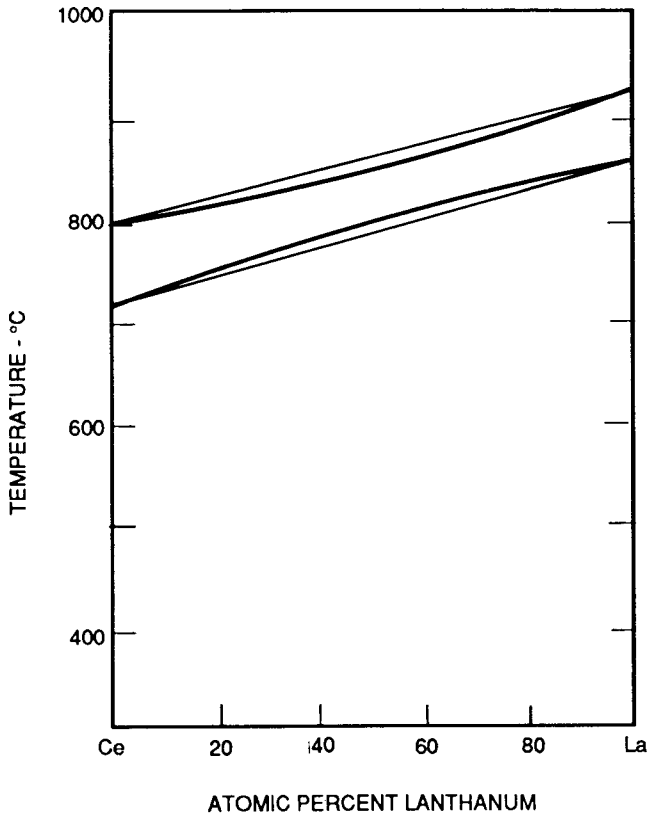

FIGURE B6. Calculated vs Experimental Ce-La Diagram Based on Empirically Determined Atomic Volumes

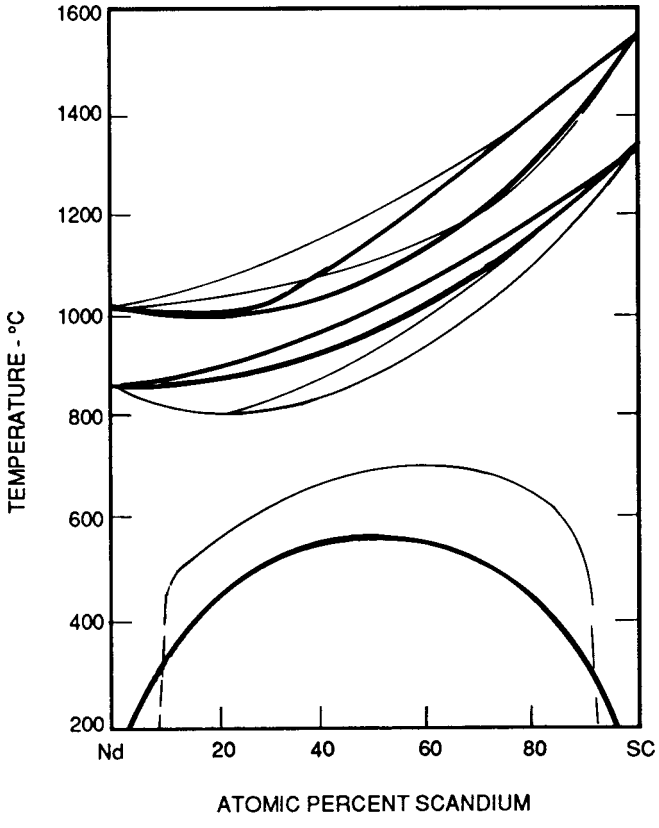

FIGURE B5. Calculated vs Experimental Nd-Sc Diagram Based on Empirically Determined Atomic Volumes

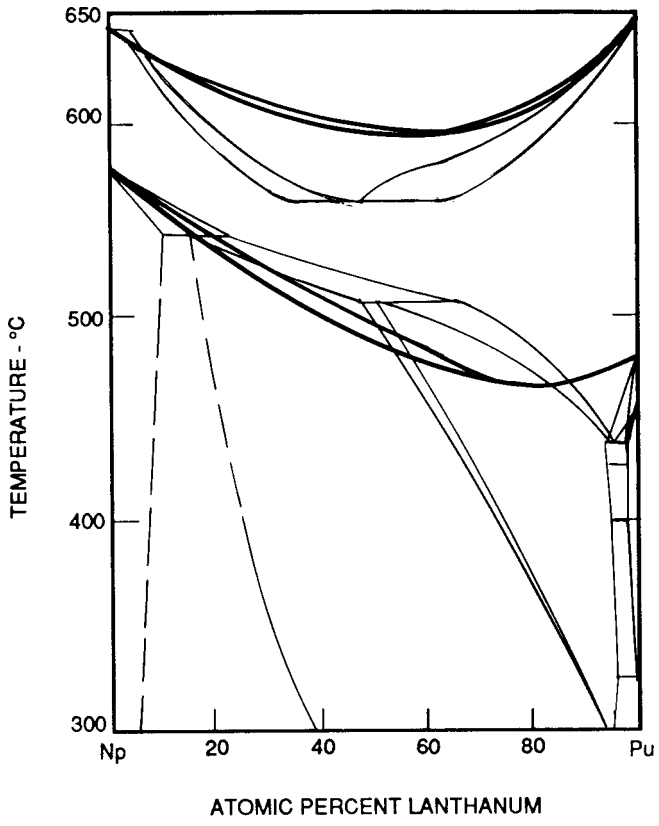

FIGURE B7. Calculated vs Experimental Np-Pu Diagram Based on Original Values for Atomic Volumes

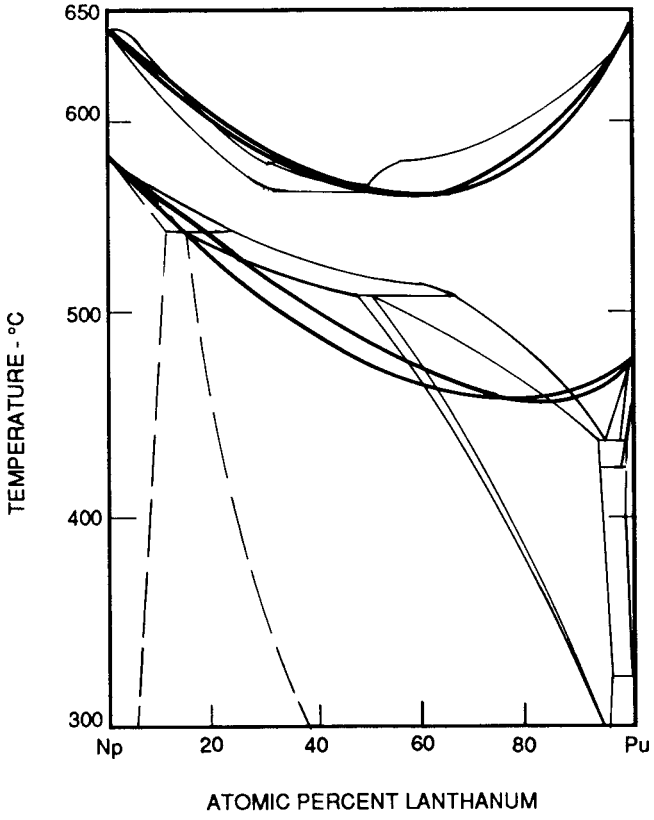

FIGURE B8. Calculated vs Experimental Np-Pu Diagram Based on Empirically Determined Atomic Volumes

☆ U.S. GOVERNMENT PRINTING OFFICE: 1992—675-757/65,103 REGION NO. 8